Electronic Structure and Electrical Properties of Conducting Polymers

Takayuki Miyamae

Electronic Structure and Electrical Properties of Conducting Polymers

(導電性高分子の電子構造と電気的特性)

宮前 孝行

Takayuki Miyamae

A Thesis Submitted to Nagoya University

for the Degree of Doctor of Science

Department of Chemistry, Faculty of Science,

Nagoya University

Furo-cho, Chikusa-ku, Nagoya 464-01, Japan

Contents

Abstract

The electronic structure and the conduction mechanism of π-conjugated conducting polymers were studied by the combination of polarized reflection spectra, temperature dependence of the conductivity, ultraviolet photoelectron spectroscopy (UPS), and molecular orbital (MO) calculations.

At first we report the polarized reflection spectra of perchlorate-doped highly conductive oriented polyacetylene, $[CH(ClO_4)_y]_x$. From the reflection spectra, measured from far infrared to ultraviolet regions, the optical conductivity spectra were obtained by Kramers-Kronig analysis. Three stages of doping were recognized from the spectral analysis, *i.e.* (1) $0<y<0.02$, where the charged soliton band is dominant; (2) $0.02<y<0.04$, where the spectra change completely and the polson band begins to grow; (3) $0.045<y$, where the spectral characteristics of metallic phase appear. The lifetime of free carrier in the metallic regime was found to be increased by the stretching of the film. From the study of the orientational effect of the stretched film, three-dimensional interchain interaction was found to be essential for the appearance of metallic conductivity.

Second, we report the temperature dependence of the electrical conductivities of perchlorate-doped highly oriented polyacetylene films measured from 290 K to 1.5 K. The conductivity and its anisotropy were significantly enhanced by stretching of the film. The value of conductivity along the direction parallel to the stretching direction was 18000 Scm^{-1} at 190 K and it remains to be a high value of 14000 Scm^{-1} even at 1.5 K. This residual conductivity at low temperature showed that the film is really metallic. The temperature dependence of conductivity was expressed by the sum of two terms; one is almost temperature independent term, which may be due to very weakly localized free carrier, and the other is due to three-dimensional variable range hopping (VRH) mechanism of more localized carrier. The temperature dependence of anisotropy and the

similar localization length for directions parallel and perpendicular to the stretching direction suggest that the hopping to the adjacent chain occurs significantly as well as intrachain hopping.

Third, we report the UPS study of sodium- and potassium-doped highly conducting polyacetylene using synchrontron radiation. Upon doping, the UPS spectra immediately show a large shift toward higher binding energy side relative to the Fermi level. At intermediate doping level, a new state is created in the originally empty energy gap region. From the correspondence with the optical properties, this gap state in the UPS spectra was assigned to the formation of quasi-one-dimensional charged soliton band. This is the first direct observation of photoemission from the charged soliton state in a doped polyacetylene. At the highly doped level (y>0.08), quasi-metallic density of states appears just below the Fermi level and the broadening of the UPS spectra was observed at the region between C 2$p\sigma$- and C 2s-derived states. However, no finite density of states were observed at the Fermi level. The spectral shape of UPS near the Fermi level and the absence of density of ststes at the Fermi level are in accordance with Tomonaga-Luttinger liquid model of strong electron correlated system. *Ab initio* molecular orbital calculation taking account of the interaction of the nearest neighbor chain gave a good description of the experimental results.

Finally, we report the UPS study of poly(pyridine-2,5-diyl) (PPy), poly(2,2'-bipyridine-5,5'-diyl) (PBPy), and their K-doped states. The two compounds show similar spectra and they were analyzed with MO calculations and the comparison with the data of related molecules. The ionization threshold energies of PPy and PBPy were found to be 6.3 and 6.35 eV, respectively. These values are higher than those of π-conjugated conducting polymers capable of p-doping. Upon K doping of PBPy, two new states appear in the originally empty energy gap, and the intensity of the state at 0.65 eV from E_F grows as the doping proceeds. This finding and the change of optical absorption spectra upon doping indicate that bipolaron bands are formed in K-doped PBPy. While

K-doped PPy also shows similar gap states, it needs higher dopant concentration to create bipolaron bands than in the case of K-doped PBPy. The difference of the dependence on dopant concentration between K-doped PPy and K-doped PBPy is discussed based on the conformational difference between these polymers.

1. Introduction

Conjugated polymers have for a long time been of interest to chemists and physicists alike. Especially polyacetylene implies the possibility of metallic conductivity, since the π band delocalized along the chain is half-filled. However, such quasi-one-dimensional system is unstable with respect to dimerization. This is the Peierls $2k_F$ instability [1], in which adjacent CH groups move toward each other, forming alternatively short bonds and long bonds, thereby lowering the energy of the system.

Polyacetylene (PA) was first polymerized by Natta *et al.* [2] in 1958 using a $Ti(OBu)_4$ - $AlEt_3$ catalyst from acetylene monomer. The polymer was an dark colored insulating semicrystalline powder, which was insoluble in any solvent, and decomposes before melting. In 1971, Shirakawa and Ikeda [3] found a method of polymerizing uniform films of PA by using concentrated solutions of Ziegler-Natta catalysts such as the $Ti(OBu)_4$ - $AlEt_3$ system. The produced films, composed of randomly oriented *fibrils* (typical fibril diameter, ca. 200 Å), are flexible and mechanically strong. The infrared absorption spectra of PA film prepared by a low-temperature (-78 °C) polymerization and the film heated after polymerization have been interpreted on the basis of all *cis-transoid* (hereafter we call it *cis*-PA) and all *trans-transoid* (hereafter we call it *trans*-PA) structures [3,4], respectively. The activation energy for the *cis-trans* isomerization was found to be 11 kcal/mol [5].

Interest in π-conjugated polymers have been enhanced greatly in recent years by several important discoveries. The first interesting aspect is that the π-conjugated compounds such as polydiacetylenes [6,7], and PA [8] possess very pronounced nonlinear optical properties, which exceed those of traditional inorganic materials. Another aspect, which constitutes the main subject of this study, is concerned with the fact that a number of intrinsically insulating π-conjugated polymers ($\sigma < 10^{-9}$ Scm^{-1}) can

be converted to be *metallic* by adding small amount of other compounds [9]. This process is often referred to as "*doping*" in analogy with the doping of inorganic semiconductors. The doping process involves chemical or electrochemical exposure of the polymer to electron donors (such as alkaline metals [10]) or acceptors (such as I_2 [10], Br_2 [9], AsF_5 [10], $FeCl_3$ [11], H_2SO_4 [12], ClO_4^- [13], *etc.*). In the terminology of solid state physics, the use of an oxidizing agent corresponds to p-type doping and that of a reducing agent to n-type doping. It leads to the increase in the conductivity by several orders of magnitude for π-conjugated conducting polymers like PA [9], poly(*p*-phenylene) (PPP) [14,15], various poly(*p*-phenylene calcogenides), polythiophene, polyaniline, and polypyrrole [16]. Note that the maximum dopant concentrations, which can be achieved by the process mentioned avove, are typically of the order of several mole percent per repeat unit of the polymer chain backbone, for instance up to 20 % in the case of PA doped by iodine, $(CHI_{0.2})_x$.

The electronic structure of conducting polymers have been explained by assuming doped structures such as soliton [17,18], polaron, and bipolaron [19]. The doped PA exhibits the charged soliton structure [17]. Undoped PA possesses twofold-degenerate ground states. The elementary process of doping is expected to be polaron formation, since the creation energy of a polaron is smaller than half of the energy of a soliton-antisoliton pair [20]. As the doping proceeds and the density of polarons increases, two polarons combine to form a pair of a charged soliton and a charged antisoliton, because of the attractive interaction between polarons, which has been discussed theoretically [19(b),21,22].

In lightly doped regime ($0<y<0.02$), the charged soliton structure is suggested to be predominant [23], and the phonon-assisted electron hopping process between soliton

bound states is expected to be the dominant conduction mechanism [24]. From the infrared absorption spectra of thin PA films, some characteristic peaks are observed at 1440-, 1370-, 1280-, 1030-, 870-, and 536 cm^{-1} [23, 25-29]. The energy and intensity of doping-induced infrared peaks are independent of dopant species, indicating that these bands are intrinsic to doped films. Mele and Rice [30] have suggested that these peaks are explained by the lattice dynamics calculations for the long chain containing a soliton using the force field model. They have claimed that a pinning mode of the carrier should exist at 300 ~ 500 cm^{-1}.

In heavy doping level ($0.06<y$), PA shows several indication of metallic states, such as the temperature-independent magnetic susceptibility [31], the metallic thermopower [32], and the metallic reflectance in far-infrared region [33]. These results suggest that free carriers are produced. The detailed nature of this free carrier, however, has not been clarified yet.

Other polymers, such as PPP, have nondegenerate ground state, in which solitons cannot be created. However, they can and apparently do, the doubly charged polarons (bipolarons) have been proposed as the spinless charge carriers in such systems. The bipolaron is defined as a pair of like charges associated with a strong local lattice distortion [19]. The bipolaron structure possesses the totally filled valence band and is not applicable for electrical conduction, However, PPP shows fairly high conductivity [14] as in the case of PA, and has unusual Pauli susceptibility [34] at heavily doped levels.

In 1987, Naarmann and Theophilou developed a new technique of PA polymerization by ageing the the Ziegler-Natta catalyst and performing polymerization in a viscous medium (*e.g.* silicone oil) [35]. In 1990 Tsukamoto *et al.* also succeeded in

improving the polymerization technique of acetylene by modifying the conventional Shirakawa- method [36]. These new-type polyacetylenes show higher conductivity than that of traditional Shirakawa-polyacetylene (S-PA). This highly conductive polyacetylene (HCPA) made by the new catalyst has a higher density (1.15 g/cm^3) and a larger maximum possible elongation ratio ($l/l_0 \sim 10$) than those of S-PA [3,32]. The conductivities of HCPA are reported to exceed 10^5 Scm^{-1}. The Pauli susceptibility for heavily iodine doped HCPA is much larger than those of S-PA [37], and is also larger than that by the one-electron band calculation without considering solitons and dimerization [38]. However, the electronic structures of doped state as well as the conduction mechanism are still open questions.

The concept of the combination of the several optical and electrical measurements is very important for understanding the changes of the electronic structure upon doping. The optical spectroscopy provides the important information on the electronic and molecular structure of the polymer chain. The electrical conductivity measurements are expected to have characteristics of the conduction mechanism of the conducting polymers. Moreover, the ultraviolet photoelectron spectroscopy (UPS) of conducting polymers have provided useful information for the valence electronic structures and electronic interaction.

In this work, we have studied the electronic structures and electrical properties of doped conducting polymers by the combination of several spectroscopical and electrical measurements. In the following chapters 2 and 3 we present the changes of the electronic structure and electrical properties of doped HCPA by the combination of the polarised reflection, temperature dependence of the conductivity measurements. So far, the UPS studies in the past have been carried out mainly p-doped conducting polymers, and n-

doped states are still limited. In chapter 4 and 5 we present the UPS study of HCPA, poly(2,5-pyridinediyl), poly(2,2'-bipyridine-5,5'-diyl), and their n-doped states.

In chapter 2 we present the study of the polarized reflection spectra of perchlorate-doped HCPA film from far-infrared to ultraviolet (80 - 30000 cm^{-1}) regions. The optical conductivity spectra are calculated by the Kramers-Kronig transformation of the polarized reflection spectra, and they are analyzed by a simple harmonic oscillator model assuming several fundamental excitations. Anisotropy of conductivity is expected in the oriented film, so the optical study with a polarized light will be helpful in analyzing the electronic structure of the doped polymers. So far only a few studies have been reported on the orientational effect of the electronic structure of the conducting polymers [39,40]. The change of the electronic structure will be discussed based on the spectra at several doping levels. Comparison will be made with the results of iodine-doped S-PA [33] and HCPA [41] films. We will also discuss the orientational effect on the polarized spectra in connection with the electronic structure and conduction mechanism of doped HCPA.

In chapter 3 we present the study of the temperature dependence of electrical conductivity of HCPA made by Tsukamoto's method [36] doped with perchlorate ion. The electrical conductivities along the directions parallel and the perpendicular to the stretching direction were measured from 290 to 1.5 K. The observed temperature dependence and anisotropy of conductivity were analyzed by assuming that it is the sum of two terms; one is almost temperature independent term and the other is Mott's three-dimensional variable range hopping conduction [42]. We will discuss the effect of orientation on the conductivity and the temperature dependence of the conductivity in connection with the conduction mechanism.

In chapter 4 we present the ultraviolet photoelectron spectric study of alkaline-metal doped HCPA. In our previous study of UPS spectra of perchlorate-doped HCPA [43], we reported a finite density of states at Fermi level in the heavily doped regime, but the intensity of the band is rather weak compared to other three-dimensional metals. In this work, we report UPS studies of Na- and K- doped HCPA, and discuss their electronic structures using the observed results. Analysis of the observed spectra were carried out with the aid of *ab initio* molecular orbital calculations [44] of the energy levels of alkaline-metal doped model compounds of polyacetylene.

Finally, in chapter 5 we present the UPS study of poly(pyridine-2,5-diyl), poly(2,2'-bipyridine-5,5'-diyl), and their potassium doped states. Recently Yamamoto *et al.* have found that poly(pyridine-2,5-diyl) (PPy) and poly(2,2'-bipyridine-5,5'-diyl) (PBPy), that have analogous structures with PPP, exhibit n-type electrically conducting properties [45]. In this work, we report UPS studies of PPy, PBPy, and their K-doped states, and discuss their electronic structures using the observed results. Analysis of the observed spectra were carried out with the aid of semiemperical PM3 molecular orbital calculations [46,47], and also by comparison with other related molecules and conducting poly(arylene)s. The changes in the electronic structure of PPy and PBPy upon *in situ* K-doping was also studied by UPS and optical absorption spectra. The origin of the new bands appearing in the observed spectra were discussed by the comparison with reported data for poly(*p*-phenylenevinylene) [48].

The results obtained through these studies give deeper insights into the doping mechanism, the changes in the electronic structure of the polymers induced by doping, and the conduction mechanism of doped conducting polymers.

References

[1] R.E.Peierls, "Quantum Theory of Solids", Oxford University Press, London, 1955.

[2] G.Natta, G.Mazzanti, and P.Corradini, *J. Polym. Sci.*, **25**, 3 (1958).

[3] H.Shirakawa and S.Ikeda, *Polym. J.*, **2**, 231 (1971).

[4] T.Ito, H.Shirakawa, and S.Ikeda, *J. Polym. Sci. Polym. Chem. Edn.*, **13**, 1943 (1975).

[5] M.Tanaka, H.Yasuda, and J.Tanaka, *Bull. Chem. Soc. Jpn.*, **55**, 3639 (1982).

[6] C.Sauteret, J.P.Hermann, R.Frey, F.Pradère, J.Ducuing, R.H.Baughman, and R.R.Chance, *Phys. Rev. Lett.*, **36**, 956 (1976).

[7] F.Kajzar, J.Messier, J.Zyss, and I.Ledoux, *Opt. Commun.*, **45**, 133 (1983).

[8] J.P.Hermann and J.Ducuing, *J.Appl. Phys.*, **45**, 5100 (1974).

[9] H.Shirakawa, E.J.Louis, A.G.MacDiarmid, C.K.Chiang, and A.J.Heeger, *J. Chem. Soc. Chem. Commun.*, 578 (1977).

[10] C.K.Chiang, M.A.Druy, S.C.Gau, A.J.Heeger, E.J.Louis, A.G.MacDiarmid, Y.W.Park, and H.Shirakawa, *J. Am. Chem. Soc.*, **100**, 1013 (1987).

[11] H.Sakai, Y.Maeda, T.Kobayashi, and H.Shirakawa, *Bull, Chem. Soc. Jpn.*, **56**, 1616 (1983).

[12] H.Shirakawa, M.Kobayashi, and S.Ikeda, *Polym. Preprints, Japan*, **28**, 463 (1979).

[13] J.LReynolds, J.C.W.Chien, F.E.Karasz, C.P.Lillya, and D.J.Curran, *J. Chem. Soc. Chem. Commun.*, 1358 (1982).

[14] D.M.Ivory, G.G.Miller, J.M.Sowa, L.W.Shacklette, R.R.Chance, and R.H.Baughman, *J. Chem. Phys.*, **71**, 1506 (1979).

[15] L.W.Shacklette, H.Eckhardt, R.R.Chance, G.G.Miller, D.M.Ivory, and R.H.Baughman, *J. Chem. Phys.*, **73**, 4098 (1980).

[16] A.F.Diaz, K.K.Kanazawa, and G.P.Gardini, *J. Chem. Soc. Chem. Commun.*, 635 (1979).

[17] N.J.Zabusky and M.D.Kruskal, *Phys. Rev. Lett.*, **15**, 240 (1965).

[18] W.-P.Su, J.R.Schrieffer, and A.J.Heeger, *Phys. Rev. Lett.*, **42**, 1698 (1979).; W.-P.Su, J.R.Schrieffer, and A.J.Heeger, *Phys. Rev. B*, **22**, 2099 (1980).

[19] (a) J.L.Brédas, B.Themans, J.M.Andre, R.R.Chance, D.S.Boudreaux, and R.Silbey, *J. Phys. (Paris)*, **44**, 373 (1983).; (b) J.L.Brédas, R.R.Chance, and R.Silbey, *Mol. Cryst. Liq. Cryst.*, 77, 319 (1981).

[20] D.K.Campbell and A.R.Bishop, *Phys. Rev. B*, **24**, 4859 (1981).

[21] J.L.Brédas, R.R.Chance, and R.Silbey, *Phys. Rev. B*, **26**, 5843 (1982).

[22] Y.Onodera and S.Okuno, *J. Phys. Soc. Jpn.*, **52**, 2478 (1983).

[23] M.Tanaka, H.Fujimoto, and J.Tanaka, *Mol. Cryst. Liq. Cryst.*, **83**, 75 (1982).

[24] S.Kivelson, *Phys. Rev. B*, **25**, 3798 (1982).

[25] M.Tanaka, A.Watanabe, and J.Tanaka, *Bull. Chem. Soc. Jpn.*, **53**, 645 (1980).

[26] M.Tanaka, H.Fujimoto, and J.Tanaka, *Mol. Cryst. Liq. Cryst.*, **83**, 1107 (1982).

[27] H.Fujimoto, M.Tanaka, and J.Tanaka, Bull. Chem. Soc. Jpn., 56, 671 (1983).

[28] I.Harada, Y.Furukawa, M.Tasumi, H.Shirakawa, and S.Ikeda, *J. Chem. Phys.*, **73**, 4746 (1980).

[29] A.J.Heeger, S.Kivelson, J.R.Schrieffer, and W.-P.Su, *Rev. Modern Phys.*, **60**, 781 (1988).

[30] E.J.Mele and M.J.Rice, *Phys. Rev. Lett.*, **45**, 926 (1980).; E.J.Mele, *Mol. Cryst. Liq. Cryst.*, 77, 25 (1981).; S.Etemad, A.Pron, A.J.Heeger, A.G.MacDiarmid, E.J.Mele, and M.J.Rice, *Phys. Rev. B*, **23**, 5137 (1981).

[31] J.Chen, T.C.Chung, F.Moraes, and A.J.Heeger, *Solid State Commun.*, **53**, 757 (1985).

[32] Y.W.Park, A.J.Heeger, M.A.Druy, and A.G.MacDiarmid, *J. Chem. Phys.*, **73**, 946 (1980).

[33] K.Kamiya and J.Tanaka, *Synth. Met.*, **25**, 59 (1988).

[34] M.Peo, S.Roth, K.Dransfeld, B.Tieke, J.Hocker, H.Gross, A.Grupp, and H.Sixl, *Solid State Commun.*, **35**, 119 (1980).

[35] H.Naarmann and N.Theophilou, *Synth. Met.*, **25**, 1 (1987).

[36] J.Tsukamoto, A.Takahashi, and K.Kawasaki, *Jpn. J. Appl. Phys.*, **29**, 125 (1990).

[37] Y.Nogami, H.Kaneko, T.Ishiguro, N.Hosoito, J.Tsukamoto, and A.Takahashi, *Synth. Met.*, **41-43**, 117 (1991).

[38] P.M.Grant and I.P.Batra, *Solid State Commun.*, **29**, 225 (1979).

[39] Y.W.Park, M.A.Druy, C.K.Chiang, A.G.MacDiarmid, A.J.Heeger, H.Shirakawa, and S.Ikeda, *J. Polym. Sci. Polym. Lett. Edn.*, **17**, 195 (1979).

[40] Y.Cao, P.Smith, and A.J.Heeger, *Synth. Met.*, **41-43**, 181 (1991).

[41] S.Hasegawa, M.Oku, M.Shimizu, and J.Tanaka, *Synth. Met.*, **38**, 37 (1990).

[42] N.F.Mott and E.A.Davis, "Electronic Processes in Non-Crystalline Materials", Oxford University Press, 2nd ed., London, 1979.

[43] K.Kamiya, M.Oku, T.Miyamae, K.Seki, H.Inokuchi, C.Tanaka, and J.Tanaka, to be published.

[44] M.J.Frish *et al.*, *Gaussian 92*, Gaussian Inc., Pittsburgh, PA, 1992.

[45] T.Yamamoto, *Prog. Polym. Sci.*, 7, 1153 (1992).

[46] J.J.P.Stewart, *J. Comput. Chem.*, **10**, 209 (1989).

[47] J.J.P.Stewart, *J. Comput. Chem.*, **10**, 221 (1989).

[48] M.Fahlman, D.Beljonne, M.Lögdlund, R.H.Friend, A.B.Holmes, J.L.Brédas, and W.R.Saraneck, *Chem. Phys. Lett.*, **214**, 327 (1993).

2. Polarized Reflection Spectra of Perchlorate-Doped Oriented Polyacetylene

2.1 Introduction

In this chapter we present the study of the polarized reflection spectra of perchlorate-doped highly conducting polyacetylene (HCPA) film from far-infrared to ultraviolet (80 - 30000 cm^{-1}) regions. Perchlorate ion is a suitable acceptor for such spectral studies, since it has no conspicuous absorption band in the visible or near-infrared region. The optical conductivity spectra are calculated by the Kramers-Kronig transformation of the polarized reflection spectra [1]. The conductivity spectra are analyzed by a simple harmonic oscillator model assuming several fundamental excitations. In HCPA, the polymer chain can be ordered by stretching to a higher degree than in the case of S-PA and the interfibril contact may be increased. Anisotropy of conductivity is expected in the oriented film, so the optical study with a polarized light will be helpful in analyzing the electronic structure of the doped polymers. Only a few studies have been presented on the orientational effect of the electronic structure of conducting polymer [2]. In our previous optical study on the iodine-doped oriented HCPA [3], we found the change of polarized reflection spectra with the level of doping. The transition to metallic state has been found at a particular dopant concentration. The optical conductivity spectra of iodine-doped HCPA showed that the free carriers with fairly long lifetime (~10^{-13} s) are formed in the heavily doped HCPA [3].

We have actually observed corresponding anisotropy of the spectra and also the change of the reflection spectra by the level of doping. The change of the electronic structure will be discussed based on the spectra observed at several doping levels. Comparison will be made with the results of iodine-doped S-PA [4] and HCPA [3] films.

We will also discuss the effect of stretching on the polarized spectra in connection with the electronic structure and conduction mechanism of doped polyacetylene.

2.2 Experimental

2.2.1 Preparation of Highly Conductive Oriented Polyacetylene Films

The polymerization catalyst was prepared according to the technique described by Tsukamoto *et al.* [5] The films were polymerized on a glass plate with the catalyst on it; this was placed in a glove box as shown in Fig. 1, where argon gas was circulated through the purification system that can keep oxygen and water contents below 1.0 ppm [6]. The catalyst was cast with uniform thickness of 10 μm on a glass plate by using Doctor Brade (Type YD-2, Yoshimitsu Seiki Co., Ltd.). Acetylene gas of six-nine grade was passed over catalyst at -10 °C at low pressure of 250 Torr (1 Torr = 133.32 Pa). The synthesized films were washed 7 times or more with distilled toluene in a specially designed self-washed Soxhlet's type extracting system as shown in Fig. 2. After washing, the films were uniaxially stretched by hands inside the glove box with stretching ratio of 5 ~ 10, and dried *in vacuo* for several hours. The typical thickness of the stretched film was around 1 μm.

2.2.2 Perchlorate Doping and DC Conductivity Measurements

The perchlorate-doping was carried out in acetonitrile solution of copper (II) perchlorate. Twenty-five grams of copper (II) perchlorate hexahydrate ($Cu(ClO_4)_2 \cdot$

$6H_2O$, Nacalai tesque) was dissolved in 500 ml distilled acetonitrile with 200 grams of molecular sieve 4A. The solution was stirred for one night and filtered, then acetonitrile was evaporated with a vacuum pump. The dried copper (II) perchlorate was dissolved in anhydrous acetonitrile (0.005 - 0.1 M, 1 M = 1 mol dm^{-3}). Polyacetylene film was immersed in the solution; the immersion time was varied from 1 minute to 2 hours, for light to heavy doping. After doping, the films were washed 5 times or more with acetonitrile, and dried *in vacuo*. The doping levels were determined from the weight uptake. The doping process was carried out under Ar atmosphere. The dc conductivity was measured by standard four probe method applying a mechanical contact between the film and platinum leads in the glove box as shown in Fig. 3.

2.2.3 Reflection Measurements of Perchlorate-Doped Polyacetylene

The reflection spectra were measured by a normal incidence setup, using three microspectrophotometers specially designed in this laboratory. The first is a far-infrared (far-IR) spectrophotometer consisted of a JASCO Michelson-type interferometer with a Mylar beam splitter (each 3 μm, 9 μm, or 25 μm thick were used) and a high pressure mercury lamp. A large-aperture reflecting type objective lens was used to collect feeble far-IR radiation reflected from the sample. All apparatuses were contained in a vacuum box and a polyethylene window was used as the exit slit leading to the detector. Liquid He cooled Si bolometer (Infrared Laboratory Ltd.) was used as the far-IR detector. This system covers wavenumber range of 30 — 650 cm^{-1}. Since the sample doped with perchlorate was sensitive to air, we treated it under argon atmosphere and under the vacuum condition during the far-IR measurements.

The second is the infrared (IR) microspectrometer, which was constructed using another JASCO Michelson-type interferometer with a KBr beam splitter, an Olympus

microscope with an Ealing objective, a siliconit light source, and an infrared detector of HgCdTe. This system covers the region of 500 — 5000 cm^{-1}.

For the measurements in the near-IR, visible and ultraviolet regions (3200 — 25000 cm^{-1}), we used the third microspectrophotometer which was made by the combination of a Carl-Zeiss double monochromator, an Olympus microscope with a Carl-Zeiss Ultrafluar objective lens, and a PbS detector and R928 photomultiplier (Hamamatsu Photonics).

Wire grid polarizers on KRS-5 plate and polyethylene plate were used as the polarized reflection measurements in the far-IR and IR regions. A MgF_2 prism was used as the polarizer in the near-IR, visible, and ultraviolet regions. The HCPA films were mounted on a universal stage to keep the surface normal to the incident beam. For obtaining the absolute value of reflectivity, calibration with standards is necessary. A gold mirror was used as reference in the far-IR and IR measurements and a SiC mirror was used for standard in the near-IR, visible, and ultraviolet measurements.

2.3 Results and Discussion

2.3.1 DC Conductivity

Figure 4 shows the relation between the dopant concentration y of $[CH(ClO_4)_y]_x$ and the dc conductivity at room-temperature for the direction parallel to the stretching direction ($\sigma_{//}$). The values of dc conductivity of perchlorate-doped HCPA were about two orders of magnitude larger than that of S-PA, but the relation of the conductivity to dopant concentration was found to be similar to that for the perchlorate-doped S-PA [7,8]. In the region for $0 < y < 0.02$ (light doping), $\sigma_{//}$ increased rapidly to the level of

10^3 Scm^{-1}. In the region for $0.02 < y < 0.04$ (intermediately doping), the conductivity increased gradually from 2×10^3 to 10^4 Scm^{-1}. Finally, in the region of $y > 0.045$ (heavy doping), the conductivity saturated and the maximum value was dependent on the sample quality. The highest conductivity we obtained for the perchlorate-doped HCPA was $\sigma_{//} = 3 \times 10^4$ Scm^{-1}.

2.3.2 Reflection Spectra

Figure 5 shows the polarized reflection spectra taken with the electric vector of incident light parallel and perpendicular to the stretching direction of perchlorate-doped HCPA films, $[CH(ClO_4)_y]_x$. The data are shown for undoped and three different dopant concentrations which correspond to the three doping stages noted in the preceding section. The reflectance of the lightly ($y = 0.013$) and intermediately ($y = 0.036$) doped films were lower than those of the heavily doped film ($y = 0.045$) for the whole measured region. The reflection spectrum of undoped film exhibited a peak at 17000 cm^{-1}, which is characteristic of the interband transition of polyacetylene. In the lightly doped film, the intensity of this peak decreased and a new broad band appeared in the near infrared region at 5000 cm^{-1} (band No. 6) and a sharp one at 1360 cm^{-1} (band No. 4). In the heavily doped film, the spectrum for the parallel direction exhibited a high reflectance reaching nearly 100 percent in the far-IR region (band No. 0) and a broad band at around 400 cm^{-1} (band No. 1). Along the perpendicular direction, sharp peaks are found at 1030 cm^{-1} and 1120 cm^{-1}. According to the theoretical calculations [9] based on the comtinuum model of Takayama, Lin-Liu, and Maki [10], the former one is due to one of the soliton bound modes. The latter peak is due to the bending mode of perchlorate. In spite of difference in the dc conductivity, the reflection spectra of further doped films, $y = 0.068$ ($\sigma_{//} = 11200$ Scm^{-1}), $y = 0.102$ ($\sigma_{//} = 28700$ Scm^{-1}) and $y = 0.132$ ($\sigma_{//} = 6600$ Scm^{-1}), have intensities and positions of peaks similar to those for the

curve of $y = 0.045$ over the whole measured region within measurement error. This behavior is in good correspondence with the result of the dc conductivity shown in Fig. 4.

2.3.3 Optical Conductivity and Simple Harmonic Oscillator Model

The Kramers-Kronig transformation of the reflection spectra were performed to obtain the optical conductivity spectra, $\sigma(\omega)$. The calculated results are shown in Fig. 6. The optical conductivity spectra $\sigma(\omega)$ in c.g.s units are given by the imaginary part of the dielectric function, $\varepsilon_2(\omega)$ as

$$\sigma(\omega) = \frac{\omega}{4\pi}\varepsilon_2(\omega) \qquad (2.1)$$

When we assume that a spectrum consists of independent contribution of each harmonic oscillators (simple harmonic oscillator model), the dielectric function $\varepsilon(\omega)$ is given by [1]

$$\varepsilon(\omega) \equiv \varepsilon_1(\omega) + i\varepsilon_2(\omega) , \qquad (2.2)$$

$$= \varepsilon_\infty + \sum_{j=0}^{7} \frac{\Omega_j\left[(\omega_j^2 - \omega^2) + i\omega\gamma_j\right]}{(\omega_j^2 - \omega^2)^2 + \omega^2\gamma_j^2} , \qquad (2.3)$$

$$\Omega_j^2 = \frac{4\pi f_j N e^2}{m_e} , \qquad (2.4)$$

where ω_j, γ_j and f_j are the resonance frequency, the band width, and the oscillator strength of the j-th transition, respectively. N is the number of species for the transition per unit volume and m_e is the mass of an electron. We assumed that seven transitions and free carrier form each spectrum. Then $\sigma(\omega)$ is given by

$$\sigma(\omega) = \sum_{j=0}^{7} \frac{\Omega_j^2 \omega^2 \gamma_j}{4\pi[(\omega_j^2 - \omega^2)^2 + \omega^2\gamma_j^2]}, \qquad (2.5)$$

$$\equiv \frac{\sigma_0^{opt}\gamma_0^2}{\omega^2+\gamma_0^2}+\sum_{j=1}^{7}\frac{\Omega_j^2\omega^2\gamma_j}{4\pi[(\omega_j^2-\omega^2)^2+\omega^2\gamma_j^2]}, \tag{2.6}$$

$$\sigma_0^{opt} \equiv \frac{\Omega_0^2}{4\pi\gamma_0}=\frac{\Omega_0^2\tau_0}{4\pi}, \tag{2.7}$$

$$\Omega_0^2=\frac{4\pi N_0 e^2}{m^*}, \tag{2.8}$$

where the first term of Eqn. (2.6) is the contribution from a free carrier, τ_0 is the lifetime of free carrier related to the scattering rate by $\gamma_0 = 1/\tau_0$, N_0 is the number of free carriers per unit volume, and m^* is the effective mass, which is assumed to be the same as m_e in this analysis. By using Eqs. (2.2) - (2.8), the optical conductivity and dielectric function spectra were simulated by fitting parameters such as ε_∞, Ω_j, ω_j, f_j, and γ_j of each transition. The values of N_0 are estimated from the fitting of $\sigma(\omega)$ in the far-infrared region and are listed in Table 1. In this analysis, the values of f_j (j = 1 to 6) were obtained using $N = n_{cs} \times N_\pi$ for the film $y > n_{cs}$, where n_{cs} is the dopant concentration [3,4] in the heavily doped region and N_π is the number of carbon $2p\pi$ electron in unit volume. The value of n_{cs} is taken as 0.025. For $y < n_{cs}$, $N = y \times N_\pi$ was assumed. Since the origin of the band No. 7 is the interband transition of polyacetylene, as described below the values of f_7 was taken as $N = N_\pi$.

2.3.4 Changes of Spectra with Doping

In Fig. 6 we show the optical conductivity spectra of films for (a) y = 0.013, (b) y = 0.036, and (c) y = 0.045 by the solid lines for the direction parallel to the stretching direction. The optical conductivity increases with the dopant concentration, particularly in the far infrared region. At a low doping level of y = 0.013, the dc conductivity was 1900 Scm^{-1}. It increases to 4450 Scm^{-1} at y = 0.036 and reaches a maximum value of

22000 Scm^{-1} at $y = 0.045$. The growing of the dc conductivity is intimately connected with the enhancement of the far infrared optical conductivity.

The dashed lines in Fig. 6 illustrate the fitted spectra by a simple harmonic oscillator model and the broken lines denote the contributions of each transition numbered from 0 to 7. The parameters for the fitting are shown in Table 1. In the table, we also showed the transition moments of each band, $\langle r_j \rangle$, calculated by the following equation.

$$\langle r_j \rangle^2 = \frac{\hbar}{2m_e\omega_j} f_j = \frac{f_j}{3.255\times10^5 \times \omega_j}, \tag{2.9}$$

where $\langle r_j \rangle$ is given in Å and ω_j in cm^{-1}. In the near infrared region, better fitting curves than the previous analysis [3] are obtained by considering two transitions, Nos. 5 and 6. They are at about 2000 cm^{-1} (No. 5) and 6000 cm^{-1} (No. 6), respectively. Besides these strong bands, a broad band around 400 cm^{-1} (No. 1) and a small sharp peak at 1360 cm^{-1} (No. 4) were found. We have proposed that this band No. 4 can be assigned to the characteristic C-H bending modes of the charged soliton structure. In the structural model of the charged soliton, it was proposed that the odd-numbered CH chains are coordinated by a dopant [11,12].

In the lightly doped film of $y = 0.013$, the bands of 6000 cm^{-1} (No. 6) and 1360 cm^{-1} (No. 4) were predominant, as shown in Fig. 6(a). In the initial stage of doping, a measurable conductivity appeared. Yang *et al.* showed that the doped film is diamagnetic at this concentration range [8]; their result is consistent with the result that the charged soliton structure, which is diamagnetic, is predominant at $y < 0.02$. The metallic state is not yet realized in the doping levels of $y < 0.02$.

From the intensity of the visible band, the content of the undoped region can be estimated. The doped region is thus evaluated to be 67 percent of the total chain at $y = 0.013$. We assume that the perchlorate-doped polyacetylene has a similar structure to the iodine doped film of $(UP)_n$ structure (Fig. 7(b)) proposed by Baughman's group [13].

Here the U layer is comprised of only undoped polyacetylene chain and the P layer is partially filled with perchlorate ions. Then each unit cell includes three chains, so that one of the three chains remains undoped at this concentration. This argument is consistent with the previous studies on Na-doped S-PA [14,15], iodine-doped S-PA [4] and perchlorate-doped S-PA [8]. The number of carbon atoms per dopant is found to be 51 carbon of the atoms in the two doped chains. This result shows that each dopant in the charged soliton chain influences over a fairly long distance.

By increasing the doping level to $y = 0.036$, the conductivity increased to $\sigma_{//} = 4450$ Scm^{-1}, and two new bands appeared at 400 cm^{-1} (No. 1) and 2000 cm^{-1} (No. 5) (Fig. 6(b)). They are indications that a new species is produced, and we have proposed that this new species is polson [11], which consists of an odd numbered CH chain coordinated by two dopants from the same side. According to the theoretical calculations [11], the polson structure has an electronically excited state at 2000 cm^{-1} and vibrational modes at about 600 cm^{-1} regions. At $y = 0.036$ (Fig. 6(b)), the undoped part of the chain is evaluated to be 33 percent, which is estimated from the intensity of 16000 cm^{-1} band. If we assume $(UP)_n$ structure at $y = 0.036$ (Fig. 7(b)), one third of polyacetylene chain is undoped, and another chain has a polson structure: the unit is composed of 23 carbon atoms, and the third chain has a charged soliton structure.

Band No. 1 has been assigned to the pinned mode of the free carrier. Woo *et al.* [16] observed a strong broad band at around 400 cm^{-1} in the iodine-doped HCPA and its intensity increased with decreasing temperature. They attributed this to the pinning of the free carrier. From the present analysis, the intensity of the free carrier band (No. 0) was transferred to band No. 1 (f_1) by lowering temperature.

By further doping to $y = 0.045$ (Fig. 6(c)), the optical conductivity increases steeply $\omega \to 0$; it indicates that the number of the free carriers increased significantly, which is consistent with the increased dc conductivity (2.2×10^4 Scm^{-1}). A similar feature was shown by Leising in AsF_5-doped polyacetylene synthesized by Durham-route

[17]. Above $y > 0.045$, the undoped chains become less than 20 percent. Accordingly, we can consider that the metallic property appears when more than 80 percent of the chains are doped to form polson chains. The number of carbon atoms per dopant is 9.5, if we assume that the polson is formed on two of five polyacetylene chains in $(UPUF)_n$ structure in the Baughman's model (Fig. 7(c)) [13]. Here the F layer denotes completely filled chain with perchlorate ions. These results indicate that the metallic state is realized when a polson lattice is formed on two-fifths of the polyacetylene chain in $(UPUF)_n$ lattice. Moreover, the dc conductivity reaches a maximum value at this level and saturates above this doping level.

We previously showed by the UPS spectra that finite density of states appears at the Fermi level in the heavily perchlorate-doped HCPA, at the conductivity level of more than 10^4 Scm^{-1} [18]. The appearance of a strong free carrier band in the far infrared region and the high dc conductivity are consistent with the results of UPS spectra.

The rapid increase of $\sigma(\omega)$ in the far-IR region with incerasing doping also indicates that the free carriers have a long lifetime of $\tau_0 \sim 1.5 \times 10^{-13}$ s. This value obtained using a simple harmonic oscillator model (Table 1). The threshold energy of a free carrier band near $\omega \approx 100$ cm^{-1} means a small half-bandwidth (γ_0). This result indicates that the free carriers have a long lifetime ($\tau_0 = 1/\gamma_0$). Following the Drude theory, the dc conductivity (σ_0) is described by the number of free carriers (N_0) and their lifetime (τ_0), as follows:

$$\sigma_0 = \frac{N_0 e^2 \tau_0}{m^*} . \qquad (2.10)$$

The high conductivity of HCPA at $y > 0.045$ is correlated to the increased N_0 and long lifetime τ_0. This result is in good agreement with the previous one on the iodine-doped HCPA [3]. The number of carbon $2p\pi$ electrons in a unit volume of polyacetylene is 4.6 $\times 10^{22}$ cm^3. Assuming $m^* = m_e$, the number of free carriers (N_0) at $y = 0.045$ is 6.63 $\times$ 10^{20} cm^3 (Table 1) and it increases to 1.43 $\times 10^{21}$ cm^3 at the final stage of doping with y

= 0.136. These numbers show that one free carrier is formed for about 30 carbon atoms. Infact, the value N_0 may be increased by a facter of m^*/m_e and the number of carbon atoms for the free carrier may be reduced by the same factor. Anyway, the heavily doped polyacetylene is characterized as a system with a small number of free carriers with long lifetime.

In Fig. 8, the intensity for each band is compared by the ratio of oscillator strengths at different dopant content, where the oscillator strengths (f_j) are calibrated by the values of lightly doped film of $y = 0.013$, where the charged soliton is the main product. From Fig. 8, the transitions are classified into three types. First, the f_4 and f_6 of the charged soliton remain constant even with the increase of dopant; this shows that the content of the charged soliton is constant for all dopant level of $y > 0.013$. The strengths of the bands No. 1 and 0 show a rapid increase with y above $y = 0.036$, like the rise of the dc conductivity. Both the band (No. 0) and the far-IR band (No. 1) shows strong correlation with the dc conductivity, and are assigned to the excitation of free carriers. These bands are enhanced by stretching with the increase of the interfibril contact. On the other hand, the oscillator strengths of the bands 2 and 5 are enhanced at $y = 0.036$, and stay constant above this level. The intensities of these bands increases at $y = 0.036$ along with N_0 and f_1. This shows good correlation with the formation of polson chains deduced from other experiments, and the band Nos. 5 and 2 can be assigned to excitations in the polson unit. Above $y > 0.045$, many polson chains are formed and the inter-polson chain interaction should be enhanced because more than two polyacetylene chains in the $(UPUF)_n$ structure are transformed to polson chains. The increase of conductivity may be correlated with the interaction between the polson chains between neighboring chains.

If we assume $(UPUF)_n$ structure at $y = 0.045$ (Fig. 7(c)), the fraction of the undoped part is evaluated from the intensity of the 16000 cm^{-1} band to be 20 percent, indicating that four-fifths of the $(UPUF)_n$ chains are doped. Furthermore, if we assume

that half of the doped chains have a polson structure, each polson, which has two dopants, is comprised of 21 carbon atoms. For constructing a polson structure, at least thirteen carbon atoms are required. Thus we can rationalize that further increase of conductivity can be achieved to the level of $y = 0.136$ by increasing the dopant content [19].

2.3.5 Anisotropy of Spectra

In Fig. 9 we show the optical conductivity spectra for the case where electric vector of light is perpendicular to the stretching direction at (a) $y = 0.013$, (b) $y = 0.036$ and (c) $y = 0.045$. The parameters obtained from the fitting by simple harmonic oscillator model are shown in Table 2.

From the optical conductivity spectra of $y = 0.045$ (Figs. 6(c) and 9(c)), the dichroic ratios of each band, f_1 (390 cm^{-1}), f_2 (700 cm^{-1}), f_4, (1360 cm^{-1}) and f_5+f_6, found to be 35:1, 7:1, 13:1 and 2.5:1, respectively. To compare with the previous study of iodine-doped HCPA [3], we have to combine bands No. 5 and No. 6. It shows that the dichroic ratios of these bands have almost the same ratios as those for iodine-doped HCPA [3]. In the heavily iodine doped sample $(CHI_{0.16})_x$, the corresponding ratios were 38:1, 10:1, 6.3:1 and 3:1, respectively.

The difference in dichroic ratios among these bands gives an insight into the nature of the transitions. Band No. 1 is more significantly polarized to the elongated direction than the bands 2 and 4. The dichroic ratio of the free carrier band 0 is 26:1, which is comparable to that of band No. 1. The dichroic ratios of the bands 5 and 6 are 7.5:1 and 1.8:1, respectively. The dichroic ratio of the bands 4 and 5 show almost the same value (13:1), the charged soliton mid-gap band (No. 6) has a small dichroic ratio.

These results indicate that the transition dipole moment of the charged soliton mid-gap band may be inclined to the chain axis.

2.3.6 Effect of Stretching on the Reflection Spectra

Figure 10 shows the polarized reflection spectra for three films of different drawing ratio (l/l_0), which were heavily doped to saturation level after drawing. The curves (a) and (d) are parallel and perpendicularly polarized reflection spectra of the draw ratio 8 (y = 0.136, σ_0 = 22300 Scm^{-1}), while curves (b) and (e) are those of the draw ratio 4 (y = 0.045, σ_0 = 22000 Scm^{-1}). The spectrum of unstretched heavily doped film is also shown as curve (c).

The effect of drawing on electrical conductivity of polyacetylene has been studied by many groups, and it has been established that the conductivity is increased by drawing [2,21]. The optical conductivity spectra (Fig. 11) clearly show that the far-IR optical conductivity increases by drawing in both stretched films, and the conductivity is larger for the more stretched film. The number of free carriers in the stretched (draw ratio l/l_0 ~ 4) and unstretched HCPA (y = 0.062, σ_0 = 2000 Scm^{-1}) are 6.6×10^{20} and 1.6×10^{21} cm^{-3}, respectively. The value for the unstretched perchlorate-doped S-PA [8] (y = 0.061, σ_0 = 700 Scm^{-1}) was 6.1×10^{20} cm^{-3} , which is estimated from $N_f = (n - n_{cs})N_\pi$, where n is the dopant content. The lifetimes of the free carriers estimated from simple harmonic oscillator model were 1.50×10^{-13} s for stretched HCPA, 2.7×10^{-15} s for unstretched HCPA, and 4.0×10^{-15} s for unstretched S-PA. These results suggest that the orientation of the fibril is important for the lifetime of free carrier in stretched HCPA than in unstretched ones. Elongation of the HCPA films aligns the PA chains parallel and will increases interfibril contact. The lifetime of free carrier will be increased by the interfibril hopping, which results in a higher conductivity than that of the unstretched HCPA. Correspondingly, stretched iodine-doped HCPA showed higher conductivity than the

unstretched sample at the same dopant level ($y = 0.13$) [20]. These results indicate the importance of three-dimensional interaction in the oriented film for the appearance of a high conductivity.

For further discussing the orientational effect on the electronic structure of HCPA, we introduce the orientational order parameter which was described by Jen *et al.* [22]. The definition of the second order parameter $\overline{P}_2$ is descrived in the Appendix. The order parameter $\overline{P}_2$ of the polymer chain in the films of draw ratio 4 and 8 are estimated from the dichroic ratio of the band at 1360 cm^{-1} which is characteristic of the charged soliton. This band appears for the whole doping range and its polarization should be parallel to the chain axis [23]. The order parameters $\overline{P}_2$ calculated from curves of Figs. 10(a)(11(a)) and 10(b)(11(b)) are 0.91 and 0.82, respectively.

Figure 12 shows the change of oscillator strength of each transition and the change of the conductivity with the order parameter, where the values are normalized to the values of unstretched sample. If we assume that these infrared bands are originated from the atomic vibrations and excited electronic states of the molecular unit, the oscillator strength is expected to increase three times from the value of randomly oriented fibril by increasing the degree of orientation of the fibril to the case of complete alignment (*oriented gas model*). The transition intensity of the 600 cm^{-1} (No. 2), 1360 cm^{-1} (No. 4) and 5000 cm^{-1} (No. 6) bands at $\overline{P}_2 = 0.82$ and 0.91 are about 3 ~ 5 times larger than that of unstretched sample. In contrast, the oriented gas model is no longer valid for the far-IR band (No. 1) and near-IR band (No. 5), since the oscillator strength of bands Nos. 1 and 5 for the parallel direction are more than three. When we consider that band No. 5 is due to the polson structure, we can explain this large enhancement by asuming that the polson is more stable in the oriented film. Since each polson structure provides an unpaired electron, which contributes to metallic conduction, this may be another reason why the oriented film is more conductive. Moreover, the far-IR No. 1 band shows good correlation with the optical dc conductivity (σ_0^{opt}). As mentioned

above, the origin of this band has a close relation to the free carriers. These results show that both free carrier band and the far-IR No. 1 band appear by the formation of many polson chains and they are aligned parallel by the interchain contact. Thus the interchain interaction is essential for the appearance of metallic bands. Figure 12 also shows the change of the dc conductivity with the order parameter. Actually, the dc conductivity does not behave similarly to the optical dc conductivity (σ_0^{opt}). This may be due to the fact that the dc conductivity includes the effect of the macroscopic defects (imperfect interfibril contact, inhomogeneity of the sample density *etc.*). Since we used a far-IR microscope for measuring of the reflectance, we obtained the reflection spectra of small fine regions (ca. 70 μm). Therefore, the optical dc conductivity may have reflected the intrinsic metallic conductivity.

Such spectra indicating the metallic state in the stretched film was also found in the spectra with the electric vector of light perpendicular to the stretching direction. In Fig. 13 we show the real part of the dielectric function for the perpendicular direction at different degrees of orientational order. The curve for $\overline{P}_z = 0.91$ shows a negative ε_1 value in the far-IR region, which is the evidence for the free carrier travelling even along the perpendicular direction. These results clearly show that the highly oriented HCPA has a metallic interaction even along the interfibril direction. From these results we can conclude that the heavily doped and highly oriented HCPA is not a simple one-dimensional conductor, but is a three-dimensional conductor. The interfibril interaction perpendicular to the chain is essential for the appearance of metallic conductivity. A three-dimensional variable range hopping is the most plausible mechanism for such highly oriented doped polyacetylene [19].

2.4 References

[1] F.Wooten, "Optical Properties of Solids," Academic Press, New York (1972).

[2] Y.Cao, P.Smith, and A.J.Heeger, *Synth. Met.*, **41-43**, 181 (1991).

[3] S.Hasegawa, M.Oku, M.Shimizu, and J.Tanaka, *Synth. Met.*, **38**, 37 (1990).

[4] K.Kamiya and J.Tanaka, *Synth. Met.*, **25**, 59 (1988).

[5] J.Tsukamoto, A.Takahashi, and K.Kawasaki, *Jpn. J. Appl. Phys.*, **29**, 125 (1990).

[6] H.Naarmann and N.Theophilou, *Synth. Met.*, **25**, 1 (1987).

[7] X.Q.Yang, D.B.Tanner, A.Feldblum, H.W.Gibson, M.J.Rice, and A.J.Epstein, *Mol. Cryst. Liq. Cryst.*, **117**, 267 (1985).

[8] X.Q.Yang, D.B.Tanner, M.J.Rice, H.W.Gibson, A.Feldblum, and A.J.Epstein, *Solid State Commun.*, **61**, 335 (1987).

[9] A.Terai, Y.Ono, and Y.Wada, *J.Phys. Soc. Jpn.*, **55**, 2889 (1986).

[10] H.Takayama, Y.R.Lin-Liu, and K.Maki, *Phys. Rev. B*, **21**, 2338 (1980).

[11] C.Tanaka and J.Tanaka, *Synth. Met.*, **41-43**, 3709 (1991).

[12] C.Tanaka and J.Tanaka, *Bull. Chem. Soc. Jpn.*, **66**, 357 (1993).

[13] N.S.Murthy, G.G.Miller, and R.H.Baughman, *J. Chem. Phys.*, **89**, 2523 (1988).

[14] J.Tanaka, Y. Saito, M.Shimizu, C.Tanaka, and M.Tanaka, *Bull. Chem. Soc. Jpn.*, **60**, 1595 (1987).

[15] T.C.Chung, F.Moraes, J.D.Flood, and A.J.Heeger, *Phys. Rev. B*, **29**, 2341 (1984).

[16] H.S.Woo, D.B.Tanner, N.Theophilou, and A.G.MacDiarmid, *Synth. Met.*, **41-43**, 159 (1991).

[17] G.Leising, *Synth. Met.*, **28**, D215 (1989).

[18] K.Kamiya, H.Inokuchi, M.Oku, S.Hasegawa, C.Tanaka, J.Tanaka, and K.Seki, *Synth. Met.*, **41**, 155 (1991).

[19] J. Tanaka, C.Tanaka T.Miyamae, M.Shimizu, S.Hasegawa, K.Kamiya, and K.Seki, *Synth. Met.* **65**, 173 (1994).

[20] J.Tanaka, S.Hasegawa, T.Miyamae, and M.Shimizu, *Synth. Met.*, **41-43**, 1199 (1991).

[21] Y.Chen, K.Akagi, and H.Shirakawa, *Synth. Met.*, **14**, 173 (1986).

[22] S.Jen, N.A.Clark, P.S.Pershan, and E.B.Priestley, *J. Chem. Phys.*, **66**, 4635 (1977).

[23] G.Zannoni and G.Zerbi, *J. Mol. Struct.*, **100**, 505 (1983).

2.5 Figure Captions

Figure 1. The glove box and the Ar gas purification system.

Figure 2. The self-washing extracting system of Soxhlet's type distillation tower.

Figure 3. Experimental setup for the dc conductivity measurements.

Figure 4. Relationship between concentration of perchlorate ion (ClO_4^-) and conductivity of HCPA.

Figure 5. Polarized reflection spectra of perchlorate-doped PA $[CH(ClO_4^-)_y]_x$; (a) pure HCPA, (b) $y = 0.013$ ($\sigma_0^{obs} = 1900$ Scm^{-1}), (c) $y = 0.036$ ($\sigma_0^{obs} = 4450$ Scm^{-1}), and (d) $y = 0.045$ ($\sigma_0^{obs} = 22000$ Scm^{-1}).

Figure 6. Optical conductivity spectra of perchlorate-doped HCPA $[CH(ClO_4^-)_y]_x$. The polarization direction of the electric vector of light is parallel to the stretching direction; (a) $y = 0.013$ ($\sigma_0^{obs} = 1900$ Scm^{-1}), (b) $y = 0.036$ ($\sigma_0^{obs} = 4450$ Scm^{-1}), and (c) $y = 0.045$ ($\sigma_0^{obs} = 22000$ Scm^{-1}).

Figure 7. Illustration of Baughman's model for doped polyacetylene projected along the chain axis; (a) undoped $(CH)_x$, (b) $(UP)_n$ lattice for lightly doped polyacetylene, where U and P denote the undoped and partially doped chain, and (c) $(UPUF)_n$ lattice doped to metallic region, where F denote the fully doped chain. Large circles illustrate dopant column.

Figure 8. Relationship between concentration of perchlorate ion (ClO_4^-) and the oscillator strength of transitions which are normalized at the transition intensities for the sample of $y = 0.013$.

Figure 9. Optical conductivity spectra of perchlorate-doped HCPA $[CH(ClO_4^-)_y]_x$. The polarization direction of the incident light is perpendicular to the stretching direction; (a) $y = 0.013$, (b) $y = 0.036$, and (c) $y = 0.045$.

Figure 10. Change of the polarized reflection spectra with the stretching ratio at heavily doped regimes ($0.04 < y$ for $[CH(ClO_4^-)_y]_x$); (a) spectrum for the electric vector of light E parallel to the stretching direction for the film with elongation ratio $l/l_0 \sim 8$, (b) spectrum with E to the stretching direction for the film with elongation ratio $l/l_0 \sim 4$, (c) unstretched film, (d) spectrum with E perpendicular to the direction of stretching for the film of (a), and (e) spectrum with E perpendicular to the direction of stretching for the film of (b).

Figure 11. Change of the optical conductivity spectra of perchlorate-doped HCPA with the draw ratio; (a) E parallel to the direction of elongation for the film of at $l/l_0 \sim 8$, (b) E parallel to the direction of elongation for the film for $l/l_0 \sim 4$, and (c) unstretched film ($y = 0.062$, $\sigma_0^{obs} = 2000$ Scm^{-1}).

Figure 12. Oscillator strength and the dc conductivity normalized at the intensities of unstretched film for each transition as functions of the order parameter $\overline{P}_2$.

Figure 13. Change of the real part of dielectric function (ε_1) with stretching for the electric field perpendicular to the stretching direction; (a) $\overline{P}_2 = 0.82$ and (b) $\overline{P}_2 = 0.91$.

2.6 Tables

Table 1. Optical parameters obtained with simulation of optical conductivity spectra (parallel direction)

	$y = 0.013$	$y = 0.036$	$y = 0.045$
σ_0^{obs}(Scm^{-1})	1900	4450	22000
σ_0^{opt}(Scm^{-1})	50	700	28000
Ω_0(Scm^{-1})	3000	4000	7700
τ(s)	1.77×10^{-15}	1.39×10^{-14}	1.50×10^{-13}
$n_{cs} \times N_\pi$(cm^{-3})	6.00×10^{20}	1.00×10^{21}	1.16×10^{21}
N_0(cm^{-3})	1.01×10^{20}	1.79×10^{20}	6.63×10^{20}
ε_∞	4.0	2.5	3.6

j	ω_j (cm-1)	γ_j (cm-1)	f_j	$\langle r_j \rangle$ (Å)	ω_j (cm-1)	γ_j (cm-1)	f_j	$\langle r_j \rangle$ (Å)	ω_j (cm-1)	γ_j (cm-1)	f_j	$\langle r_j \rangle$ (Å)
1	250	360	0.075	3.04	370	340	0.23	4.37	390	460	0.87	8.28
2	620	400	0.070	1.86	650	500	0.39	4.29	700	480	0.35	3.92
3	960	450	0.085	1.65								
4	1380	50	0.020	0.67	1360	50	0.02	0.67	1380	50	0.02	0.67
5	2500	3000	1.15	3.76	2500	3500	3.85	6.88	2000	3000	3.85	7.64
6	5500	7000	9.30	7.21	6500	7000	3.60	4.13	5600	8000	7.70	6.50
7	19000	6500	0.092	0.39	17500	12000	0.086	0.39	14500	10000	0.043	0.30

Table 2. Optical parameters obtained with simulation of optical conductivity spectra (perpendicular direction)

	$y = 0.013$				$y = 0.036$				$y = 0.045$			
σ_0^{opt}(Scm^{-1})	15				51				150			
Ω_0(Scm^{-1})	1000				1200				1500			
τ(s)	4.77×10^{-15}				1.13×10^{-14}				2.12×10^{-14}			
$n_{cs} \times N_\pi$(cm^{-3})	6.00×10^{20}				1.00×10^{21}				1.16×10^{21}			
N_0(cm^{-3})	1.12×10^{19}				1.61×10^{19}				2.52×10^{19}			
ε_∞	2.4				2.4				2.3			
j	ω_j (cm^{-1})	γ_j (cm^{-1})	f_j	$\langle r_j \rangle$ (Å)	ω_j (cm^{-1})	γ_j (cm^{-1})	f_j	$\langle r_j \rangle$ (Å)	ω_j (cm^{-1})	γ_j (cm^{-1})	f_j	$\langle r_j \rangle$ (Å)
1	270	180	0.0048	0.74	400	490	0.0397	1.75	300	300	0.025	1.60
2	600	400	0.019	0.99	600	500	0.0183	0.97	600	450	0.051	1.62
3	880	500	0.025	0.93	900	400	0.0093	0.56	1000	450	0.022	0.82
4	1380	50	0.003	0.26	1360	50	0.0024	0.23	1380	50	0.0015	0.18
5	3000	4000	0.413	2.06	3000	2800	0.290	1.72	2700	4100	0.51	2.41
6	5800	7300	1.03	2.34	5500	7000	0.548	1.75	6500	8000	4.20	1.41
7	17000	12000	0.01	0.13	14500	12000	0.01	0.15	14000	12000	0.01	0.15

3. Electrical Transport Properties of Perchlorate-Doped Oriented Polyacetylene

3.1 Introduction

In this section we present the study of the temperature dependence of electrical conductivity of HCPA doped with perchlorate ion. Perchlorate ion is a useful acceptor because it has no spin. Most of other acceptors, *e.g.* $FeCl_4^-$ ion, have a spin which may influence on the conductivity [1]. The electrical conductivities along the directions parallel and the perpendicular to the stretching direction were measured from 290 to 1.5 K. The observed temperature dependence and anisotropy of conductivity were analyzed in terms of Mott's three-dimensional variable-range hopping model [2]. Comparison is made with our previous study, where the temperature dependence of conductivity of iodine doped S-PA was analyzed by using one- and two-dimensional variable-range hopping models [3]. We will discuss the effect of orientation on the conductivity and the temperature dependence of the conductivity in connection with the conduction mechanism.

3.2 Experimental

The Ziegler-Natta catalyst was prepared according to a technique described by Tsukamoto *et al.* [4] and treated as mentioned in chapter 2. Polyacetylene films were synthesized in a glove box, where argon gas was circulated through the purification system that could keep the oxygen and water contents below 1.0 ppm, respectively [5]. The catalyst was cast with a uniform thickness of 10 μm on a glass plate by using Doctor Brade (Type YD-2, Yoshimitu Seiki Co., Ltd.). Acetylene monomer gas of six-nine grade was passed over the catalyst cooled at -10 °C. After polymerization, the films were washed repeatedly with toluene, stretched by hands in the glove box with a stretching ratio of 3 ~ 8, and then dried *in vacuo*. The thickness of the stretched film was ~ 1 μm.

HCPA films were prepared and elongated in a glove box as described in chapter 2. The perchlorate doping was carried out in the glove box at room-temperature in an acetonitrile solution of dried copper (II) perchlorate by the same technique as described in chapter 2. The doping levels were determined based on the weight uptake. Polymerization, stretching, washing and perchlorate doping were carried out under a purified argon atmosphere. The temperature dependence of the electrical conductivity was measured by a conventional four-probe method with low-frequency (80 Hz) alternating current under vacuum condition. Electrical contacts were achieved by using silver paste. The temperature was monitored by a copper-constantan thermocouple (290 K — 30 K) and a calibrated carbon resistor (30 K — 1.4 K).

3.3 Results and Discussion

3.3.1 Temperature Dependence of Conductivity of Perchlorate-Doped Polyacetylene.

Figure 1 shows the temperature dependence of the conductivity of perchlorate-doped with polyacetylene, $[CH(ClO_4)_y]_x$, parallel to the stretching direction. The doping was carried out immediately after synthesis. Films (a) (y = 0.074) and (b) (y = 0.082) were doped to a saturated level, but film (b) was exposed to air for 30 minutes after doping. Film (c) was also a freshly prepared sample doped to y = 0.022. The orientational order parameter $\overline{P}_2$ (for the definition of $\overline{P}_2$, see Appendix) of these films were estimated from the infrared absorption spectra to be 0.68. The room-temperature conductivity (σ_{RT}, Fig. 1 (a)) was 17000 Scm^{-1}, and it increased upon cooling, as in the case of $FeCl_4^-$-doped polyacetylene [1,6]. This showed the maximum value to be at 190 K ($\sigma_{190K}/\sigma_{RT}$ = 1.09) as shown in the inset of Fig. 1, and then decreases to $\sigma_{1.5K}/\sigma_{RT}$ = 0.84 at 1.5 K. High conductivity ($\sigma > 10^4$ Scm^{-1}) down to 1.5 K implies that the heavily perchlorate-doped stretched polyacetylene is a metal with a weak localization of carriers.

The temperature dependence of the conductivity is illustrated in Fig. 2 by a ln σ plot to $1/T$. The activation energy (ΔE) for curve (a) in the 3 - 1.5 K region is only 1.2 μeV, which is obtained by fitting to the equation

$$\sigma = \sigma_0 \exp(-\Delta E/k_B T). \tag{3.1}$$

This means that most of the carriers are very weakly localized, even in the 1 K region. We also analyzed the conductivities of other films at very low temperature, and found σ_0 and ΔE of Eq. (3.1) as shown in Table 1. The most ordered heavily doped film (Fig. 1 (a) and (b), $\overline{P}_2$ = 0.68) shows a large σ_0 for the chain direction. In the study on the reflection spectra in Chapter 2, we found that elongation of the film increases the inter- and intrachain interaction producing a metallic reflectance [7]. The elongation results in an increase of σ_0 along the chain direction. In this respect, perchlorate-doped polyacetylene is highly anisotropic. It is remarkable that neither phonon scattering nor electron-electron scattering were found at very low temperature.

A comparison of curves (a) and (b) of Fig. 1 shows the effect of oxidation by air. A decrease of conductivity of the film of Fig. 1 (b) was noticed below 230 K, while that of curve (a) was observed from 190 K. These results may mean that the conductivity mechanism which dominates in the low-temperature region is more influenced by air. The activation energy for 2.5 ~ 5 K, estimated by the plot of Fig. 2 (b), was 7.2 μeV. This value is six-times larger than that of curve (a), suggesting the formation of deeper traps by oxidation in film (b) than in film (a). The oxidation enhances sp^3 defects in the conjugated double bonds of the polyacetylene chain [8]. Curve (c) of Fig. 1 shows the conductivity of a less-doped film (y = 0.02); it indicates that a really metallic state is not realized at this level of doping. The room-temperature conductivity for y = 0.022 was 300 Scm^{-1}; the conductivity decreased monotonically from room temperature to 1.5 K with $\sigma_{1.5K}/\sigma_{RT}$ = 0.44.

Above 10 K, the more tightly bound electrons are activated; the activation energy (ΔE) estimated from Fig. 2 and Eq. (3.1) is 0.88 meV for curve (a). Accordingly, the conduction mechanism in doped polyacetylene may be considered based on the combination of two terms: one is almost the temperature-independent conduction mentioned above; the other is a process requiring thermal activation. In fact, the contribution from the latter, which can be described by three-dimensional variable-range hopping (3D-VRH) conduction, becomes significant for a higher temperature region as shown below.

3.3.2 Variable-range Hopping Analysis of the Conductivity of Oriented Polyacetylene.

Following Mott's treatment, [2] the 3D-VRH conductivity is given by

$$\sigma(T) = 0.39\left[N(E_F)/\alpha k_B T\right]^{1/2} \nu_0 e^2 \exp\left[-(T_0/T)^{1/4}\right], \tag{3.2}$$

where $T_0 = 16\alpha^3/k_B N(E_F)$, α^{-1} is the decay length of a localized state, or $L = \alpha^{-1}$ is the localization length (we will use this terminology in the following discussion), ν_0 is the hopping attempt frequency, and $N(E_F)$ is the density of states near E_F per unit volume [9] The optimum hopping distance, R, is given by

$$R = \left(\frac{3}{2\pi\alpha N(E_F) k_B T}\right)^{1/4}. \tag{3.3}$$

We applied Eqs. (3.2) and (3.3) to the values of the conductivity after subtracting the contribution of the almost temperature-independent conduction expressed by Eq. (3.1) by using σ_0 and ΔE of Table 1. The residual conductivities follow the relation of Eq. (3.2) fairly well, as shown in Fig. 3. It is remarkable that the relation between ln $\sigma T^{1/2}$ and $T^{-1/4}$ holds over a wide temperature range. In this analysis we used the value of the

density of states, $N(E_F)$ to be 0.22 and 0.31 state/eV·(C atom), for the stretched and unstretched films, respectively, at the saturated doping level [10]. The lattice parameters for two CH chains are assumed to be as shown in Table 1 [11].

Combining Eqs. (3.1) and (3.2), the conductivity is given by

$$\sigma(T) = \sigma_0 e^{-\Delta E/k_B T} + 0.39\left[N(E_F)L/k_B T\right]^{1/2} \nu_0 e^2 e^{-(T_0/T)^{1/4}} \qquad (3.4)$$

The calculated conductivities with the parameters of Table 1 are shown in Fig. 4 together with the experimental points. Good agreement between the experimental and calculated values throughout the examined temperature range can be seen. Above 200 K, the observed conductivity, $\sigma(T)$, decreased, which may have been caused by phonon scattering. The rotational motion of the perchlorate ion may be freed above 186 K [12], leading to enhanced phonon scattering above this temperature. For film (c), the conductivity increased monotonously to 290 K; this may mean that the dominant conduction mechanism is not the same between these two films.

Concerning the temperature dependence of different conduction mechanisms, one is T^{-1} and the other is $T^{-1/4}$ on the exponent; this has been discussed in detail by Mott [13]. Table 1 gives the cross-over temperature T_1 from a nearly free to the VRH conduction according to this type of analysis. Below T_1 the conduction of nearly free, or very weakly localized, carrier is dominant. The weakly localized carrier has an extended localization length L, which it is effective for the transport at a very low temperature, where thermal excitation is not feasible. From an activation energy of 1.2 μeV below 3 K, the value of L at 1.5 ~ 3 K was estimated using

$$\Delta E \approx \frac{1}{L^3 N(E_F)} \qquad (3.5)$$

to be as large as 680 Å. In a stretched fresh film, the $T^{-1/4}$ dependence exists above T_1 = 30 K.

More reliable values for L and R above T_1 were obtained by an analysis using Eq. (4), and are tabulated in Table 1. These values are 13 and 18 Å, respectively. These

values are compared in the latter discussion, with the estimated minimum values of L and R, based on the polson model.

3.3.3 Effect of Stretching and Anisotropy of the Conductivity

The room-temperature conductivity of unstretched fims is only 500 Scm^{-1}. By stretching the film, the room-temperature conductivity parallel to the stretching direction is increased by a factor of 30 ~ 40, and metallic property appears, as shown in Fig. 1. The anisotropy of the conductivity is given by the ratio of the conductivity parallel and perpendicular to the stretching direction ($\sigma_{//}/\sigma_{\perp}$); its temperature dependence is shown in Fig. 5. The most ordered film of $\overline{P}_2 = 0.68$ exhibited a conspicuous temperature dependence, as shown in curve (a) of Fig. 5. The anisotropy was 92 at 280 K and 250 at 1.5 K. A strongly oriented, but mediumly doped, film of $y = 0.039$ ($\overline{P}_2 = 0.68$) showed a similar behavior as shown in Fig. 5 (b). In contrast, the anisotropy of a less-stretched film ($\overline{P}_2 = 0.55$) was almost constant (22 ~ 35), as shown in Fig. 5 (c).

In the preceding section the conductivity is expressed using two terms. At very low temperature, conduction by extended carriers dominates, whereas the 3D-VRH term becomes significant above 30 K. The temperature dependence of anisotropy suggests that the extended carrier moves along the chain with a large anisotropy of 250 at very low temperature, while the VRH conduction involves interchain hopping. The anisotropy of the conductivity can be reasonably explained using the parameters given in Table 1; the calculated anisotropy for curves (a) and (c) for heavily doped films are shown by solid lines in Fig. 5; they show satisfactory agreement with the observed values. The result provides additional support for Eq. (3.4), and the overall scenario of the conduction mechanism.

The values of σ_0 dramatically increase by extensive stretching, as shown in Table 1; the σ_0 of a $\overline{P}_2 = 0.68$ film is 12000 Scm^{-1}, a $\overline{P}_2 = 0.55$ film is 8200 Scm^{-1}, and an unstretched ($\overline{P}_2 = 0$) one is only 70 Scm^{-1}, respectively. We can ascrive this increase to the appearance of metallic conductivity causes due to an extended ordering of fibrils leading to enhanced interchain interaction.

For the direction perpendicular to the stretching direction, the values of R and L are of the same order of magnitude as that for the parallel direction. This indicates that the 3D nature of the interaction is conceivable. However, the hopping to the perpendicular direction requires a slightly larger activation energy, as indicated by the larger T_0 in Table 1. The hopping frequency ν_0 in the direction perpendicular to the stretching direction is more than one order of magnitude smaller than that in the parallel direction; this means that the phonon density of states is larger along the chain direction.

According to the transmission electron microscope (TEM) observation of an ultra-thin stretched film [14], a small part of fibril was found to still exist along the perpendicular direction. One may suppose that the electrical conductivity for the perpendicular direction is caused by this component, rather than the intrinsic property of perpendicular transport in a less-ordered system. However, the trend of the temperature-dependent anisotropic conductivity of Fig. 5 (a) is not compatible with the expected behavior based on this misoriented fibril transport, since the anisotropy of the conductivity is a temperature dependent in the low-temperature region. In chapter 2, the real part of the dielectric function of a highly ordered film showed a negative value for the perpendicular direction in the far-infrared region. This implies that a metallic state is realized even for the perpendicular direction in a highly ordered system. The temperature dependence of the anisotropy, and a similar localization length for parallel and perpendicular directions, suggest that the hopping to an adjacent chain (interchain hopping) occurs significantly, as well as doed intrachain hopping in the high-temperature region.

3.3.4 Polson Model of Perchlorate-Doped Polyacetylene

By studying the optical and structual aspects of doped polyacetylene, we proposed the polson model for the heavily doped polyacetylene [15-17]. The characteristic point of the model is that an unpaired electron is enclosed by two charged soliton structures which are comprise dopant-coordinated allylic groups. Figure 6 shows an idealized model of a polson-antipolson chain (a) and interchain contacts in the ordered fibril structure (b).

Although the crystal structure of perchlorate-doped polyacetylene is not perfectly determined [11], we can estimate the structure based on the dopant concentration and polson model. The polyacetylene chain perchlorate-doped to saturation contains 8 mole percent of ClO_4^- ion per repeat unit of the $(CH)_x$ chain. Accordingly, twenty-five carbon atoms involving two dopant-coordinated groups form a polson unit. This chain unit is the smallest polson structure in the perchlorate-doped polyacetylene, suggesting that the minimum polson unit length is ca. 30 Å, since each C-C bond length would be ca. 1.2 Å along the chain direction. If we consider the structure of the polson unit (Fig. 6) more strictly, an unpaired electron is contained within 11 carbon atoms between the dopants, and a value of 13 Å is found for L, as mentioned in the preceding section. The carrier (an unpaired electron) in the polson unit moves freely within the unit, making the minimum L to be ca. 13 Å. The hopping distance R ~ 18 Å to the nearest neighbor is naturally explained in Fig. 6 by the hopping to the inter- or intrachain neighboring polson unit.

Along the one-dimensional polson chain, we can estimate the conductivity using

$$\sigma = \frac{e^2}{4\pi^3\hbar} v_F S_F \tau, \tag{3.7}$$

where v_F is the Fermi velocity, S_F is the area of Fermi surface, and τ is the relaxation time of a free carrier.

From the energy-band calculation of the one-dimensional polson chain [15-17] we estimated v_F to be 10^8 cm/s; τ was estimated to be 10^{-13} s by an optical experiments [7,17]. By using the lattice parameters of a = 8.0, b = 8.4, and c = 2.46 Å, the conductivity was estimated to be 2×10^5 Scm^{-1}. The experimentally obtained σ_0 is one order of magnitude smaller than this value, presumably because of the scattering due to impurities and defects in the π-conjugated system. However, a pretty good agreement between the theoretical and experimental values supports the picture of a one-dimensional metallic band of the polson chain structure.

A one-dimensional metal is not stable to a Peierls distorsion, and it seems paradoxical that the doped polyacetylene shows highly anisotropic conduction. In fact, high metallic conductivity is realized by extensive stretching with intimate contact among the chain, thus expanding the dimensionality due to the interchain interaction. The interchain contact is essential for realizing a metallic state. Therefore, the doped polyacetylene should be regarded as being a three-dimensional metal with a large anisotropy, but not as being a one-dimensional conductor.

3.4 References

[1] H.Kaneko and T.Ishiguro, *Synth. Met.*, **65**, 141 (1994).

[2] N.F.Mott and E.A.Davis, "Electronic Processes in Non-Crystalline Materials", Oxford University Press, 2nd ed., London, 1979.

[3] K.Kamiya and J.Tanaka, *Synth. Met.*, **25**, 59 (1988).

[4] J.Tsukamoto, A.Takahashi and K.Kawasaki, *Jpn. J. Appl. Phys.*, **29,** 125 (1990).

[5] H.Naarmann and N.Theophilou, *Synth. Met.*, **22**, 1 (1987).

[6] Y.W.Park, C.Park, Y.S.Lee, C.O.Yoon, H.Shirakawa, Y.Suezaki and K.Akagi, *Solid State Commun.*, **65**, 147 (1988).

[7] T.Miyamae, M.Shimizu and J.Tanaka, *Bull. Chem. Soc. Jpn.*, **67**, 2407 (1994) .

[8] Th.Schimmel, G.Denninger, W.Riess, J.Voit, M.Schwoerer, W.Schoepe, and H.Naarmann, *Synth. Met.*, **28**, D11 (1989).

[9] A.J.Epstein, H.Rommelmann, R.Bigelow, H.W.Gibson, D.M.Hoffmann and D.B.Tanner, *Phys. Rev. Lett.*, **50,** 1866 (1983).

[10] Y.Nogami, H.Kaneko, T.Ishiguro, A.Takahashi, J.Tsukamoto and N.Hosoito, *Solid State Commun.*, **76,** 583 (1990).

[11] J.P.Pouget, J.C.Pouxviel, P.Robin, R.Comes, D.Begin, D.Billaud, A.Feldblum, H.W.Gibson, and A.J.Epstein, *Mol. Cryst. Liq. Cryst.*, **117,** 75 (1985).

[12] J.L.de Boer and A.Vos, *Acta. Cryst.*, **B28,** 835 (1972).

[13] N.F.Mott, "Metal-Insulator Transitions", Taylor & Francis, 2nd ed, London, 1990.

[14] J.Tanaka, C.Tanaka, T.Miyamae, K.Kamiya, M.Shimizu, M.Oku, K.Seki, J.Tsukamoto, S.Hasegawa, and H.Inokuchi, *Synth. Met.*, **55-57,** 121 (1993).

[15] C.Tanaka and J.Tanaka, *Bull. Chem. Soc. Jpn.*, **66,** 357 (1993).

[16] C.Tanaka and J.Tanaka, *Synth. Met.*, **55-57,** 4377 (1993).

[17] J.Tanaka, C.Tanaka, T.Miyamae, M.Shimizu, S.Hasegawa, K.Kamiya, and K.Seki, *Synth. Met.*, **65,** 173 (1994).

3.5 Figure captions

Figure 1. Temperature dependence of conductivity parallel to the stretching direction; (a) stretched fresh sample, $y = 0.074$, (b) $y = 0.083$ (measured after 30 min. exposure to air), and (c) $y = 0.022$. The inset shows the expansion of the region from room temperature to 100 K.

Figure 2. $\ln\sigma$ against $1/T$ for the $[CH(ClO_4)_y]_x$; (a) $y = 0.074$, (b) $y = 0.083$ (measured after 30 min. exposure to air), and (c) $y = 0.022$.

Figure 3. $\ln\sigma(T)T^{1/2}$ against $T^{-1/4}$ plots for perchlorate-doped polyacetylene; (a) $\overline{P}_2 = 0.68$ parallel to the stretching direction, (b) $\overline{P}_2 = 0.55$ parallel to the stretching direction, (c) perpendicular to the stretching direction of (a), (d) perpendicular to the stretching direction of (b), and (e) unstretched film.

Figure 4. Observed and calculated temperature dependence of conductivity ; (a) $y = 0.074$, $\overline{P}_2 = 0.68$ parallel to the stretching direction of fresh sample, (b) $y = 0.072$, $\overline{P}_2 = 0.55$ (measured after 30 min. exposure to air), and (c) $y = 0.07$ unstretched. The solid lines are simulated temperature dependences of conductivity. For details, see text.

Figure 5. Observed and calculated temperature dependence of anisotropic ratio for perchlorate-doped $(CH)_x$; (a) $\overline{P}_2 = 0.68$, y = 0.083, (b) $\overline{P}_2 = 0.68$, $y = 0.039$, and (c) $\overline{P}_2 = 0.55$, $y = 0.072$.

Figure 6. Structural formula for perchlorate ions in doped polyacetylene (a) and the interchain contact between the nearest neighbor polson-antipolson chain of doped polyacetylene (b). Unpaired electrons are shown by block circles.

Table. I Parameters of the modified three-dimensional variable range hopping model.

sample	$\overline{P}_2$ [a)]	ΔE	T_1	σ_0	T_0	ln(A)[b)]	α	L	R	ν_0
		10^{-6} eV	K	Scm^{-1}	K		10^5 cm^{-1}	Å	Å	cm^{-1}
y=0.074 fresh film (a)[c)]	0.681	1.2	30	14200	32700	14.61	77.1	13.0	17.4	149200
y=0.083 film (b) parallel[d)]	0.554	7.2	5	8200	18670	14.31	64.1	15.6	18.3	100400
perpendicular		9.0	2	220	26500	11.78	71.9	13.9	17.7	8500
y=0.072 parallel	0.681	10	10	12000	17000	14.36	62.0	16.1	18.4	104800
perpendicular		13	2	50	30500	10.81	75.3	13.3	17.5	3300
y=0.070 unstretched	0.0	17.8	5	70	29300	12.15	83.3	12.0	15.7	11200

[a)]For the definition of $\overline{P}_2$, see Appendix.

[b)]For 3D VRH model $A = 0.39\left[N(E_F)/\alpha k_B T\right]^{1/2} \nu_0 e^2$. $N(E_F)$=0.22 states/eV·(C atom) (for stretched sample) and 0.31 state/eV·(C atom) (for unstretched sample), respectively.[14)] The lattice parameters are taken to a=8.0 Å, b=8.6 Å, and c=2.46 Å.

[c)]These parameters are obtained from the curve of Fig. 1(a).

[d)]These parameters are obtained from the curve of Fig. 1(b).

4. Ultraviolet Photoelectron Spectroscopy of Alkaline-metal Doped Polyacetylene

4.1 Introduction

In chapter 4 we present the ultraviolet photoelectron spectric study of alkaline-metal doped polyacetylene.

During the last decade, photoelectron spectroscopy (PES) of conducting polymers has provided useful information for the electronic structure and electronic interaction. Works utilizing X-ray photoelectron spectroscopy (XPS) and ultraviolet photoelectron spectroscopy (UPS) have been performed for examining the valence and core level electronic structures of π -conjugated conducting polymers [1-5], and their change upon doping [6-10]. Energy levels characteristic of metallic state in conducting polymer may be found by UPS. In fact, by Salaneck *et al.* [9] found that the top of the valence band of $NOPF_6$-doped poly(3-hexylthiophene) exists at the same position of the Fermi level of gold. Including this work, the UPS studies in the past have been carried out mainly on p-doped conducting polymers such as AsF_5-doped S-PA [6] and ClO_4^--doped polypyrrole [8], and studies on n-doped conducting polymers are still limited.

Polyacetylene, $(CH)_x$, can be doped by either n- or p-type dopants. In our previous study of UPS spectra of perchlorate-doped (p-doped) polyacetylene [11], we reported a finite density of states at Fermi level in the heavily doped regime, but the intensity of the band is rather weak compared to other three-dimensional metals.

In this work, we report UPS studies of Na- and K- doped PA, and discuss their electronic structures using the observed results. Analyses of the observed spectra were carried out with the aid of ab initio molecular orbital calculations [12] of the energy levels of alkaline-metal doped model compounds of PA.

4.2 Experimental

4.2.1 Sample Treatment and UPS Measurements

Thin polyacetylene films were synthesized using the high-temperature aged catalyst prepared with Tsukamoto's method [13] in the glove box described in chapter 2. The catalyst was cast with uniform thickness of 1 μm on a flat glass plate. Acetylene monomer gas of six-nine grade was passed over the catalyst cooled at -78 °C for a few minutes. After polymerization, the film was stripped from the glass plate, washed repeatedly with toluene, put carefully on a molybdenum substrate, and then dried *in vacuo*. Typical thickness of the film was 0.5 μm.

Photoelectron spectra were measured at the beamline 8B2 in the UVSOR Facility, Institute for Molecular Science. Energy calibration of the spectrometer was carried out using the Fermi edge of gold film evaporated *in situ*. The photon of 40 eV energy was used with the incident angle of 50° from surface normal, and the photoelectrons were collected in normal emission from the sample surface. The total energy resolution of the spectrometer was about 200 meV, as judged from the Fermi edge of gold [14].

Thin films were used for measurements of pristine polymer for avoiding sample charging at UPS measurements due to ionization. Immediately after synthesis, polyacetylene contains 93 - 95 percent of *cis* form. For measuring both *cis*- and *trans*-forms, synthesized fresh film was kept in argon filled vessel which was cooled at -78 °C before UPS measurement to avoid isomerization to *trans*-form at room temperature. The *cis*-film was completely isomerized to *trans*-form in the preparation chamber attached to the UPS spectrometer at 200 °C for 1 hour. The results for these undoped films and their discussions are reported elsewhere [11]. After the isomerization were completed, sodium or potassium doping of polyacetylene was carried out *in situ* at 170 °C ± 10 °C in the preparation chamber (base pressure 5×10^{-8} Torr, 1 Torr=133.32 Pa) using a SAES alkaline metal getter source. Subsequently the doped

films were transferred to the measurement chamber (base pressure 1×10^{-10} Torr). The SAES getter was heated with a current of 5.8 - 6.5 A dc to evaporate alkaline metal. The amount of metal deposited onto the polymer film was monitored by a quartz thickness monitor. The potassium doping levels were determined from the ICP analysis after UPS measurements.

4.2.2 MO Calculations on Polyacetylene Model Compounds

Ab initio RHF and UHF SCF-MO calculations for simplified model systems of doped states were carried out by Gaussian 92 program [12] at the Computer Center of Institute for Molecular Science. The basis set for the calculation was 3-21G. Also explicit energy band structures of doped polyacetylene for the π levels were calculated by Pariser-Parr-Pople's (P-P-P) method [15] by using the structural data obtained by *ab initio* method.

4.3 Results and Discussion

4.3.1 UPS Spectra of Na-Doped Polyacetylene

Figure 1 shows the UPS spectra of Na-doped polyacetylene at increasing doping levels. The abscissa is the binding energy E_b from the vacuum level (E_{vac}). The curve (a) is the spectrum of undoped film, where the top of the valence band is at 0.9 eV below E_F. A shoulder at 8 eV is absent in the film manipulated exclusively under inert gas or vacuum. Thus this peak is ascribed to a defect induced by exposure to air for a few minutes before introducing into the spectrometer [11]. The curve (b) of Fig. 2 illustrates the UPS spectrum of lightly Na-doped film, where E_F shifts to the lower binding energy side by 0.8 eV from E_{vac}.

The expanded spectra in this region with energy relative to E_F are illustrated in Fig. 2, where the curve (b) shows downward shift of the valence band relative to E_F.

By further doping to the saturated level, the UPS spectrum changed drastically and the occupied states become extended close to E_F (Fig. 1(c) and Fig. 2(c)). However, a sharp Fermi-edge was not observed at the top of the occupied state. The position of E_F was still shifted toward E_{vac} by about 0.25 eV compared to the lightly doped regime (Fig. 2(b)).

Being afraid of possible presence of metallic sodium on polyacetylene, we also measured the UPS spectrum of Na evaporated on a gold substrate, which is shown in Fig. 2(d). The spectrum is much different from the heavily Na-doped polyacetylene in Fig. 2(c). Also we heated the heavily doped film at 200 °C for 1 hour in the preparation chamber for removing the excess sodium, and confirmed that the spectrum was not changed by heating. Moreover, even when sodium film remained on the surface of polyacetylene, sodium valence band emission near E_F is very weak due to the small cross section of Na 3*s* levels [16]. In addition, Na 2*p* emission of the heavily doped polyacetylene film was found at 31.1 eV relative to E_F, which was 0.6 eV larger than that of sodium metals (30.5 eV). The shift might be caused by the formation of the sodium ion. These results indicate that the density of states near E_F can be assigned to the emission from the quasi-metallic band of the heavily-doped polyacetylene chain.

4.3.2 UPS Spectra of K-Doped Polyacetylene

The UPS spectra of K-doped polyacetylene for increasing doping levels are shown in Fig. 3, and those of by expanded scale near E_F are shown in Fig. 4. At initial stage of doping (Figs. 4b and 4c), the UPS spectra are shifted to the higher binding energy side relative to E_F as in the case of the lightly Na-doped polyacetylene. The shift may be caused by the generation of a new state in the energy gap, although its peak could not be seen in the lightest doping

stage because of its small content. At intermediate doping levels (Figs. 4d, and 4e), a new state appears in the originally empty electron energy gap (the band gap). The position of the new level shifts toward E_F with increasing doping, as shown in Fig. 4. At intermediate doping level of (d), the new state appears at 1.0 eV below E_F. This broad peak moves uniformly toward E_F with increasing doping level.

By further doping to the stage (f) with $[CHK_y]_x$, $y = 0.10$, finite density of states was found just below E_F as for the case of Na-doped polyacetylene. The position of E_F in the stage (f) was still shifted about 0.11 eV in Fig. 3 from the intermediately doped film (e), where $y = 0.06$. In the Raman spectral study of Na-doped polyacetylene [17], new Raman lines appear beyond $y = 0.08$, and the spectra changed completely into a new pattern at the stage of $y = 0.13$. Moreover, Chung *et al.* [18] discussed a transition occurring into a metallic state at $y > 0.08$ from the magnetic susceptibility measurement. In the heavily doped region, the appearance of large density of states near E_F thus corresponds to the transition found in the Raman spectra and magnetic susceptibility studies.

4.3.3 Comparison of the UPS Spectra of Doped Polyacetylene to the Charged Soliton and Polson Model Calculations

We will discuss the observed spectra described above by comparing with theoretical calculations. We have proposed that the charged solitons are generated by light doping of polyacetylene and this turns into the polson by further doping [19-23]. We also suppose that the transition from the charged soliton to the polson lattice from lightly- to heavily-doped state occurs at around $y = 0.08$ in $[CHM_y]_X$ described above.

In Fig. 5, we show the π electron density of states obtained by P-P-P method for these states by Na-doping, together with the results for undoped state [21]. The abscissa is binding

energy relative to vacuum level. In the undoped state (Fig. 5(a)), the HOMO band is at the top of the C $2p\pi$ band. In the lightly-doped state (Fig. 5(b)), a new band appears in the band gap region due to the charged soliton formation. The charged soliton band becomes the HOMO band, and E_F is raised by the formation of this band. In the heavily-doped state, a metallic state is generated by the polson formation with finite density of states across E_F (Fig. 5(c)). At the same time, E_F is further raised from that of the charged soliton states.

The observed trend of the UPS spectra is in accordance with the calculated results. In the case of light-doping, E_F is shifted closer to the vacuum level, and a new state (Figs. 3(d) and 3(e)) in the band gap region is observed for the case of K-doping. This is the first observation of the charged soliton state in the doped polyacetylene. On further doping, E_F shifts further, as sshown in Figs. 3 and 4. From the stage (e) to (f), and the spectral shape changes drastically from those of lightly-doped ones. This transition occurs at $y = 0.08$, where the Raman and the magnetic measurements also showed significant changes of electronic and molecular structures. In the heavily-doped polyacetylene, finite density of states were calculated across the Fermi level by the polson chain. The observed spectra in Figs. 2(c) and 4(f) show occupied states extending close to E_F, which may be due to the metallic energy band of the polson chain [19-23].

However, finite density of states with a sharp Fermi step was not observed at E_F. This apparent contradiction may arise from two reasons. Firstly, a real metallic state may not be achieved by the present method of sample treatment. In the previous optical measurements on perchlorate-doped polyacetylene [24], the real metallic state was achieved by stretching of polyacetylene film before doping. By stretching, the interchain interaction might be enhanced. In fact, in the case of perchlorate-doped polyacetylene, a finite density of states at E_F was actually observed by using the stretched film [11]. In the present experiment, thin films were

not stretched to keep the surface clean. In this situation, the carriers might be localized because of insufficient interchain interaction [24].

Another possibility is that a characteristic property of the strongly electron correlated one-dimensional system appeared in UPS experiments [25,26]. In a one-dimensional conductor, a metallic Fermi-step has not been found on the E_F level, and it has been discussed as an evidence for Tomonaga-Luttinger (T-L) liquid [26]. According to the T-L liquid theory of one-dimensional system, the UPS spectra near the Fermi edge will exhibit a spectral shape of $\sim |\omega|^{\alpha}$, where ω is the energy measured from E_F and $\alpha > 1$. The observed spectra in Figs. 2(c), 4(f), and also the UPS spectrum of perchlorate-doped polyacetylene [11] showed a large value of $\alpha > 1.0$, which suggests the effect of strong long-range repulsive interaction [26]. This result is close to other one-dimensional systems such as $(TMTSF)_2PF_6$ [27], $K_{0.3}MoO_3$, and $(TaSe_4)_2I$ [28].

The theoretical calculations by the P-P-P method give information only for the C $2p\pi$ states, which composes the topmost part of the valence states. On the other hand, in the UPS spectra of metallic state (Fig. 1 (c) or Fig. 4 (f)), a quite different band shape was found in the 5 - 20 eV region of C $2p\sigma$ and C $2s$ bands from those of neutral trans- and lightly-doped polyacetylene (Figs. 6 (a) and (b)). To analyze the spectra in this region, we performed ab initio calculations for the simplified model systems. For the lightly-doped polyacetylene, the energy levels of isolated charged soliton model compound ($C_{30}H_{32}Na_2$) were calculated, using the optimized geometry reported previously [23]. In Fig. 6(b), the simulated UPS spectrum using these results is shown, with corresponding UPS spectrum of K-doped polyacetylene shown in Fig. 5(e) ($y = 0.06$). For a better fit with the observed spectrum, each molecular orbital energy was convoluted with a Gaussian function of 0.5 eV FWHM. The simulated spectrum was contracted along the energy scale by a factor of 0.7 and shifted to higher binding energy by 0.5 eV. Correspondence between the calculated and observed curves in Fig. 6(b) is

quite satisfactory, supporting that the intermediately doped polyacetylene can be regarded as the charged soliton chain.

In contrast to the case of undoped, lightly- ,and intermediately-doped polyacetylene, the UPS spectra of heavily alkaline-metal doped films were difficult to explain by the calculations for the isolated model compounds. We found that the only way to explain the observed broad band is to consider the interaction between the doped chains [23]. Considering the crystal structure studies of alkaline-metal doped polyacetylene by Fischer *et al.* [29] and Saldi *et al.* [30], we have proposed the structural model of alkaline-metal doped polyacetylene as shown in Fig. 7 for Na-doped polyacetylene [23]. The crystal structural model was obtained by putting the polson model compounds in the crystal lattice, where each polson chain is numbered as in Fig. 7. The energy levels are calculated for two types of $C_{13}H_{15}Na_2$ pairs composed of (1) the polson chain No. 1, (2) one of the surrounding polson chains at position No. 3 or 4, and (3) two Na atoms. In Fig. 6(c), we show the simulated UPS spectrum as the overlap of the contribution from the two types of pairs. The interactions between the chains are found to be effective to shift the energy bands in the C $2p\sigma$ region, leading to good correspondence between the simulated and observed UPS spectra. The interaction is also effective for the broadening of the top most C$2p\pi$ band. These results suggest the importance of the interchain interactions in the heavily alkaline-metal doped polyacetylene. In contrast to this, similar calculation for the charged soliton chains indicated only small effect of interchain interaction. This is consistent with our conclusion from optical (chapter 2) [24] and electrical conductivity measurements (chapter 3) [31] that a three-dimensional interaction in heavily-doped polyacetylene is important for the appearance of the metallic state.

4.4 References

[1] K.Seki, U.Karlsson, R.Engelhardt, E.-E.Koch, and W.Schmidt, *Chem. Phys.*, **91**, 459 (1984).

[2] S.Asada, K.Seki, and H.Inokuchi, *Chem. Phys. Lett.*, **130**, 155 (1986).

[3] K.Seki, S.Asada, T.Mori, H.Inokuchi, I.Murase, U.O.Karlsson, R.Engelhart, and E.E.Koch, *Synth. Met.*, **17**, 629 (1987).

[4] K.Seki, S.Asada, T.Mori, H.Inokuchi, I.Murase, T.Ohnishi, and T.Noguchi, *Solid State Commun.*, **74**, 677 (1990).

[5] K.Seki, H.Tanaka, T.Ohta, K.Sanechika, and T.Yamamoto, *Chem. Phys. Lett.*, **178**, 311 (1991).

[6] W.R.Salaneck, H.R.Thomas, C.B.Duke, A.Paton, E.W.Plummer, A.J.Heeger, and A.G.MacDiarmid, *J. Chem. Phys.*, **71**, 2044 (1982).

[7] P.Pfluger and G.B.Street, *J. Chem. Phys.*, **80**, 544 (1984).

[8] A.J.Nelson, S.Gleins, and A.J.Frank, *J. Chem. Phys.*, **87**, 5002 (1987).

[9] R.Lazaroni, M.Lögdlund, S.Stafström, W.R.Salaneck, and J.L.Brédas, *J. Chem. Phys.*, **93**, 4433 (1990).

[10] M.Fahlman, D.Beljonne, M.Lögdlund, R.H.Friend, A.B.Holmes, J.L.Brédas, and W.R.Salaneck, *Chem. Phys. Lett.*, **214** (1993) 327.

[11] K.Kamiya, H.Inokuchi, M.Oku, S.Hasegawa, C.Tanaka, J.Tanaka, and K.Seki, *Synth. Met.*, **41**, 155 (1991); K.Kamiya, M.Oku, T.Miyamae, K.Seki, H.Inokuchi, C.Tanaka, and J.Tanaka, to be published.

[12] M.J.Frisch, G.W.Trucks, M.Head-Gordon, P.M.W.Gill, M.W.Wong, J.B.Foresman, B.G.Johnson, H.B.Schlegel, M.A.Robb, E.S.Replogle, R.Gomperts, J.L.Andres, K.Raghavachari, J.S.Binkly, C.Gonzalez, R.L.Martin, D.J.Fox, D.J.Defrees, J.Baker, J.J.P.Stewart, and J.A.Pople, *Gaussian 92*, Revision C, Gaussian Inc., Pittsburgh, PA,1992.

[13] J.Tsukamoto, A.Takahashi, and K.Kawasaki, *Jpn. J. Appl. Phys.*, **29**, 125 (1990).

[14] K.Seki, H.Nakagawa, K.Fukui, E.Ishiguro, R.Kato, T.Mori, K.Sasaki, and M.Watanabe, *Nucl. Instr. Methods*, **A246**, 264 (1986).

[15] R.Pariser and R.G.Parr, *J. Chem. Phys.*, **21**, 456 (1953); R.Pariser and R.G.Parr, *J. Chem. Phys.*, **21**, 767 (1953); J.A.Pople, *Trans. Faraday Soc.*, **49**, 1375 (1953).

[16] J.J.Yeh and I.Lindau, *Atomic Data and Nuclear Data Tables*, **32**, 1 (1985).

[17] J.Tanaka, Y.Saito, M.Shimizu, C.Tanaka, and M.Tanaka, *Bull. Chem. Soc. Jpn.*, **60** (1987) 1595.

[18] T.-C.Chung, F.Moraes, J.D.Flood, and A.J.Heeger, *Phys. Rev.*, **B 29**, 2341 (1984).

[19] C.Tanaka and J.Tanaka, *Synth. Met.*, **41-43**, 3709 (1991)

[20] C.Tanaka and J.Tanaka, *Proc. Mat. Res. Soc.*, **247**, 577 (1991).

[21] J.Tanaka and C.Tanaka, in Conjugated Polymers and Related Materials, edited by W.R.Salaneck, I.Lundström, and B.Ranby (Proc. 81st Nobel Symp., Oxford University Press, London, 1993).

[22] J.Tanaka and C.Tanaka, *Prog. Theor. Phys. Suppl.*, **113**, 61 (1993).

[23] J.Tanaka, C.Tanaka, T.Miyamae, M.Shimizu, S.Hasegawa, K.Kamiya, and K.Seki, *Synth. Met.*, **65**, 173 (1994).

[24] T.Miyamae, M.Shimizu, and J.Tanaka, *Bull. Chem. Soc. Jpn.*, **67**, 2407 (1994).

[25] J.Voit, *Phys. Rev.* **B 47**, 6740 (1993); J.Voit, *J. Phys.* **CM5**, 8305 (1993).

[26] J.Voit, in The Physics and Mathematical Physics of the Hubbard model, edited by D.K.Campell, J.M.P.Carmelo, and F.Guinea (Proc. NATO Advanced Research Workshop, Plenum Press, New York, 1994).

[27] B.Dardel, D.Malterre, M.Grioni, P.Weibel, Y.Baer, J.Voit, and D.Jérôme, *Europhys. Lett.*, **24**, 687 (1993).

[28] B.Dardel, D.Malterre, M.Grioni, P.Weibel, and Y.Baer, *Phys. Rev. Lett.*, **67**, 3144 (1991).

[29] J.E.Ficher, P.A.Heiney, and J.Ma, *Synth. Met.*, **41-43**, 33 (1991).

[30] F.Saldi, M.Lelaurain, and D.Billaud, *Synth. Met.*, **41-43**, 63 (1991).

[31] T.Miyamae, T.Mori, K.Seki, and J.Tanaka, Submitted to *Bull. Chem. Soc. Jpn.*

4.5 Figure captions

Figure 1. Changes of the UPS spectra of Na-doped polyacetylene: (a) *trans*-polyacetylene, (b) lightly Na-doped, and (c) heavily Na-doped polyacetylene.

Figure 2. The expanded UPS spectra near E_F for (a) *trans*-polyacetylene, (b) lightly Na-doped, (c) heavily Na-doped polyacetylene, and (d) metallic Na evaporated film on Au film. The location of E_F is determined from the Fermi edge of Au evaporated film.

Figure 3. Changes of the UPS spectra of K-doped polyacetylene for increasing dopant concentration.

Figure 4. Expanded UPS spectra of K-doped polyacetylene in the low binding energy region.

Figure 5. The calculated density of states of (a) *trans*-polyacetylene, (b) lightly Na-doped charged soliton chain, and (c) heavily Na-doped polson chain.

Figure 6. The observed (solid line) and simulated (dotted line) UPS spectra of neutral and alkaline-metal doped polyacetylene; (a) *trans*-polyacetylene and isolated *trans*-$C_{20}H_{22}$ [23], (b) intermediately-doped polyacetylene, $[CHK_{0.06}]_x$, and the isolated charged soliton model compound ($C_{30}H_{32}Na_2$), and (c) heavily-doped polyacetylene, $[CHK_{0.10}]_x$ and the molecule of the polson structure ($C_{13}H_{15}Na_2$) put on the crystal lattice.

Figure 7. Projection of the heavily Na-doped polyacetylene crystal onto *ab* plane [23].

5. Ultraviolet Photoelectron Spectroscopy of Poly(pyridine-2,5-diyl), Poly(2,2'-bipyridine-5,5'-diyl), and Their K-doped States

5.1 Introduction

In this chapter we present the UPS study of poly(pyridine-2,5-diyl), poly(2,2'-bipyridine-5,5'-diyl), and their potassium doped states. Recently Yamamoto *et al.* have found that poly(pyridine-2,5-diyl) (PPy) and poly(2,2'-bipyridine-5,5'-diyl) (PBPy), that have analogous structures with poly(*p*-phenylene) (PPP), exhibit n-type electrically conducting properties [1-3]. These polymers can be easily reduced due to the π-deficient nature of pyridine. The reduction of PPy or PBPy starts about -1.9 V *vs* Ag/Ag^+ (0.34 V *vs* SCE) from the cycrlic voltammetry, and the the reduction peak appears at -2.43 V [4]. In contrast to the ease of reduction (n-doping), PPy (or PBPy) is electrochamically inactive in the anodic sweep range (0 ~ 1.7 V vs Ag/Ag^+) [4], whereas PPP and polythiophene show oxidation (p-doping) peaks at 1.10 ~ 1.34 [5,6] and 0.71 V, respectively. By Na-doping, the neutral PPy and PBPy ($\sigma < 10^{-14}$ Scm^{-1}) become semiconducting with a conductivity of 1×10^{-1} Scm^{-1} as measured with a compressed powder, while these polymers are inactive to electron acceptors [1]. Moreover, PBPy forms electrochemically active complexes with Ru and Ni [7]. A $RuCl_3$-PBPy system behaves as good catalyst for photoevolution of hydrogen in an aqueous medium [7].

In this work, we report UPS studies of PPy and PBPy, and discuss their electronic structures using the observed results. Analysis of the observed spectra were carried out with the aid of semiempirical PM3 molecular orbital calculations [8,9] for oligomers of PPy and PBPy, and also by comparison with other related molecules and conducting poly(arylene)s. We also studied the changes in electronic structure of PPy and PBPy upon in situ doping with potassium by UPS and optical absorption spectra, and examined the origin of the new bands appearing in the observed spectra.

5.2 Experimental

5.2.1 Potassium-Doping and UPS Measurements on PPy and PBPy.

The samples of PPy and PBPy were prepared by dehalogenation-polycondensation of 2,5-dibromopyridine and 5,5'-dibromo-2,2'-bipyridine, respectively, with Ni (0)-complex technique described elsewhere [1-3]. Photoelectron spectroscopic measurements were carried out on an angle-resolving UPS spectrometer at BL8B2 of UVSOR Facility, Institute for Molecular Science. Monochromatized synchrotron radiation of $h\nu$ = 40 eV obtained with a plane-grating monochromator [10] was used. Energy calibration of the spectrometer was carried out using the Fermi edge of gold film, which was vacuum-deposited on the molybdenum substrate before depositing polymer samples. Thin films of PPy and PBPy for UPS measurements were prepared on this gold-coated substrate by vacuum evaporation in the preparation chamber (base pressure 1×10^{-9} Torr, 1 Torr = 133.32 Pa), and was subsequently transferred to the measurement chamber with a base pressure of 1×10^{-10} Torr. It has been already known that these polymers can be evaporated keeping the polymer structure, although the molecular weight is somewhat reduced [4]. UPS spectra were measured for the normal emission from the sample surface with the incident angle of the light beam of 50° from the surface normal.

Potassium doping of PPy and PBPy was carried out *in situ* at 125 °C ± 5 °C using a SAES K-getter source in the preparation chamber. The getter was heated with a dc current of 5.8 A for potassium evaporation. Thickness of the films and the amount of potassium deposited onto the polymer films were monitored by a quartz thickness monitor. The thickness of the PPy and PBPy films was 10 - 30 nm. By limiting the photocurrent below 20 pA by inserting an appropriate mesh in the optical path, cherging effect could be avoided.

5.2.2 MO Calculations on PPy and PBPy.

The molecular orbital (MO) calculations for model molecules of PPy and PBPy were carried out with a MOPAC semiempirical PM3 [8,9] program on a SX-3R computer at the Computer Center of Institute for Molecular Science. Geometry optimization was carried out for two- and four-ring neutral oligomers of PPy and PBPy, and their molecular orbitals were calculated. We assumed planar molecular structures to simplify the calculations, although small torsion between pyridine rings is expected from the analogy with PPP oligomers [11]. In PBPy, only head-to-head (H - H) type (Scheme 1) connections exist. Although the H - H / H - T ratio of PPy is unknown, ^{1}H-NMR data of poly(3-methylpyridine-2,5-diyl) and poly(6-hexylpyridine-2,5-diyl) indicate the H - T contents of 65 and 55 percent [4], suggesting that PPy is also consists of both H - H and H - T units with comparable quantity. Since the analysis of sequence in the used PPy revealed that the contents of the H - H units are lower than that of H - T units [4], we used head-to-tail (H - T) type oligomers (Scheme 1) for comparison of the UPS data.

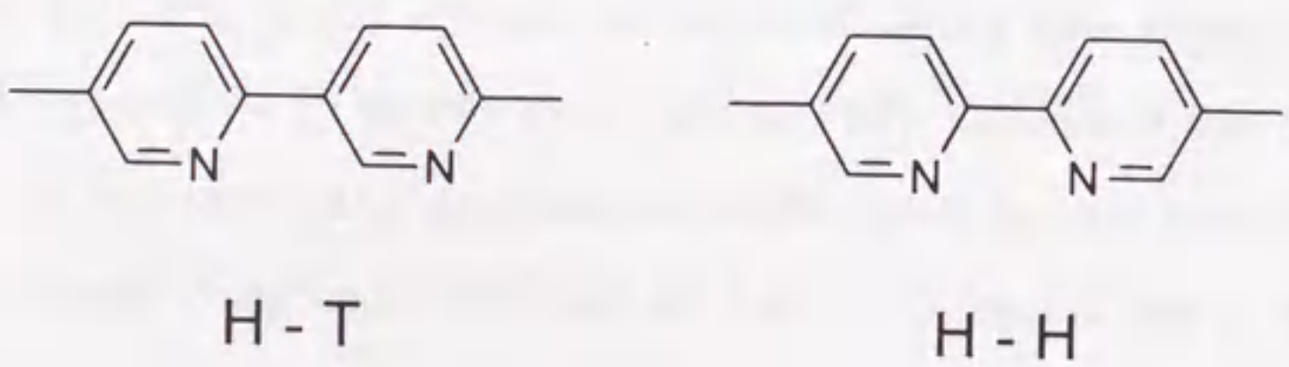

H - T H - H

Scheme 1

5.3 Results and discussion

5.3.1 UPS spectra of neutral PPy and PBPy

5.3.1-1 UPS spectra of PPy and PBPy

Figure 2 shows the UPS spectra of PPy (a) and PBPy (b) at the incident photon energy $h\nu = 40$ eV. The abscissa is the binding energy E_b from the vacuum level. From the UPS spectra of PPy and PBPy, the threshold energies I_{th}, which were determined from the righthand onset T, for photoemission from the solid films were found to be 6.3 eV, 6.35 eV, respectively. Six features (A-F) are seen in the UPS spectrum of PPy at 7.1, 9.2, 12.4, 15.0, 18.8, and 22.7 eV, respectively, while those of PBPy are seen at 7.0, 9.0, 12.4, 14.6, 18.6, and 22.7 eV, respectively. Principally these two spectra resemble each other, indicating analogous electronic structures. To compare with these, in Fig. 2 we also show the orbital energies obtained from the PM3 semiempirical calculations of four-ring pyridine oligomers by vertical lines and the simulated spectra obtained as the density of states (DOS) by convoluting the delta functions at each orbital energy with a Gaussian function of 0.5 eV FWHM. For a better fit with the solid-state UPS data, orbital energies and simulated spectra were shifted to higher binding energies by 1.4 eV for PPy and 1.2 eV for PBPy. One should note that these spectra have heen observed for solid polymer samples, while the DOS is calculated for an isolated model compounds. This shifts are due to two reasons; one is due to the electronic polarization of the surrounding molecules [12], and the other is due to the fact that theoretical calculations are perfomed on oligomers which have planer conformations. The simulated spectra are also similar, indicating that the difference in H - H and H - T connections does not significantly affect the electronic structures of neutral polymers.

5.3.1-2 Comparison with the results of MO calculations

We will hereafter focus our attention on the uppermost occupied states, since they are most important for determining the doping behavior and electronic properties. The features A and B can be interpreted in a similar way to those for PPP [13], poly(*p*-phenylene sulfide) (PPS) [14], and poly(*p*-phenylenevinylene) (PPV) [15] as follows. In Fig. 3 we illustrate the correlation among the calculated energy levels of pyridine, 2,2'-bipyridine, and 2,3-bipyridine molecules (Fig. 3 (b)), and the corresponding correlation among experimentally observed levels of pyridine solid [16] and PPy (Fig. 3 (a)). It is known that the top part of the occupied states of pyridine is formed by the three orbitals shown in Fig. 4 (a), which are well separated in energy from other orbitals. They consist of the $11a_1$ (n) orbital originating from the lone pair electrons of the nitrogen atom and $1a_2$ and $2b_1$ π orbitals, as depicted in Fig. 3 (b). The assignments of the observed peaks of pyridine solid are conformable to the assignments of the Penning ionization electron spectroscopy [17]. The uppermost part of the occupied states of PPy should be also formed by these three orbitals. In the calculated energy levels of bipyridines, two of them with $2b_1$ and $11a_1$ symetry do not strongly interact with the neighboring pyridine ring due to the small contribution from the bridge-head C atoms. On the other hand, the $1a_2$ π orbital strongly interacts with the corresponding π levels of neighboring pyridine ring to form the well split bonding and anti-bonding states.

In a long PPy (or PBPy) chain, this $1a_2$ level forms a widely dispersed π band. The $11a_1$ and $2b_1$ orbitals form the bands with smaller dispersion. These aspects are actually seen in the MO results used for the simulation in Fig. 2. The correspondence among observed and simulated UPS spectra of PPy and PBPy are quite good in this region, and we can easily assign the peak A in the UPS spectra to the top of the dispersive and well delocalized π band derived from the $1a_2$ level, and peak B to the less dispersive band derived from the $11a_1$ and $2b_1$ levels, respectively. The dispersion of the $11a_1$ and $2b_1$ derived orbitals, although not large, gives rise to the broadeness of the peak B of the spectra of PPy and PBPy.

5.3.1-3 Comparison with Other Pyridine-Derived Systems

The considerations described above are confirmed by the comparison with the results for other related molecules in Fig. 4. Here we show the UPS spectra of pyridine vapor (a) [18], 2,2'-bipyridine vapor (b) [19], 2,2':6',2":6",2"'-quarterpyridine vapor (c) [20], and PPy (d). The vapor phase spectra (a), (b), and (c) are shifted by 1.0, 0.8, 0.2 eV to the low binding energy side, respectively, for achieving the best correspondence with the solid spectra. This shift corresponds to the solid-state stabilization of the photo-formed cation due to electronic polarization of the surroundings [12]. In Fig. 4, we find a good correspondence among the spectra of 2,2'-bipyridine (c), 2,2':6',2":6",2"'-quarterpyridine vapor (c) and PPy (d).

These trends can be explained by a similar consideration of interaction among pyridine units as that for PPy described above, although the connecting positions are not common among these compounds. In the $1a_2$ orbital of pyridine (Fig. 3), C atoms at 5 and 6 sites have the same phase and electron density. Therefore the interaction between the $1a_2$ orbitals caused by 2,6-bonding in Fig. 4 (c) will be similarly effective as that by the 2,5-bonding. In contrast, the $11a_1$ and $2b_1$ orbitals do not interact strongly through the bonding at the 2,6-sites, because of the small contribution from the C atoms at these sites. This small interaction is also similar with the case of 2,5-bonding. In the case of 4,4'-bipyridine [19], on the other hand, the $11a_1$ orbital strongly interacts through the bonding at the 4 sites. Thus we can ascribe the resemblance among the UPS spectra of 2,6-oligomers and PPy to the similarity in the contribution from the 5 and 6 positions to the MOs of pyridine.

5.3.1-4 Comparison with Other Polymers

The key parameters in discussing the electronic structure of conducting polymers are the ionization potential (I_{th}), electron affinity (E_a), and band gap (E_g). In

Table 1, we compare these values for PPy and PBPy with those of other π-conjugated conducting polymers. They give a measure of the ease of carrier formation by doping.

The values of I_{th} of PPy and PBPy indicate that acceptor doping to these polymers should be difficult due to the large I_{th}. Their values, 0.7 eV larger than that of PPP [13], are consistent with the fact that even the treatment of PPy with a strong oxidant AsF_5 does not give electrically conducting property to PPy (9.7×10^{-12} Scm^{-1}) [4]. In contrast, PPP can release the π electrons upon interaction with AsF_5 to give the p-doped state showing the conducting property (500 Scm^{-1}) [21]. The electron affinities (E_a) of PPy and PBPy, which are estimated from the relation $E_a = I_{th} - E_g$, are larger than that of other π-conjugated conducting polymers, indicating the ease of carrier formation by donor doping. This trend was already pointed out by electrochemical measurements [4]. The ease of oxidation and reduction of aromatic polymers reflects the ease of oxidation (abstraction of electron) and reduction (addition of electron) of the monomer unit [3]. The values of E_a of pyridine, benzene, and pyrrole are -0.62, -1.15, and -2.38 eV, respectively [22], and the order of these values is in good agreement with that for the E_a of corresponding polymers as tabulated in Table 1. It isgenerally accepted in the field of organic chemistry that pyridine shows electron-donating Lewis base nature, originating from the lone pair electrons of nitrogen, while its 6π-conjugation system has an electron-deficient character [23]. π-defitient systems are expected to stabilise the highest occupied molecular orbital because of the decreased electron density on the carbon ring, resulting in large E_a and I_{th}. Thus we can conclude that the PPy and PBPy have electron-accepting property due to the π-deficient nature of pyridine.

5.3.2 UPS spectra of Potassium-doped PBPy

In Fig. 5, we show the UPS spectra of K-doped PBPy for increasing doping levels in the most intriguing energy region from E_{vac} to binding energy E_b = 14 eV. The average potassium content for the most heavily doped film (Fig. 5 g) was determined by Auger electron spectroscopy (AES) to be 2.5 K-atoms per pyridine ring. At this stage, K metallic layers may be formed on the polymer surface. The K concentrations for intermediate stages were estimated from the exposure time to K vapor, resulting in 0.2 ± 0.1 (d), 0.5 (e), and 1(f) K-atom per pyridine ring, respectively.

At the initial stage of K doping, two new peaks X and Y appear in the energy gap region. With increasing K content, the peak X gradually grows up. Also the peak B shows decrease of intensity with increasing K content. At the final stage of doping (g), peak B shifts back slightly to the lower binding energy. We also observed a fairly large change of work function ϕ (energy difference between E_F and vacuum level) determined from the low-energy cutoff of the UPS spectra (not shown), as shown in Fig. 6. At the initial stage of doping, ϕ shows a large decrease of 0.83 eV. On further doping, only a small additional decrease of 0.45 eV occurs at the doping stage of one K atom per ring (f).

The intensity of the peak X appearing in the originally empty electron energy gap increases with doping, as shown in Fig. 5, while that of peak Y seems to be almost constant. The possibility of these peaks being emission from K metal can be examined by the data in Fig. 7, which shows the UPS spectra of K-doped PBPy and metallic thick K film (ca. 400 Å) deposited on this film. With the 40 eV radiation, the cross section for K 4*s* levels is very low [23]. The intensity of the 4*s* emission observed for the metallic K layer is approximately one order of magnitude lower than that for the gap states in K-doped PBPy. These results clearly indicate that the gap states cannot be assigned to emission from the 4*s* levels of metallic K adsorbed onto the polymer, but should be derived from the orbitals of carbon 2*p* character.

The two gap states X and Y are at 3.7 and 5.5 eV from the vacuum level, being separated by 1.8 eV. Similar observation has been reported in the UPS study of Na-doped PPV by Fahlman *et al.* [24]. While the band gap of PPV (2.5 eV) [25] is 0.4 eV smaller than that of PBPy (2.95 eV) [4], their peak positions are similar among them. There are two ways in which these aromatic polymers can accept the added charges; forming two polaron bands or two bipolaron bands in the originally empty electron energy gap. Fahlman *et al.* [24] pointed out from the valence effective Hamiltonian calculation that the two polaron bands would lead to a large broadening of the polaron peaks in the UPS spectra with a finite density of states at Fermi level, while polaron formation will result in only a peak with a shallow valley in the band gap region. On the other hand, the two bipolaron bands would lead to two well separated peaks in the UPS spectra and there should not be any finite density of states at the Fermi level [25]. Thus the gap states observed here can be ascribed to two well-separated bipolaron peaks.

Following the calculations by Brédas *et al.* for alkali-metal doped quarterphenyl [26,27], the gap state at 3.7 eV (peak X) of K-doped PBPy can be assigned to the lowest unoccupied molecular orbital (LUMO) of PBPy filled by electron donated from K atoms and stabilized by geometric relaxation, and the 5.5 eV states (peak Y) to the destabilized highest occupied molecular orbital (HOMO). The UPS spectra of K-doped PBPy are in good correspondence with predicted bipolaron states of Brédas *et al.* for Na-doped quarterphenyl [26]. The formation of bipolaron states should lead to a substantial shift of E_F relative to the vacuum level. This is experimentally observed as the decrease in the work function ϕ (Fig. 6) and increase of the binding energy of the deeper orbitals relative to the Fermi level.

These assignments can be further tested by examining the optical absorption. In Fig. 8 we show the change in the electronic spectra of heavily K-doped PBPy film caused by the compensation of dopant by H_2O in air. The curve 0 is the spectrum of a PBPy film cast from formic acid solution before K-doping, and curve 1 is that of a heavily doped film. The undoped PBPy film exhibits a peak at 3.0 eV, corresponding

of the interband transition. At the saturated doping level (curve 1), two new broad peaks are seen at 0.9 eV and 2.7 eV. The energies of the these new bands are different from those of absorption bands (1.5 and 2.23 eV) of the cation radical of 2,2'-bipyridine (Na^+bpy^-) [28]. The interval between the doping-induced two bands is 1.8 eV, which is consistent with the interval of the gap states observed in the UPS spectra.

After measuring these spectra, the sample was exposed to air diluted with Ar. The intensities of the doping-induced bands decreased and the intensity of the interband transition is increased by the reaction of the K-doped film with H_2O. A side reaction, such as bond cleavage, can be excluded since the final curve 8 in Fig. 8 is coincident with that of a native PBPy film (curve 0). The presence of bipolarons on polymer chains will result in the possibility of two optical transition below the band gap transition: for n-type doping, from the lower bipolaron level to the conduction band and from the upper bipolaron level to the conduction band [27]. In the case of polaron formation, a third absorption is possible below the gap, corresponding to an optical transition between the two polaron levels. The changes of the absorption spectra of K-doped PBPy resemble that for heavily ClO_4^--doped PP [29] and AsF_5-doped PPV [30]. For AsF_5-doped PPV, two peaks were found at 0.8 and 2.1 eV, which are assigned to the bipolaron excitations [30]. The appearance of two doping-induced absorption bands in PBPy at K-doped states thus confirms the bipolaron formation.

Next we will discuss the change of peak B. Its intensity decreases continuously with increasing K-doping. This means that the $2b_1$ (π) and $11a_1$ (n) molecular orbitals forming peak B, with large contributions from the N atom of pyridine ring, strongly interact with the K cations. This suggests that the K cations are preferentially located close to the N atoms of bipyridine unit. The shift of peak B towards lower binding energy side (g) may be ascribed to the enhanced screening of the photoformed hole by free carriers created by doping.

5.3.3 UPS spectra of Potassium-doped PPy

Figure 9 shows the UPS spectra of neutral and increasingly K-doped PPy. The doping steps and conditions were carefully controlled to be similar to the corresponding stages of doping of PBPy film in Fig. 5. The potassium content for the most heavily doped film (Fig. 9 g) was also to be 2.5 K-atoms per pyridine ring, as in the case of K-doped PBPy. At the initial stage of doping (Fig. 9 b), the UPS spectra of PPy show smaller change than in the PBPy. The work function (ϕ) decreased only by 0.36 eV (Fig. 6), which is much smaller than the value of 0.83 eV for PBPy. At intermediate stages of doping up to 0.5 K-atom per pyridine ring (Fig. 9 e), only a slight decrease in the value of ϕ occurs (Fig. 6) and the relative intensity of the peak B in the UPS spectra also shows little decrease. The formation of bipolaron states is expected to cause a substantial rise of E_F relative to the vacuum level, as seen in the preceding section. At the last stage of doping (Fig. 9 f), we see a large change of work function (1.08 eV), and the intensity of the peak B shows a large decrease. At the last stage of doping (f), two gap states X and Y appear at the same positions with those of PBPy, and they can be assigned to bipolaron bands. The peak can be recognized, and the energy position of peak B is shifted toward lower binding energy (Fig. 9 g). This low energy shift can be assigned with relaxation due to electronic screening as in the case of PBPy. Thus we can summerize that PPy is slow in changing by K-doping, although the heavily doped state is similar to that of PBPy.

As for the reason why PPy requires higher dopant concentration to create bipolarons than PBPy, it is suggestive that Yamamoto *et al.* found that PBPy forms electrochemically active transition metal complex with Ru(II), Ni(II), Ni(I), and Fe(III) [3,4] due to the chelating ability accompanied by the head-to-head (H - H) structure of PBPy (Scheme 1). In contrast to PBPy, PPy has only a weak coordinating ability toward the metals, presumably because of the mainly head-to-tail (H - T) structure of PPy. Thus we can conclude that more effective doping to PBPy comes from its strong ability to coordinate with potassium, while it is almost absent in PPy.

5.4 References

[1] T.Yamamoto, T.Ito, K.Sanechika and M.Hishinuma, *Synth. Met.*, **25**, 103 (1988).

[2] T.Yamamoto, Z.-H.Zhou, T.Kinbara and T.Maruyama, *Chem. Lett.*, 223 (1990).

[3] T.Yamamoto, *Prog. Polym. Sci.*, 7, 1153 (1992).

[4] T.Yamamoto, T.Maruyama, Z.-H.Zhou, T.Ito, T.Fukuda, Y.Yoneda, F.Begum, T.Ikeda, S.Sasaki, H.Takezoe, A.Fukuda, and K.Kubota, *J. Am. Chem. Soc.*, **116**, 4832 (1994).

[5] G.Schiavon, G.Zotti, and G.Bontempelli, *J. Electroanal. Chem. Interfacial Electrochem.*, **161**, 323 (1984).

[6] T.Yamamoto, H.Wakayama, T.Fukuda, and T.Kanbara, *J. Phys. Chem.*, **96**, 8677 (1992).

[7] T.Yamamoto, Y.Yoneda, and T.Maruyama, *J. Chem. Soc. Chem. Commun.*, 1652 (1992).

[8] J.J.P.Stewart, *J. Comput. Chem.*, **10**, 209 (1989).

[9] J.J.P.Stewart, *J. Comput. Chem.*, **10**, 221 (1989).

[10] K.Seki, H.Nakagawa, K.Fukui, E.Ishiguro, R.Kato, T.Mori, K.Sasaki, and M.Watanabe, *Nucl. Instr. Methods*, A**246**, 264 (1986).

[11] J.L.Baudour, Y.Delugeard, and P.Rivet, *Acta Cryst.*, B**34**, 625 (1978).

[12] L.E.Lyons, *J. Chem. Soc.*, 5001 (1957).

[13] K.Seki, U.Karlsson, R.Engelhardt, E.E.Koch, and W.Schmidt, *Chem. Phys.*, **91**, 459 (1984).

[14] S.Asada, K.Seki and H.Inokuchi, *Chem. Phys. Lett.*, **130**, 155 (1986).

[15] K.Seki, S.Asada, T.Mori H.Inokuchi, I.Murase, T.Ohnishi and T.Noguchi, *Solid State Commun.*, **74**, 677 (1990).

[16] K.Y.Yu, J.C.McMenamin, and W.E.Spicer, *Surf. Sci.*, **50**, 149 (1975); J.-H.Fock, J.Schmidt-May, and E.-E.Koch, *J.Electron Spectrosc.*, **34**, 225 (1984).

[17] T.Suzuki, T.Hirooka, T.Kondow, and K.Kuchitsu, *Surf. Sci.*, **158**, 515 (1985).

[18] K.Kimura, S.Katsumata, Y.Achiba, T.Yamazaki, and S.Iwata, "Handbook of He I Photoelectron Spectra of Fundamental Organic Molecules" Japan Scientific Societies Press, Tokyo (1981).

[19] J.P.Maier and D.W.Turner, *Faraday Disc. Chem. Soc.*, **54**, 149 (1972).

[20] I.Novac and L.Klasinc, *Z. Naturforsch.*, **33a**, 247 (1978).

[21] L.W.Shacklette, R.R.Chance, D.M.Ivory, G.G.Miller, and R.H.Baughman, *Synth. Met.*, **1**, 307 (1980).

[22] M.T.Bowers, Gas Phase Ion Chemistry, vol. 2, Academic Press, New York, 1979; K.D.Jordan and P.D.Burrow, *Acc. Chem. Res.*, **11**, 341 (1978).

[23] G.R.Newkome and W.W.Paudler, Contemporary Heterocyclic Chemistry, John Wiley, New York (1982).

[24] J.J.Yeh and I.Lindau, *Atomic Data and Nuclear Data Tables*, **32**, 1 (1985).

[25] M.Fahlman, D.Beljonne, M.Lögdlund, R.H.Friend, A.B.Holmes, J.L.Brédas and W.R.Salaneck, *Chem, Phys. Lett.*, **214**, 327 (1993).

[26] "Handbook of Conducting Polymers. vols. 1 & 2", Ed. by T.Skotheim, Marcel Dekker, New York, 1986.

[27] J.L.Brédas, B.Thémans, J.G.Fripiat, J.M.André and R.R.Chance, *Phys. Rev. B* **29**, 6761 (1984).

[28] J.L.Brédas and G.B.Street, *Acc. Chem. Res.*, **18**, 309 (1985).

[29] Y.Kaizu and H.Kobayashi, *Bull. Chem. Soc. Jpn.*, **45**, 470 (1972).

[30] K.Yakushi, L.J.Lauchlan, T.C.Clarke, and G.B.Street, *J. Chem. Phys.*, **79**, 4774 (1983).

[31] J.Obrzut, and F.E.Karasz, *J. Chem. Phys.*, **87**, 6718 (1987).

[32] S.Hino, K.Iwasaki, and K.Matumoto, *Bull. Chem. Soc. Jpn.*, **63**, 2199 (1990).

5.5 Figure Captions

Figure 1. The molecular structures of PPy (a) and PBPy (b).

Figure 2. UPS spectra of PPy (a) and PBPy (b) evaporated films at the incident photon energy of 40 eV. Observed (solid line) and simulated (dotted line) UPS spectra. The virtical lines indicate the orbital energies calculated for the four-ring oligomers. The vacuum level (E_{vac}) is taken as the origin of the energy scale.

Figure 3. The correlation of the energy levels among the experimentally observed upper ocupied levels (a) of pyridine solid [16] and PPy, and the correlation of the calculated energy levels (b) among pyridine, 2,2'-bipyridine, and 2,5-bipyridine molecules.

Figure 4. UPS spectra of (a) pyridine vapor [18], (b) 2,2'-bipyridine vapor [19], (c) 2,2':6',2":6",2"'-quarterpyridine vapor [20], and (d) PPy film. The vapor spectra (a) and (b) are shifted by 1.0 eV to the low binding energy side for achieving the best correspondence with the solid spectra [12]. The dashed lines show the correlation of the uppermost level being shifted lower binding energy with increasing pyridine unit.

Figure 5. UPS spectra of neutral and increasingly K-doped PBPy. The abscissa is the binding energy from the vacuum level.

Figure 6. Change of the work function ϕ of the PBPy (open circles) and PPy (filled circles) upon K-doping. The K content (x) on the abscissa was estimated from the exposure time to K vapor. For details, see text.

Figure 7. UPS spectra of (a) K-doped PBPy and (b) metallic K thick film on the K-doped PBPy.

Figure 8. Absorption spectral change of K-doped PBPy film by exposure to air diluted with Ar.

Figure 9. UPS spectra of neutral and increasingly K-doped PPy. The abscissa is the binding energy from the vacuum level.

Table I. Comparison of ionization threshold (I_{th}), band gap (E_g), and electron affinity (E_a).

polymer	Abbreviation	I_{th}	E_g	E_a[a]	References[b]
		eV	eV	eV	
poly(2,5-pyridinediyl)	PPy	6.3	2.82[c]	3.5	this work
poly(2,2'-bipyridine-5,5'-diyl)	PBPy	6.35	2.95[c]	3.4	this work
poly(*p*-phenylenesulfide)	PPS	6.0	3.4 [c]	2.6	[14]
poly(*p*-phenylene)	PPP	5.65	2.93 [c]	2.2	[13]
poly(*p*-phenylenevinylene)	PPV	5.2	2.4 [c]	2.7	[15]
polypyrrole	PP	4.0	2.5 [c]	0.4	[32]

[a] E_a values are estimated from the simple equation, $E_a = I_{th} - E_g$, where E_g is the band gap.

[b] Experimental I_{th} values are taken from the UPS of solid films.

[c] E_g values are estimated from the edge of the absorption spectra of solid film [4,30,31].

6. Appendix

For further discussing the orientational effect on the electronic structure of polyacetylene, we introduce the orientational order parameter $\overline{P}_2$ which was described by Jen *et al.* [1] We consider two coordinate systems: (1) the laboratory frame (x, y, z) fixed with respect to the polyacetylene film and chosen to reflect the macroscopic symmetry of the system; and (2) the molecular frame (1, 2, 3) fixed on the polyacetylene chain and chosen by considering the molecular symmetry. The z-axis is taken to be parallel to the stretching direction, and the 3-axis parallel to the major chain axis. The orientation of a particular polyacetylene chain is described by the three Euler angles (α,β,γ) that link the two coordinate systems. The orientational order of the polymer chain is described by a distribution function $f(\alpha,\beta,\gamma)$, which can be expanded by the generalized spherical harmonics,

$$f(\alpha,\beta,\gamma)=\sum_{n=0}^{\infty}\sum_{m'm}^{n}\frac{2n+1}{8\pi^2}a_{m'm}^{(n)}D_{m'm}^{(n)}(\alpha,\beta,\gamma), \tag{A.1}$$

with

$$a_{m'm}^{(n)}=\int_0^{2\pi}d\alpha\int_0^{\pi}\sin\beta d\beta\int_0^{2\pi}d\gamma\, D_{m'm}^{(n)*}(\alpha,\beta,\gamma)f(\alpha,\beta,\gamma)=\left\langle D_{m'm}^{(n)*}(\alpha,\beta,\gamma)\right\rangle, \tag{A.2}$$

where $D_{m'm}^{(n)}(\alpha,\beta,\gamma)$ are the Wigner matrices [2] and $\langle\cdots\rangle$ represents the thermal average. The distribution function, Eqn. (A.1), can be simplified and the number of nontrivial order parameters can be reduced by imposing the known symmetries of the individual constituent molecules and macroscopic symmetry. For a uniaxial macroscopic phase with the unique axis parallel to the z axis, the distribution function is independent of α, and only the terms with $m' = 0$ contribute to the summation. If the polyacetylene chains are made up by cylindrically symmetrical rigid rods, we obtain

$$f_{\hat{u}}(\beta)=\int_0^{2\pi}d\alpha\int_0^{2\pi}d\gamma\, f(\alpha,\beta,\gamma)=\sum_{n=even}\frac{2n+1}{2}\overline{P}_nP_n(\cos\beta), \tag{A.3}$$

and

$$\overline{P}_n = \int_0^{\pi} \sin\beta d\beta \, P_n(\cos\beta) \, f_{\hat{u}}(\beta) = \langle P_n(\cos\beta) \rangle \,, \qquad \text{(A.4)}$$

where $P_n(\cos\beta)$ are the Legendre polynomials and $\hat{u}$ is the unit vector along the symmetry axis of the molecule.

The second order parameter, $\overline{P}_2$, is thus given by

$$\overline{P}_2 = \langle P_2(\cos\theta) \rangle = \frac{1}{2} \langle 3\cos^2\theta - 1 \rangle, \qquad \text{(A.5)}$$

where θ is the angle between the axis of individual polymer chain direction and macroscopic symmetry axis. The order parameter $\overline{P}_2$ vanishes in isotropic media, while it takes non-zero value in an ordered media. It is equal to unity when the chain is completely aligned. The dichroic ratio R is given by using $\overline{P}_2$ as,

$$R = \frac{1 + 2\overline{P}_2}{1 - \overline{P}_2} \qquad \text{(A.6)}$$

It is assumed that the polymer chains are linear and that each chain has a series of independent absorbing groups, in which the transition dipole moments are inclined at a common angle α to the chain axis. The order parameter $\overline{P}_2$ of the polyacetylene films are estimated from the dichroic ratio of the band at 1360 cm^{-1}, which is characteristic of the charged soliton. This band appears for whole doping range and its polarization should be parallel to the chain axis [3]. From the dichroic ratio R, we could obtain the second order parameter $\overline{P}_2$ as follows by allowing α to tend to be zero [4]. The order parameter is obtained according to the following equation;

$$\overline{P}_2 = \frac{R - 1}{R + 2}. \qquad \text{(A.7)}$$

References

[1] S.Jen, N.A.Clark, P.S.Perchan, and E.B.Priestly, *J. Chem. Phys.*, **66**, 4635 (1977).
[2] M.E.Rose, "Elementary Theory of Angular Momentum," Wiley, New York (1957).
[3] G.Zannoni and G.Zerbi, *J. Mol. Strust.*, **100**, 505 (1983).
[4] R.D.B.Fraser, *J.Chem. Phys.*, **28**, 1113 (1958).

7. Figures in Chapter 2

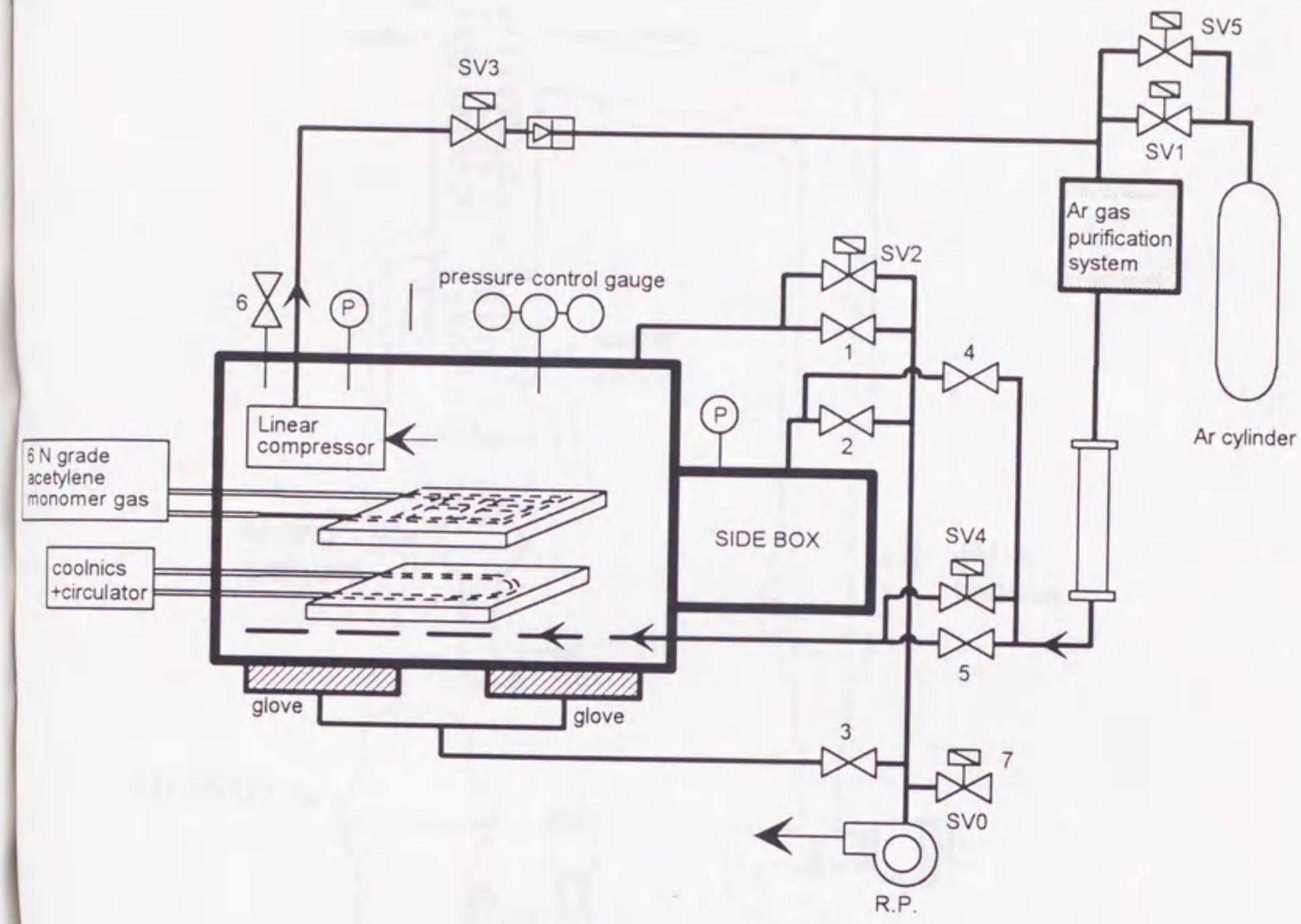

: solenoid valve

: hand-operated valve

Figure 1

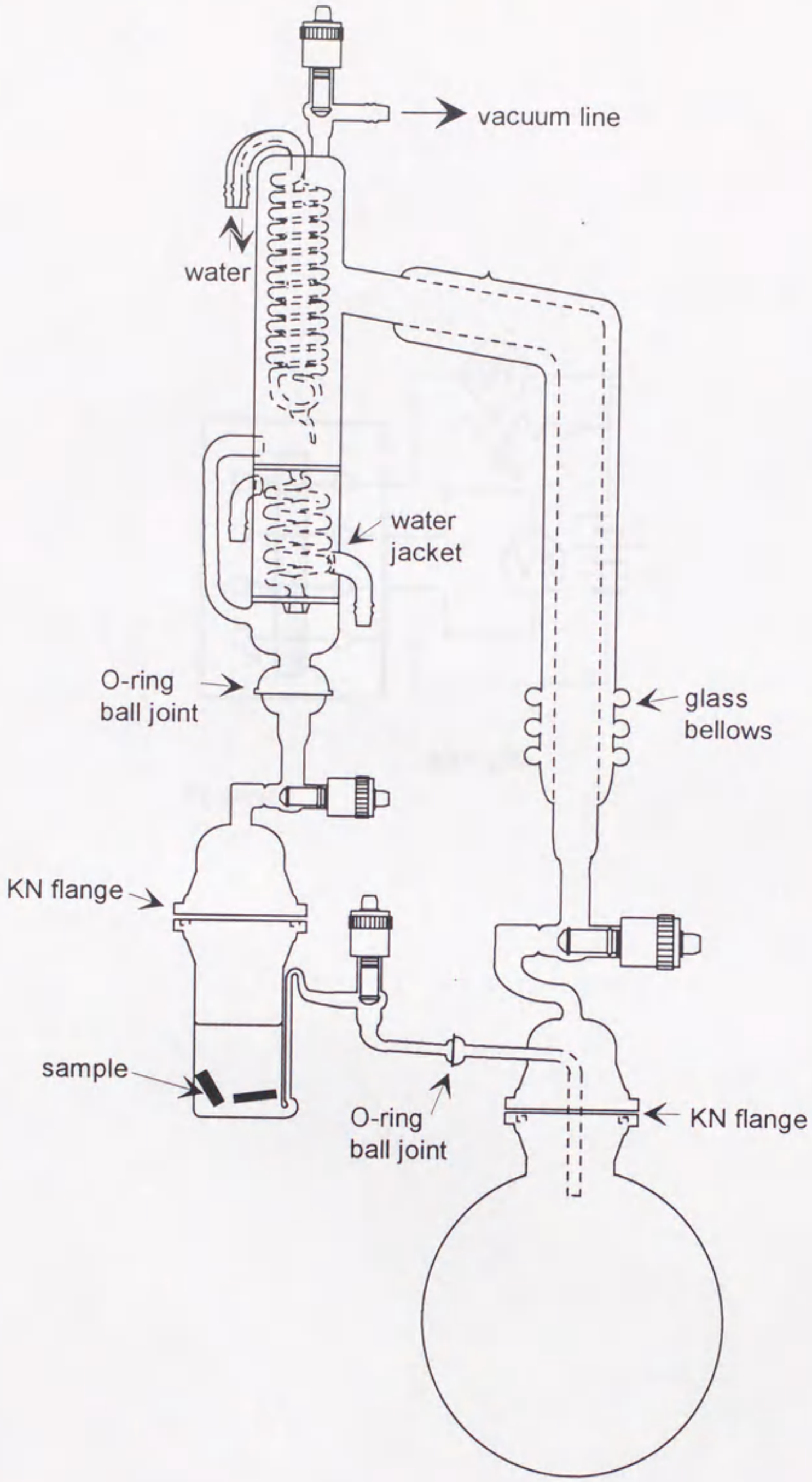
vacuum line
water
water
jacket
O-ring
ball joint
glass
bellows
KN flange
sample
O-ring
ball joint
KN flange

Figure 2

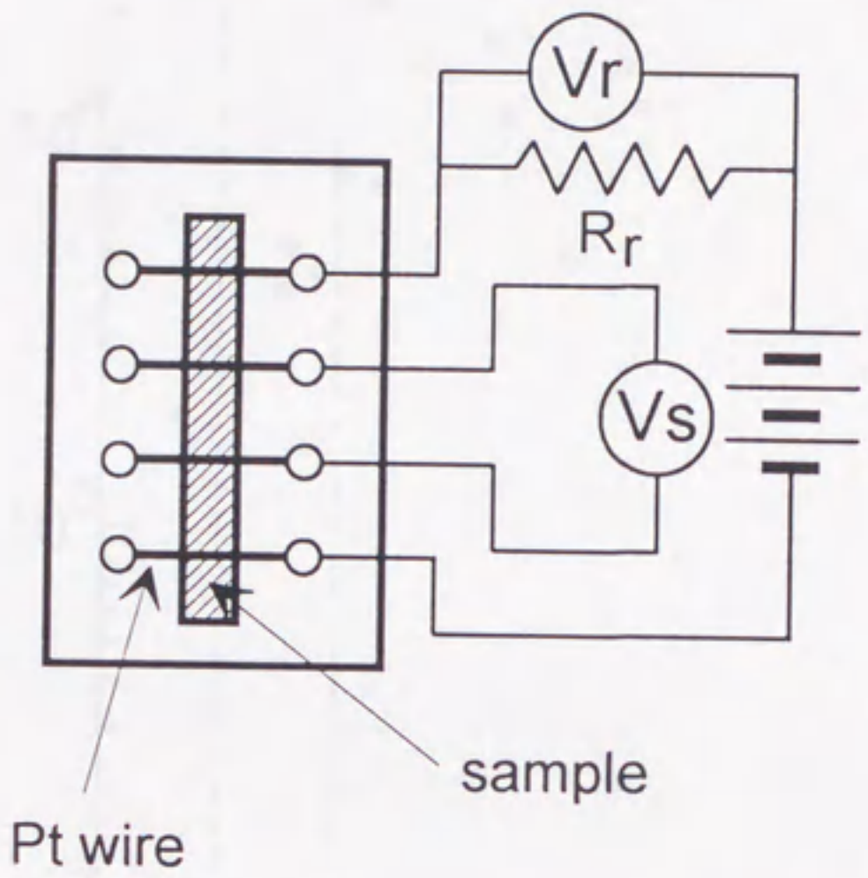

Figure 3

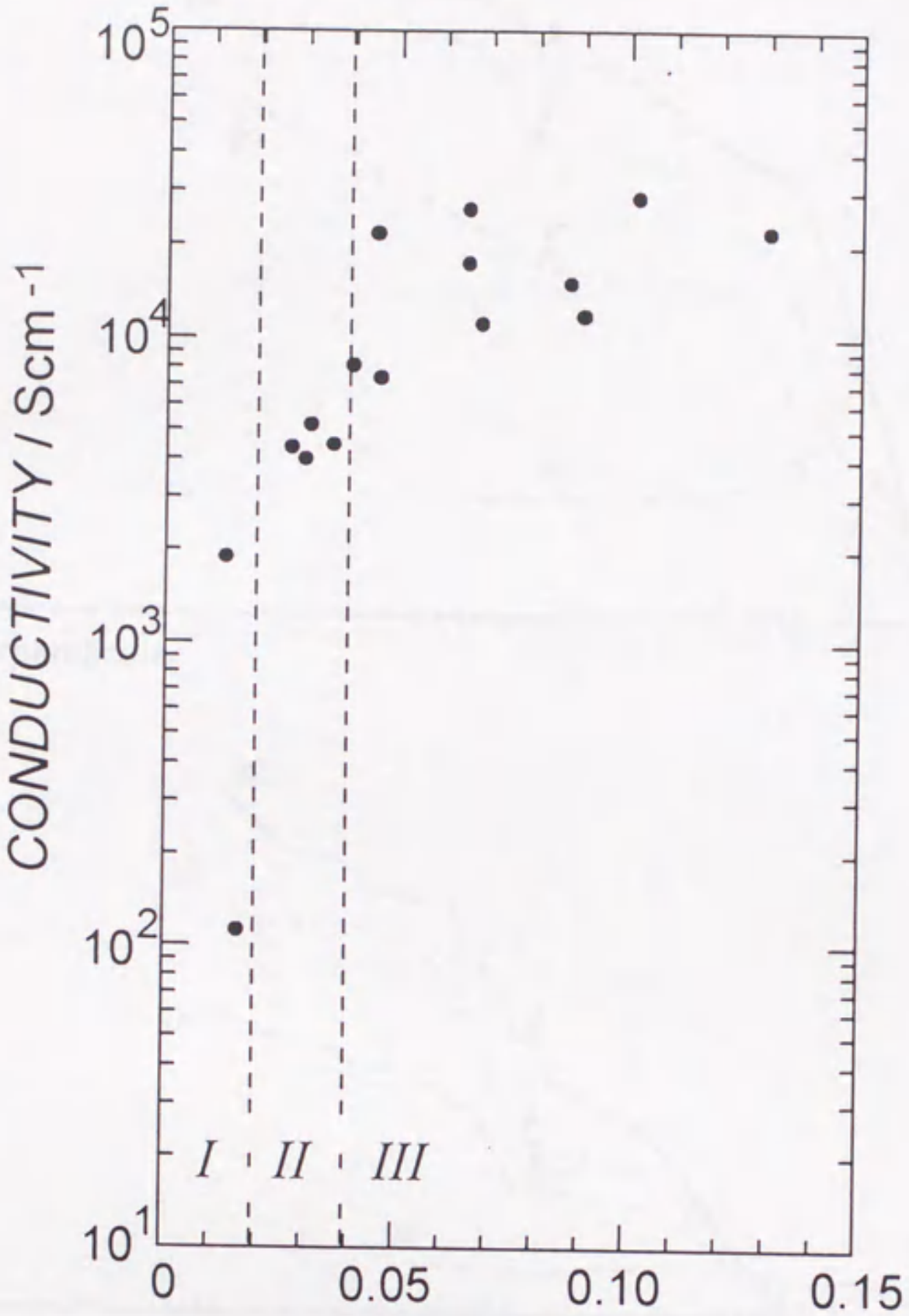
10^5
10^4
10^3
10^2
10^1
CONDUCTIVITY / Scm^{-1}
I
II
III
0
0.05
0.10
0.15
CONCENTRATION, y

Figure 4

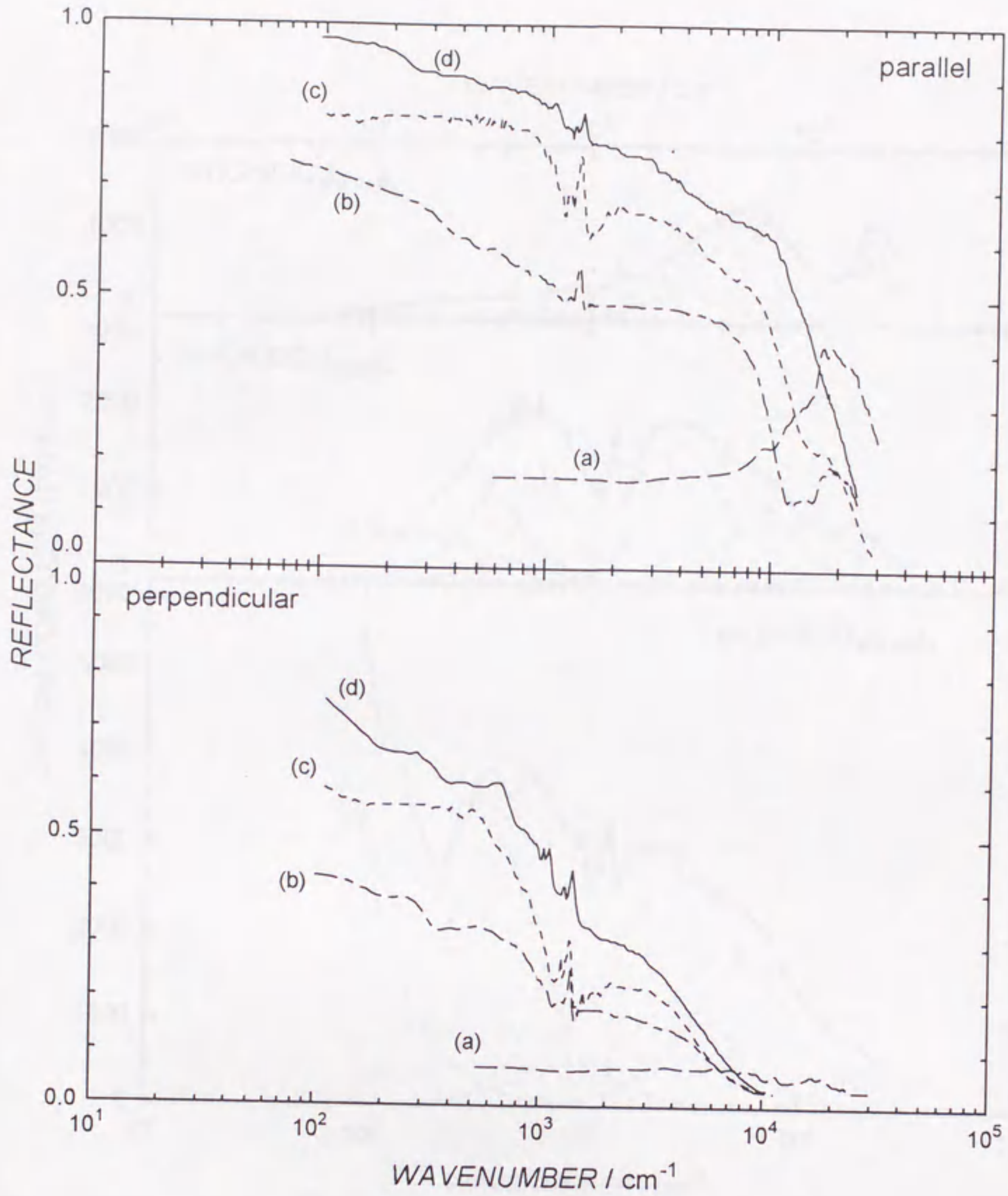
1.0
0.5
0.0
REFLECTANCE
parallel
perpendicular
(a)
(b)
(c)
(d)
10^1
10^2
10^3
10^4
10^5
WAVENUMBER / cm^{-1}

Figure 5

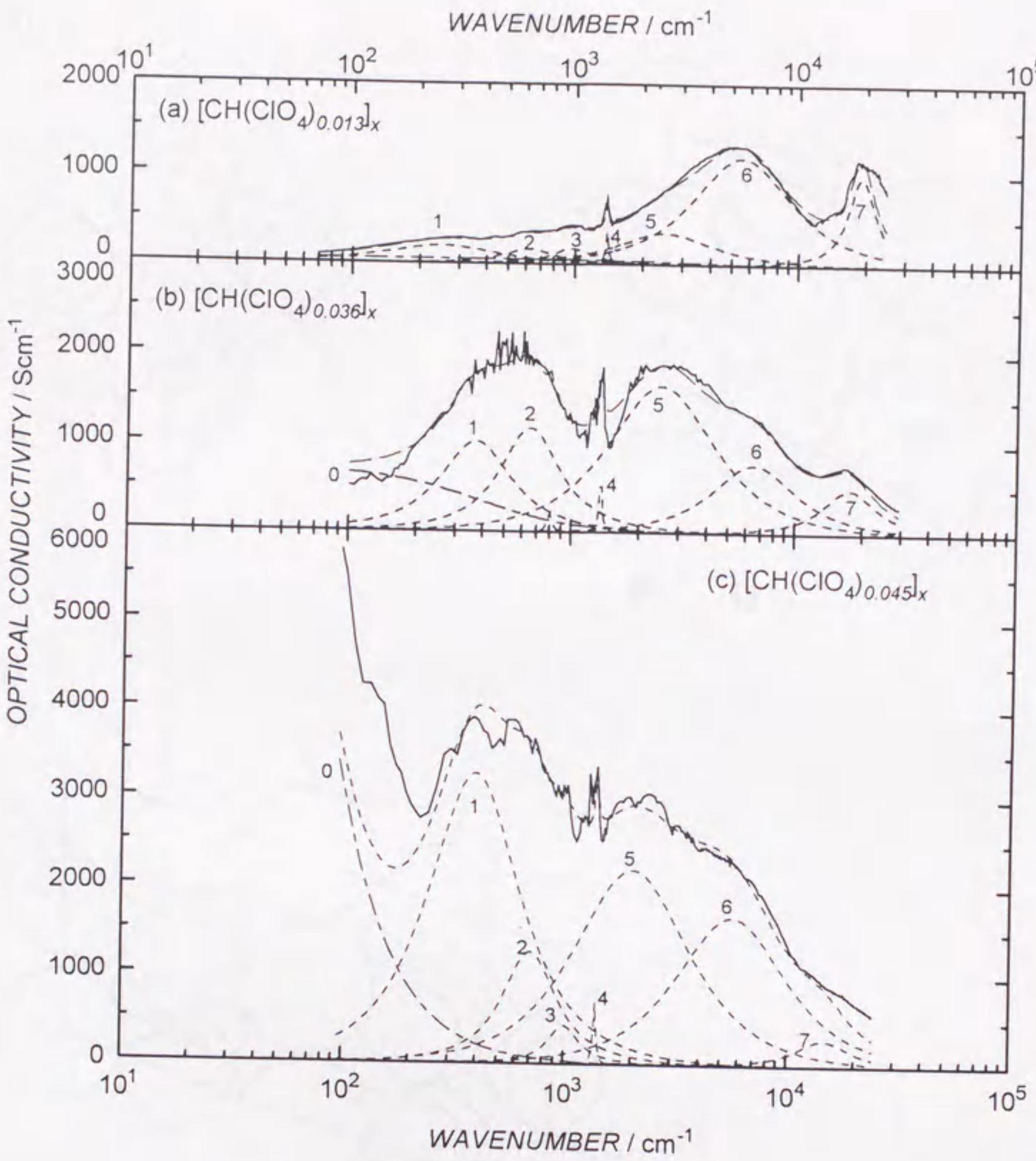
WAVENUMBER / cm-1
(a) [CH(ClO4)0.013]x
(b) [CH(ClO4)0.036]x
(c) [CH(ClO4)0.045]x
OPTICAL CONDUCTIVITY / Scm-1
WAVENUMBER / cm-1

Figure 6

(a)

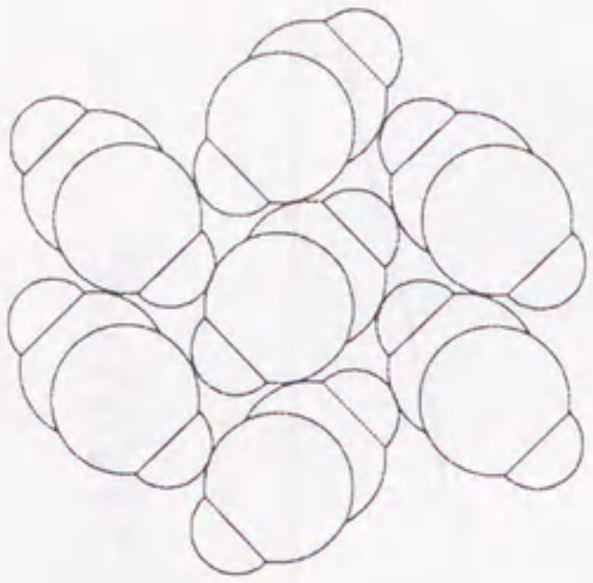

P U

(b)

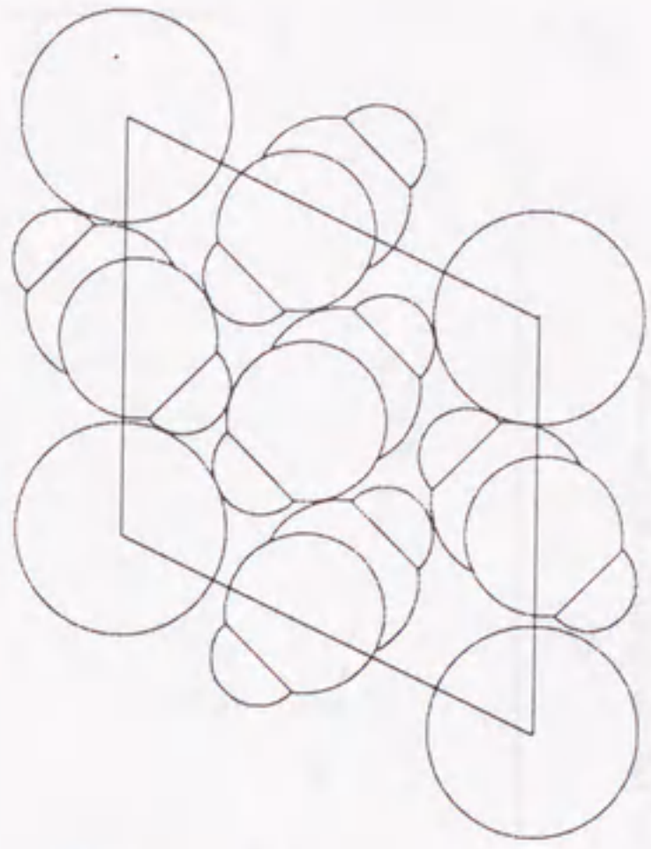

P U

(c)

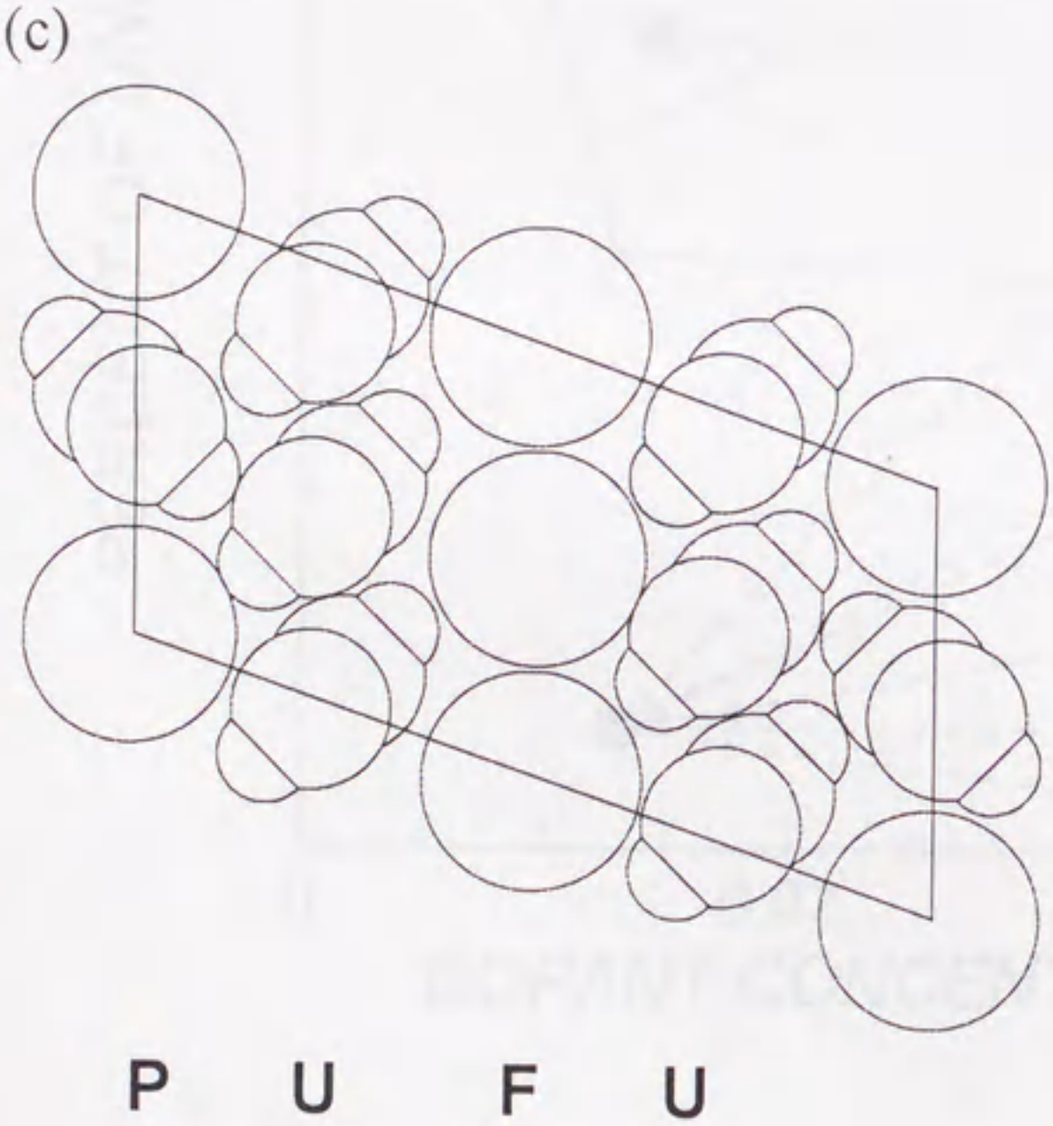

P U F U

Figure 7

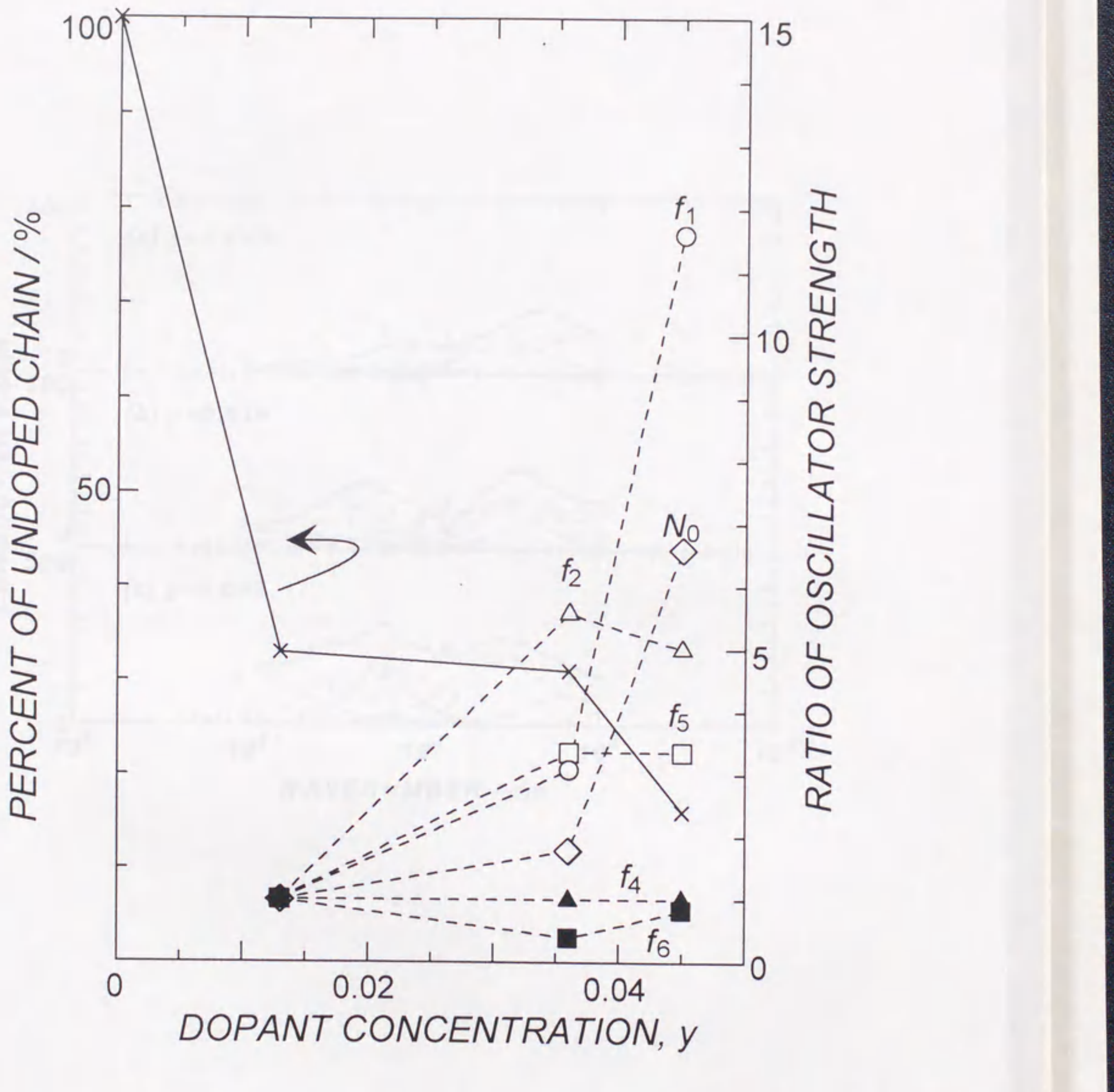
100
50
0
15
10
5
0
0
0.02
0.04
PERCENT OF UNDOPED CHAIN / %
RATIO OF OSCILLATOR STRENGTH
DOPANT CONCENTRATION, y
f_1
f_2
N_0
f_5
f_4
f_6

Figure 8

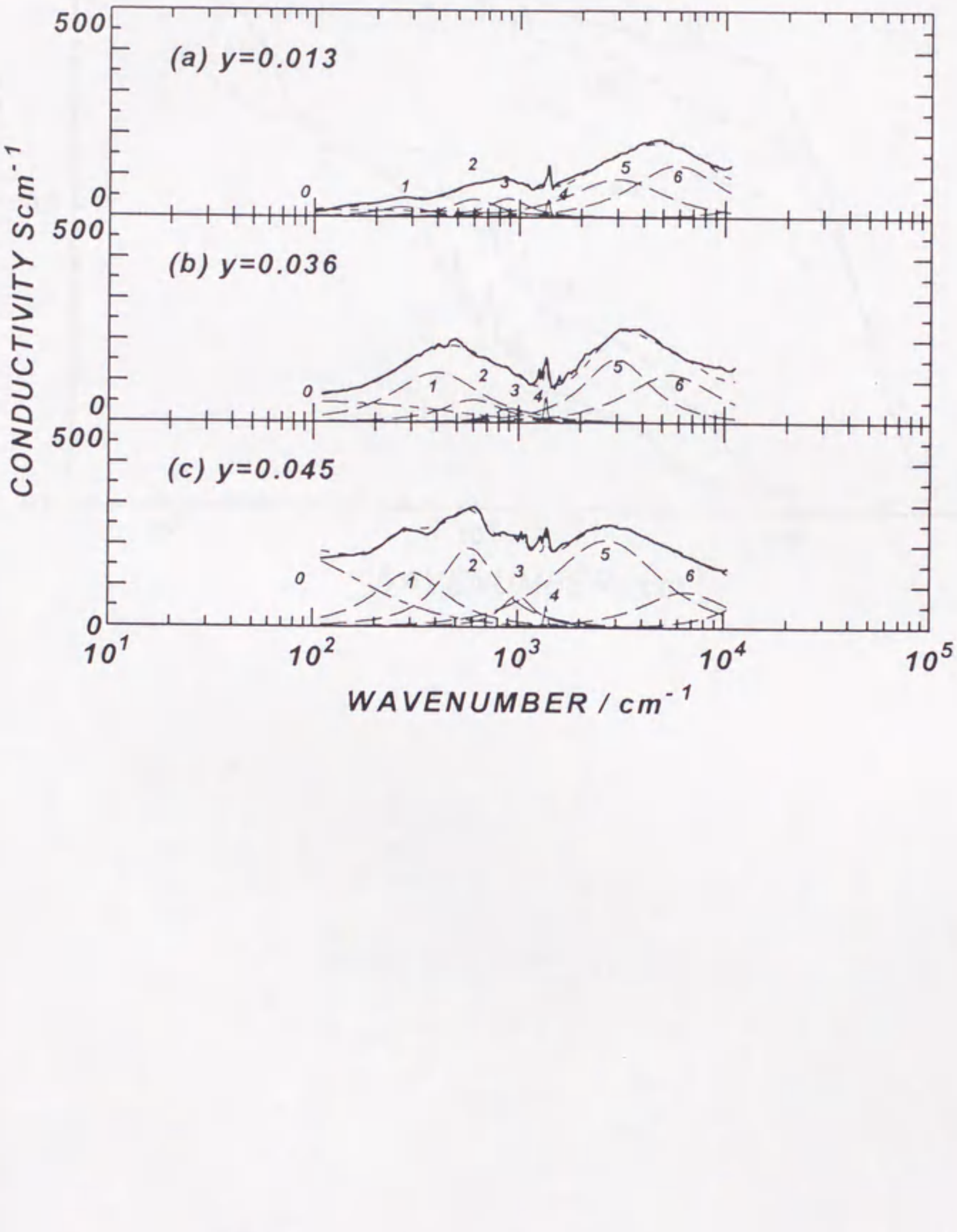
500
(a) y=0.013
0
500
(b) y=0.036
0
500
(c) y=0.045
0
0
1
2
3
4
5
6
CONDUCTIVITY Scm-1
10^1
10^2
10^3
10^4
10^5
WAVENUMBER / cm-1

Figure 9

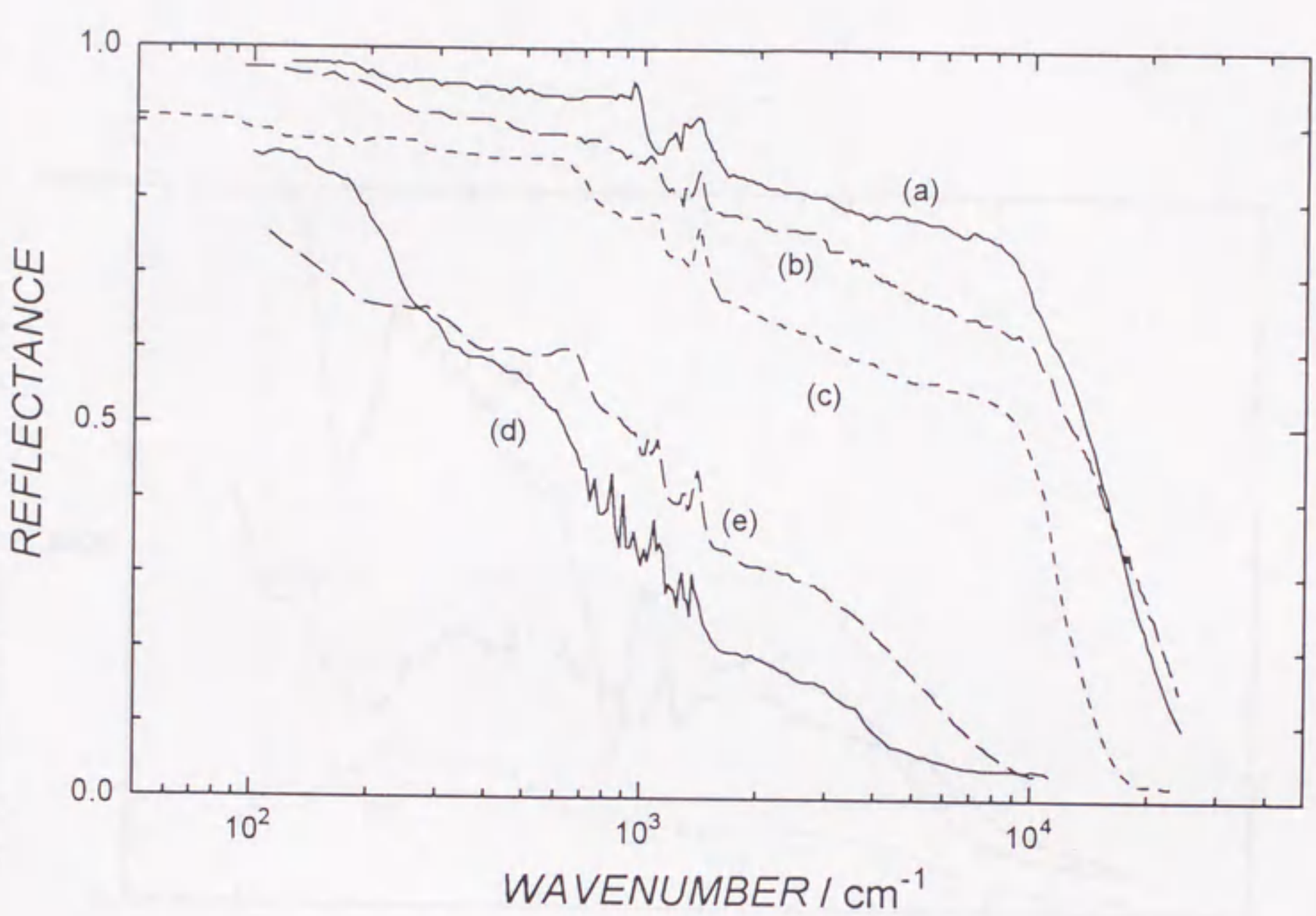

Figure 10

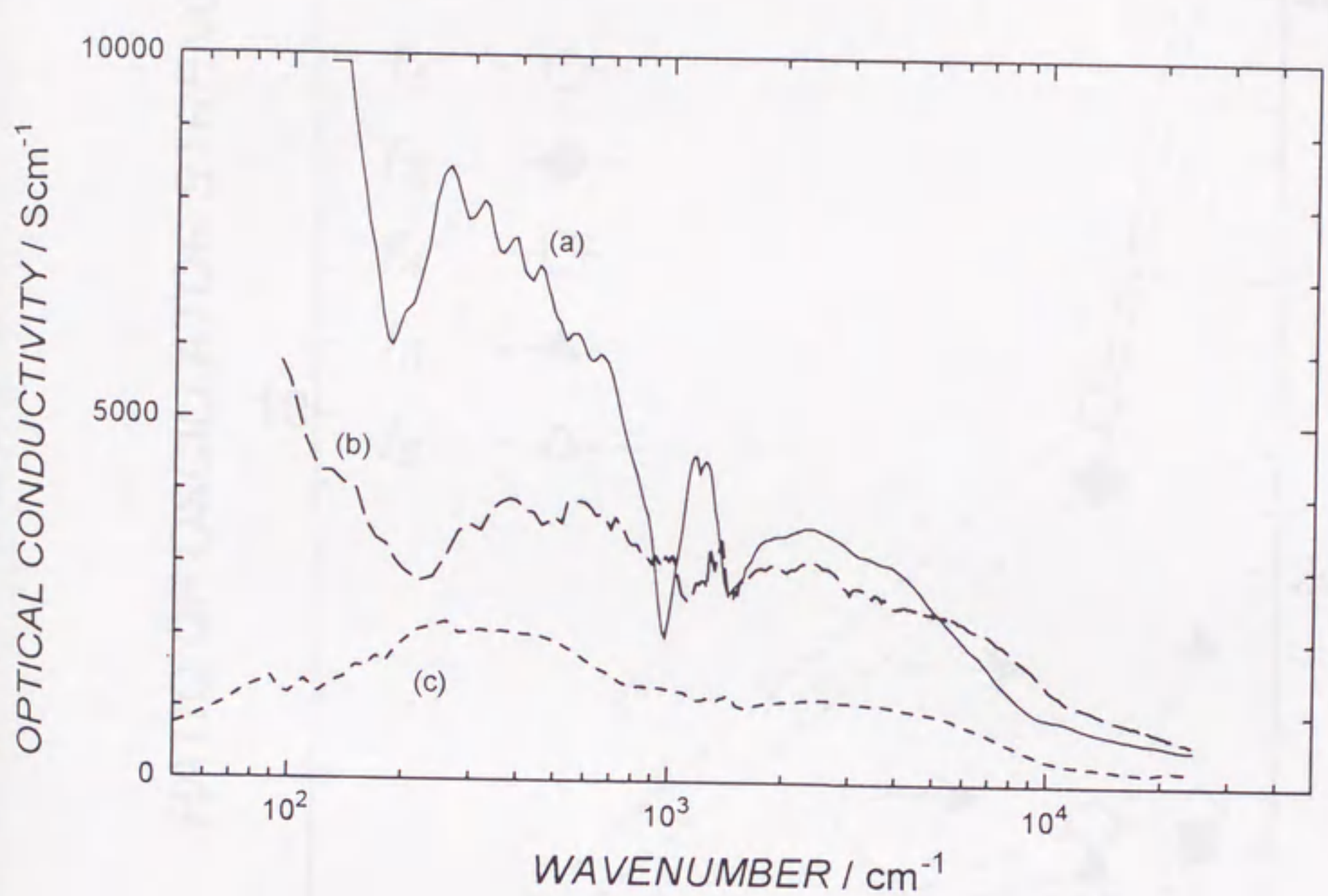
10000
5000
0
OPTICAL CONDUCTIVITY / Scm-1
(a)
(b)
(c)
10^2
10^3
10^4
WAVENUMBER / cm-1

Figure 11

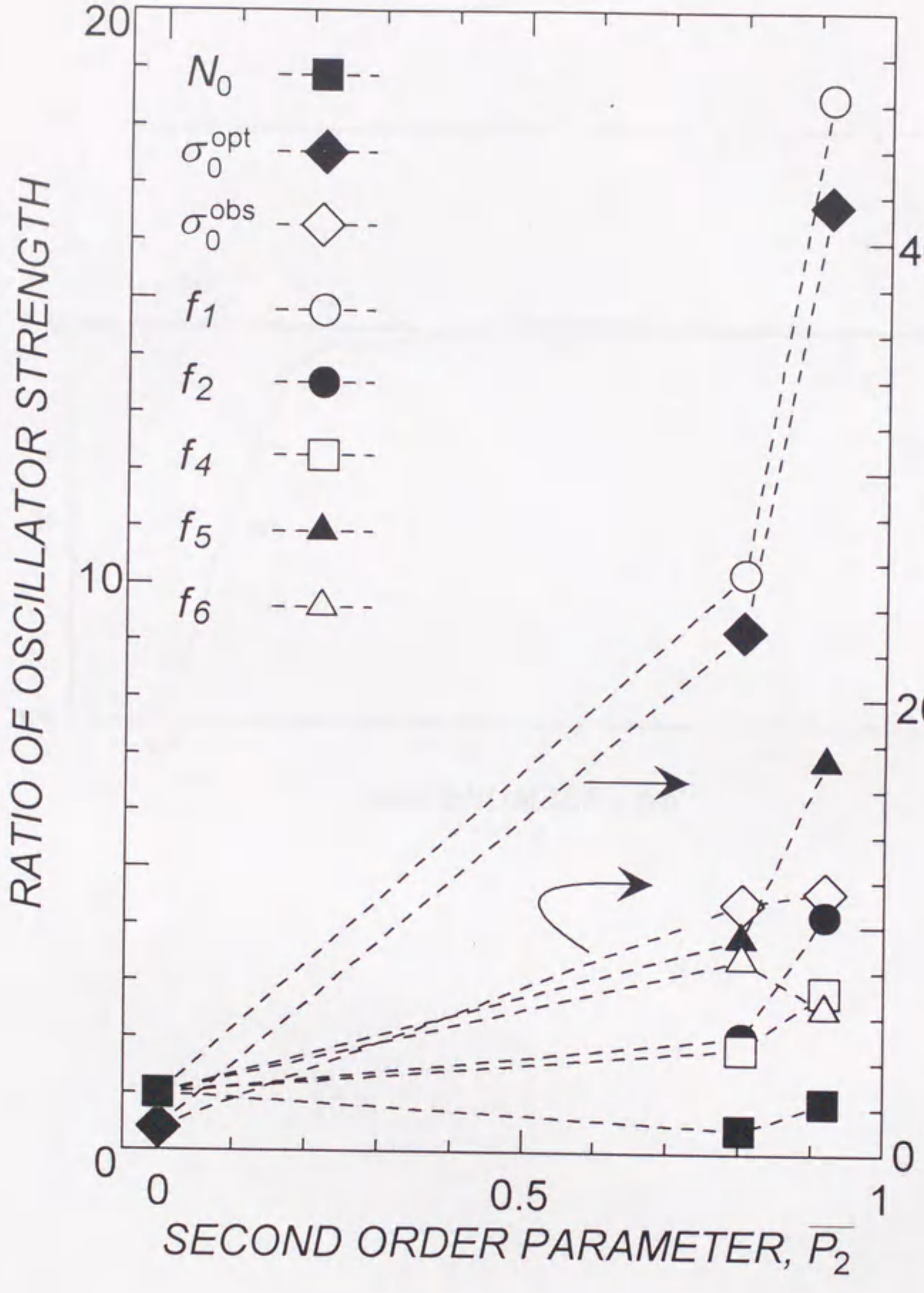
20
10
0
0
0.5
1
40
20
0
N_0
σ_0^{opt}
σ_0^{obs}
f_1
f_2
f_4
f_5
f_6
RATIO OF OSCILLATOR STRENGTH
RATIO OF DC CONDUCTIVITY
SECOND ORDER PARAMETER, $\overline{P_2}$

Figure 12

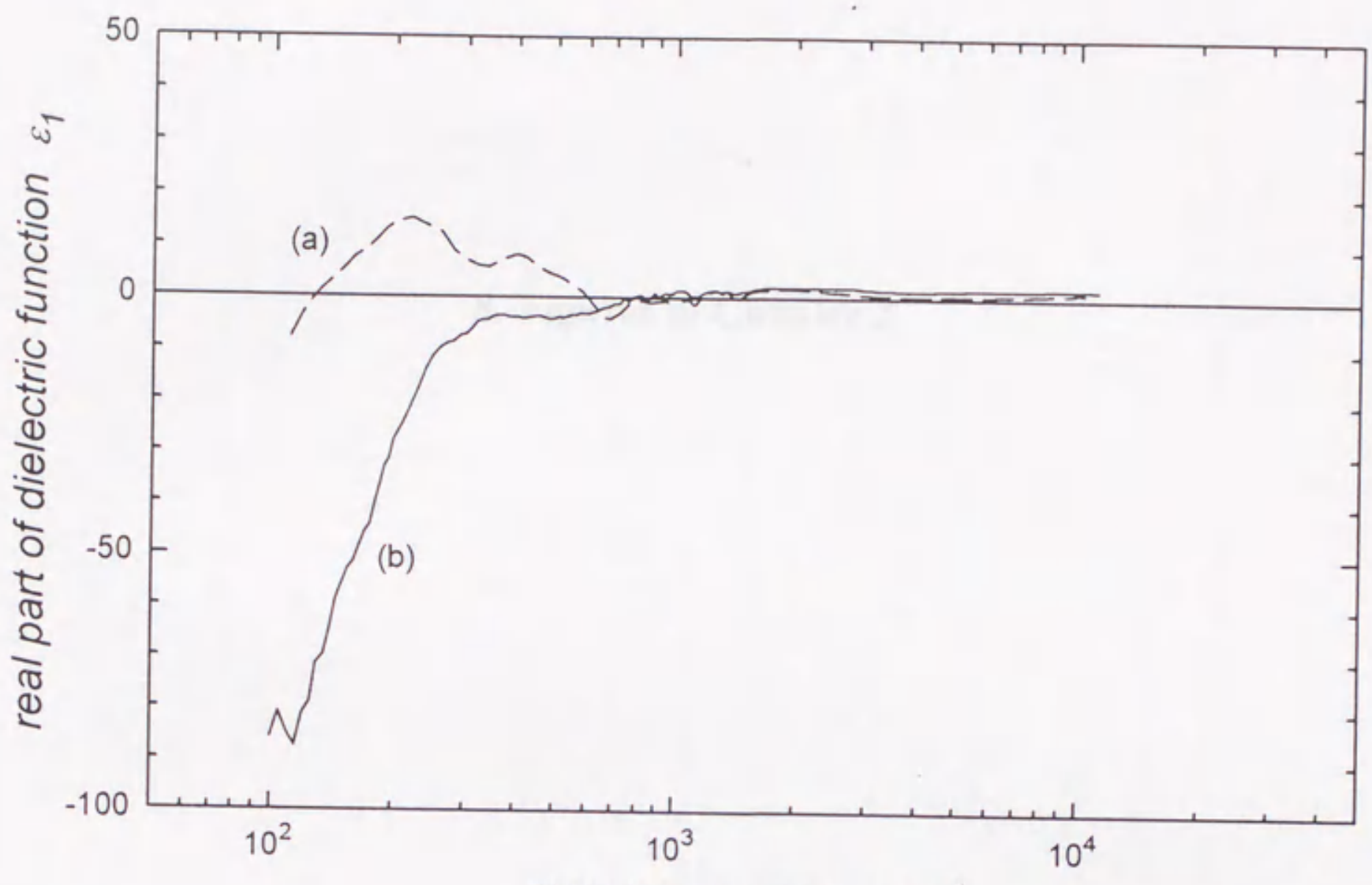
50
0
-50
-100
real part of dielectric function ε1
(a)
(b)
10^2
10^3
10^4
WAVENUMBER / cm^-1

Figure 13

8. Figures in Chapter 3

Figure 1

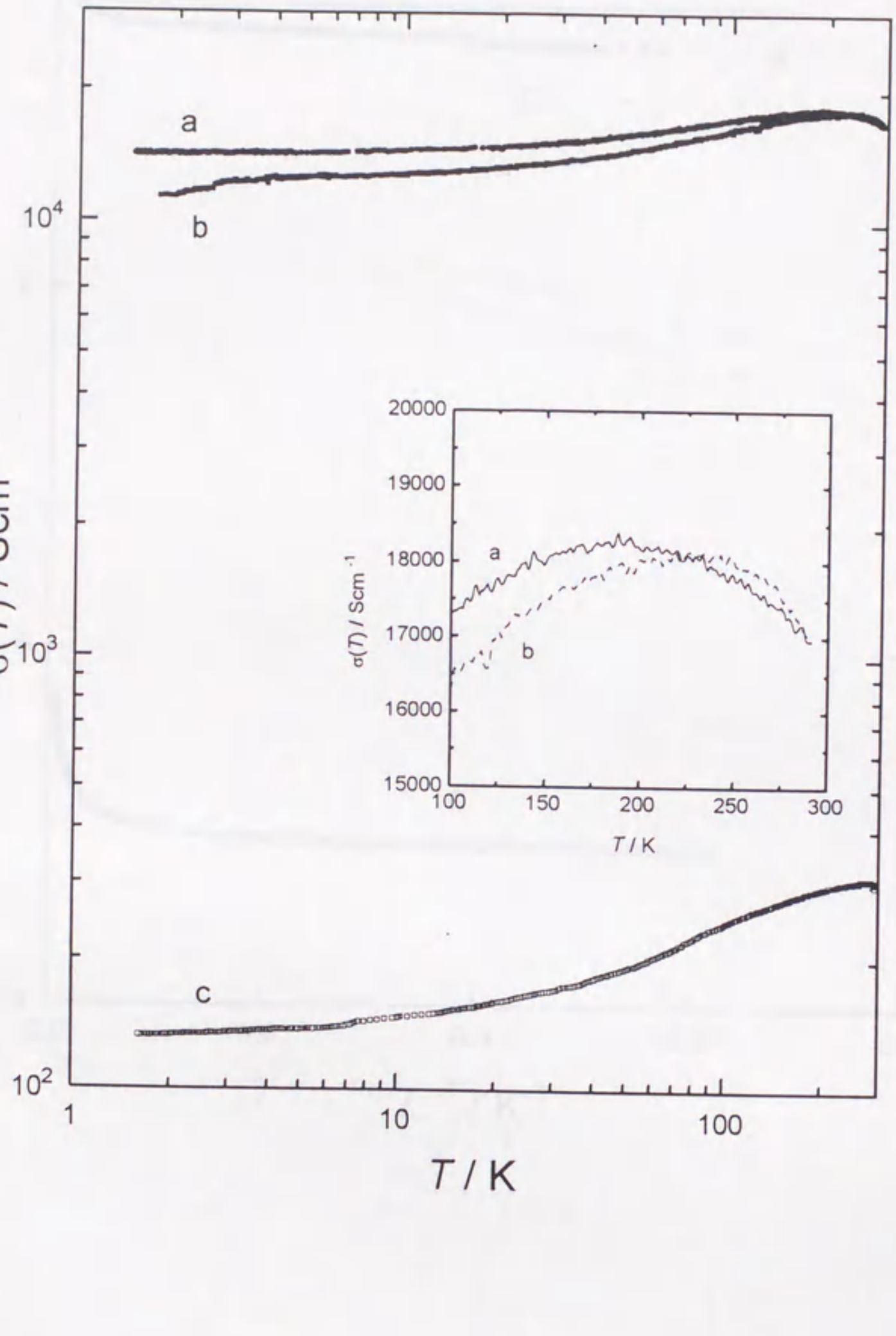
a
b
c
10^4
10^3
10^2
$\sigma(T)$ / Scm^{-1}
1
10
100
T / K
20000
19000
18000
17000
16000
15000
100
150
200
250
300
$\sigma(T)$ / Scm^{-1}
T / K

Figure 1

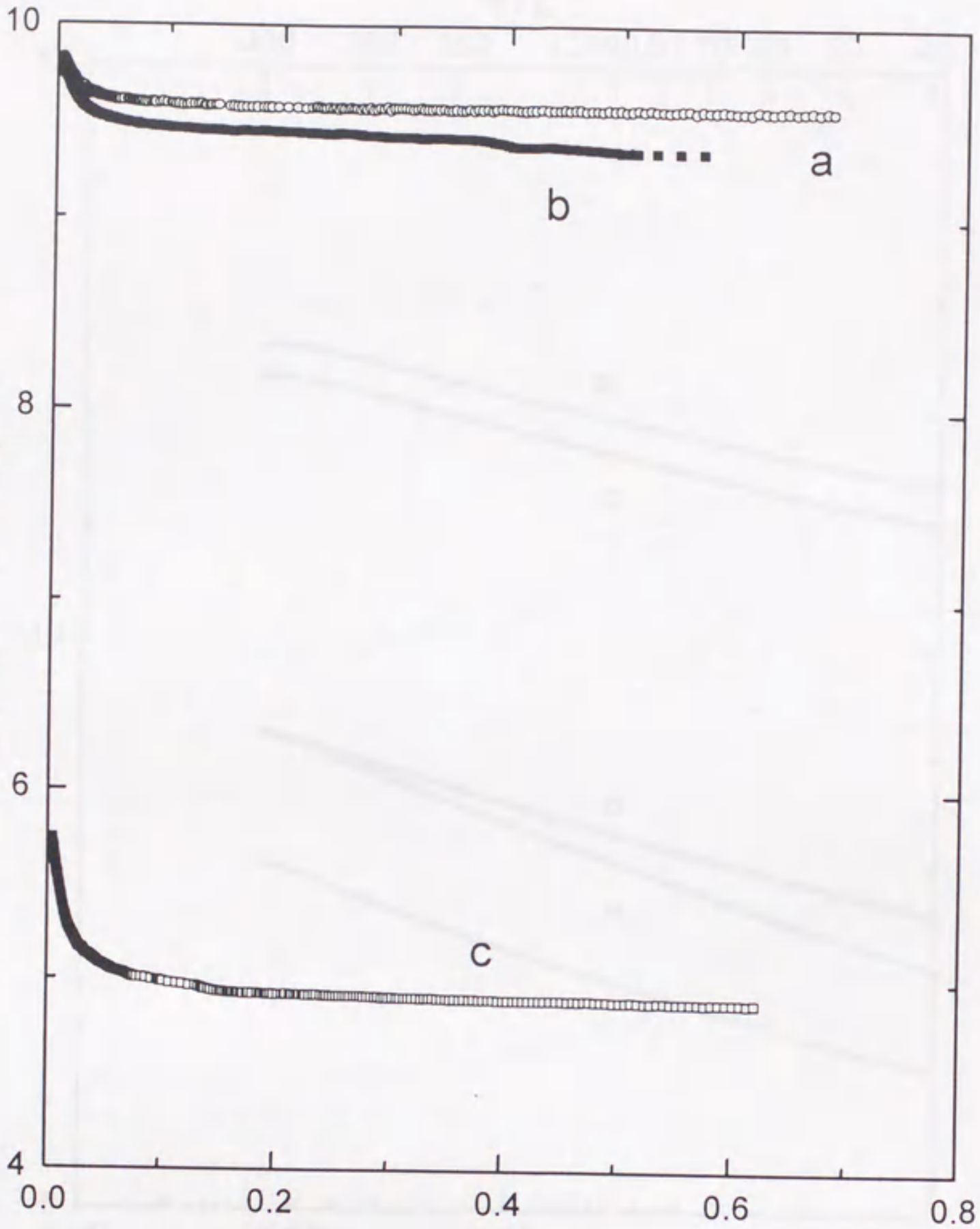

Figure 2

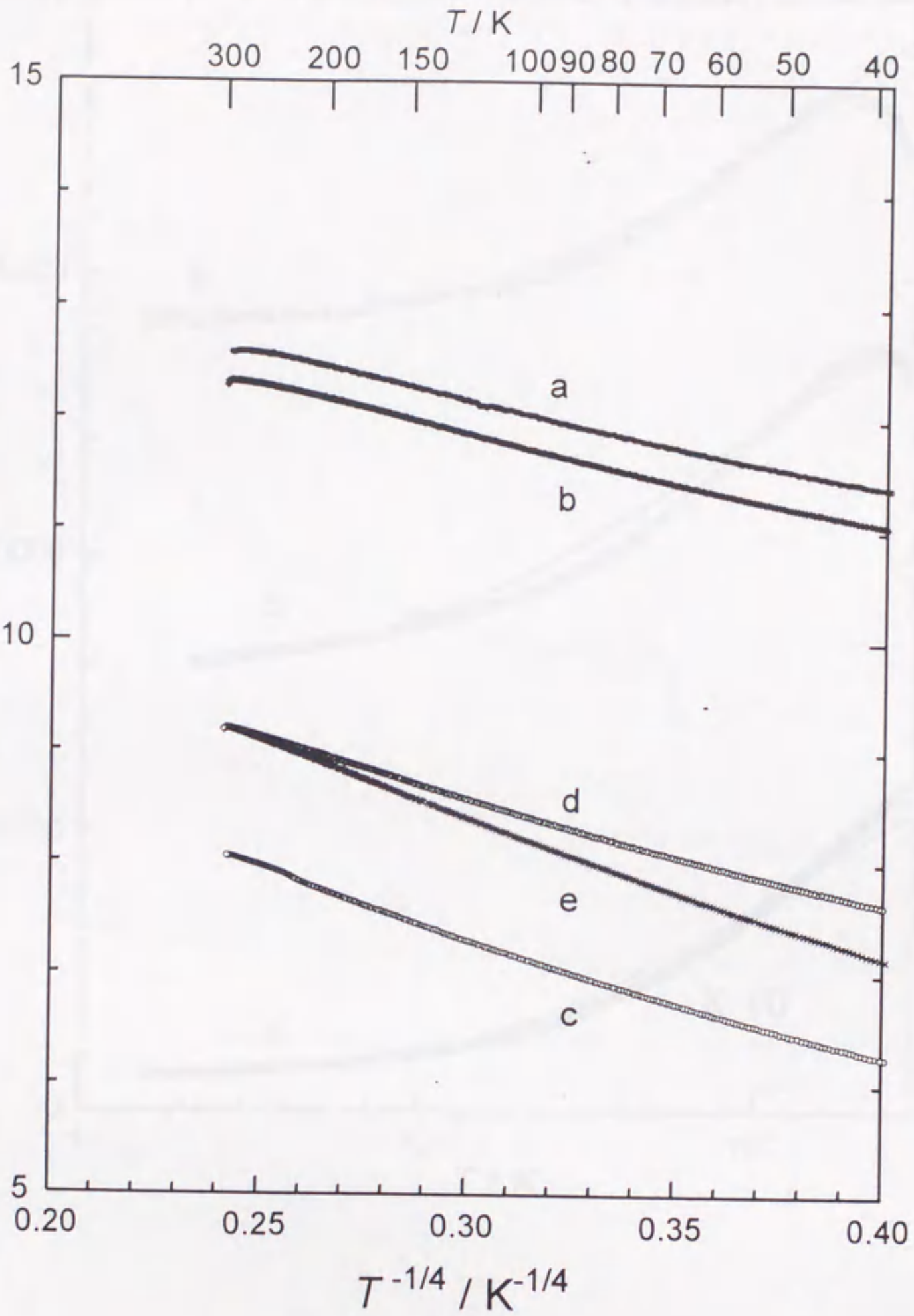
T / K
300
200
150
100
90
80
70
60
50
40
15
10
5
a
b
c
d
e
ln[σT^1/2 / Scm^-1K^1/2]
0.20
0.25
0.30
0.35
0.40
T^-1/4 / K^-1/4

Figure 3

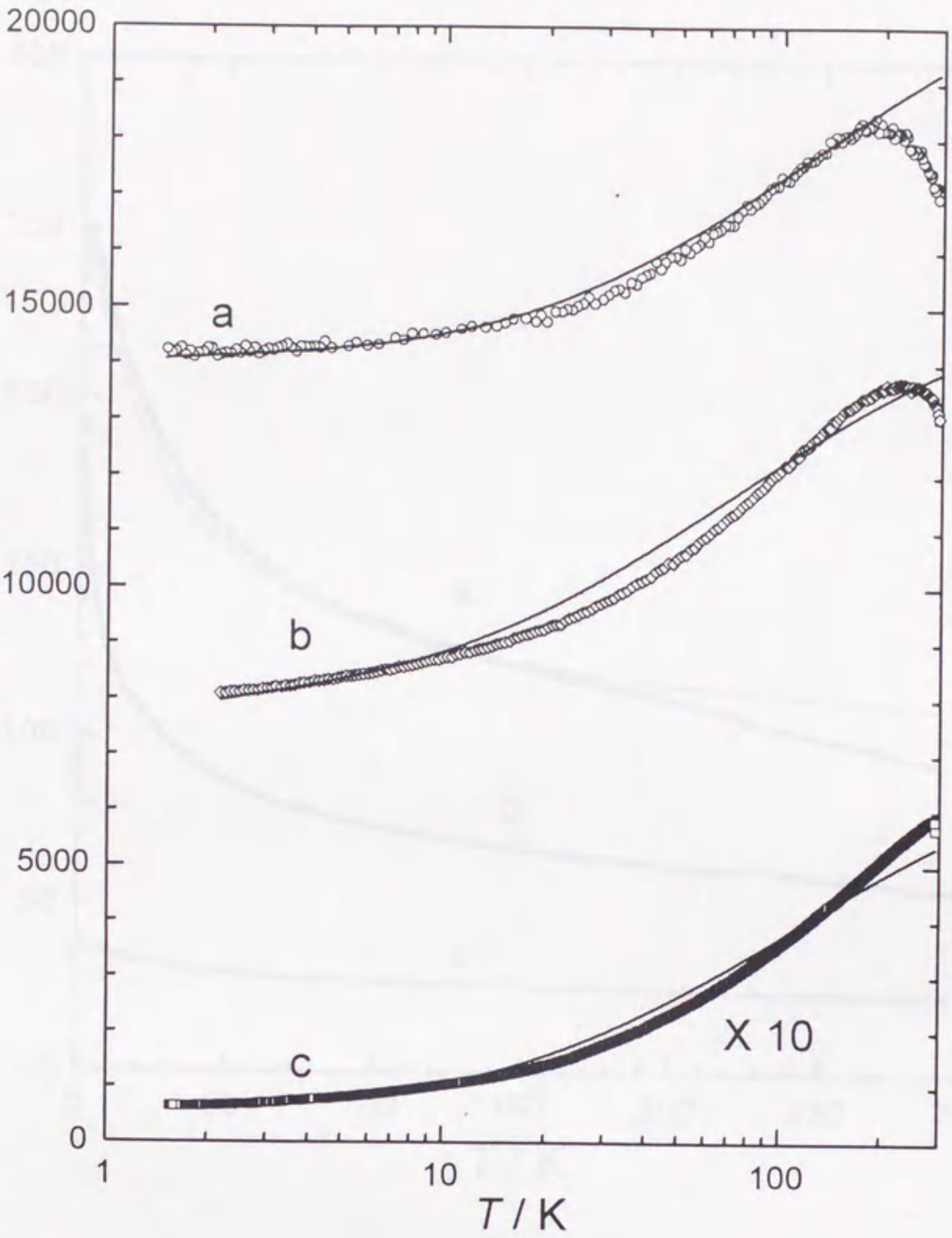

Figure 4

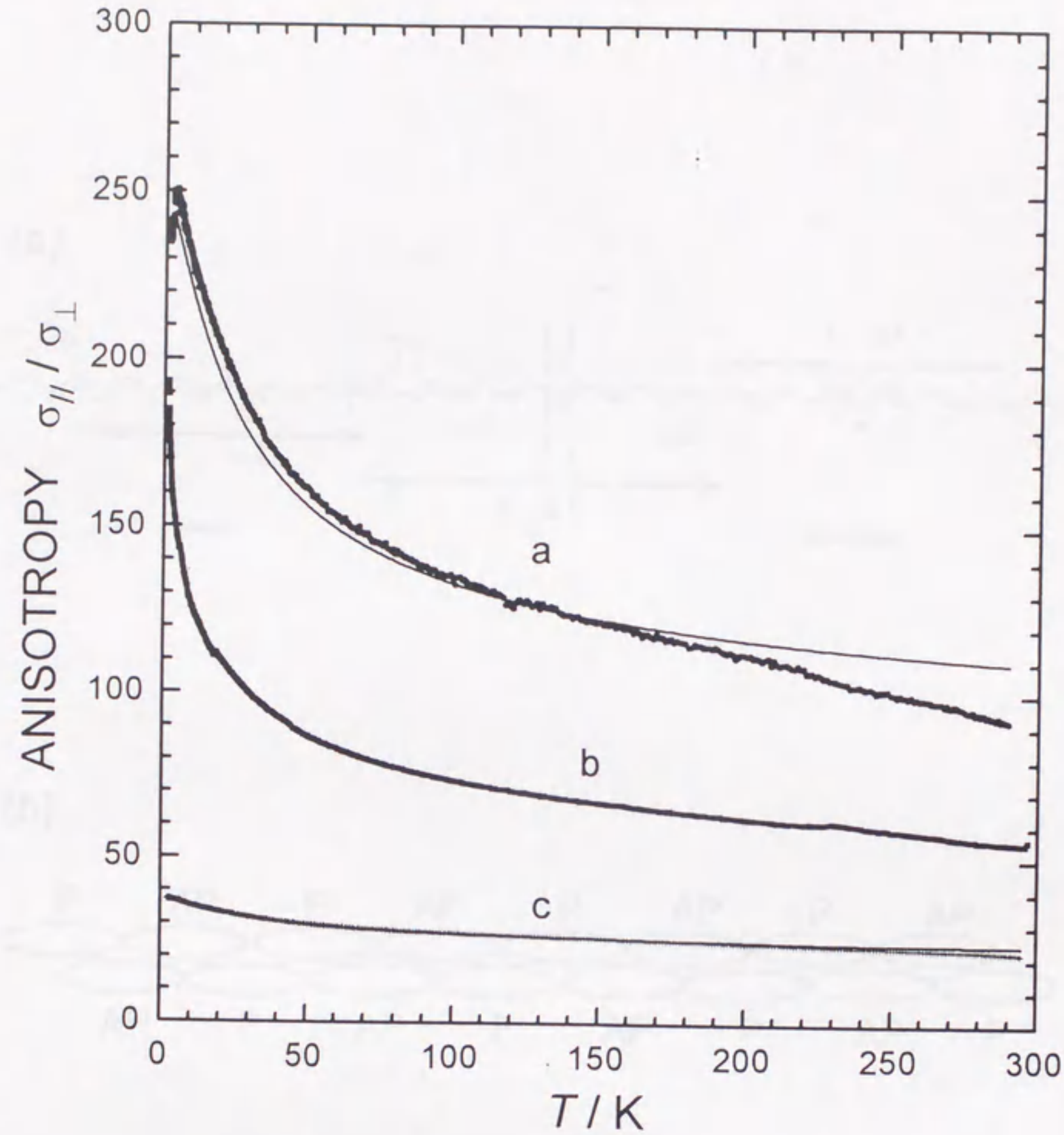
300
250
200
150
100
50
0
ANISOTROPY $\sigma_{//} / \sigma_{\perp}$
a
b
c
0
50
100
150
200
250
300
T / K

Figure 5

(a)

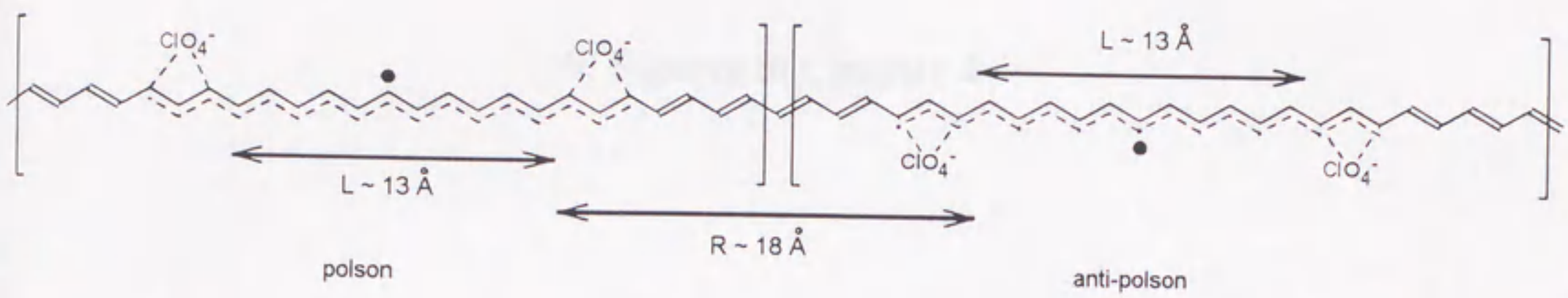
ClO4-
ClO4-
L ~ 13 Å
R ~ 18 Å
polson
L ~ 13 Å
ClO4-
ClO4-
anti-polson

(b)

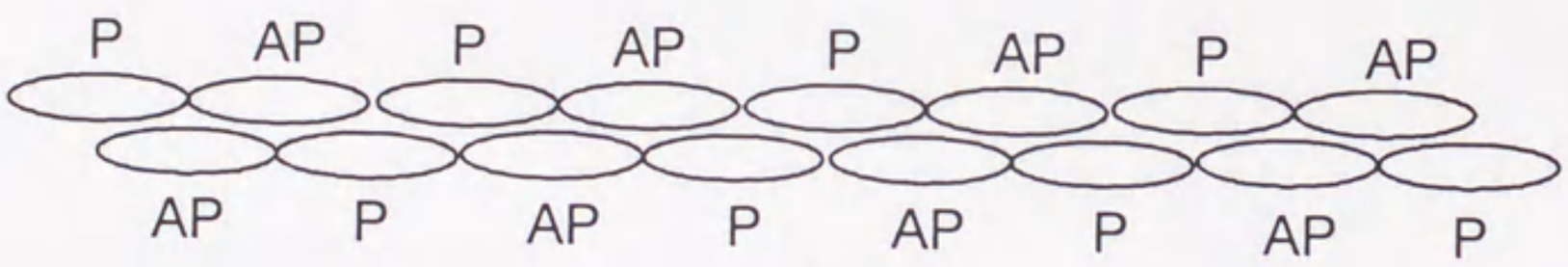
P
AP
P
AP
P
AP
P
AP
AP
P
AP
P
AP
P
AP
P

Figure 6

9. Figures in Chapter 4

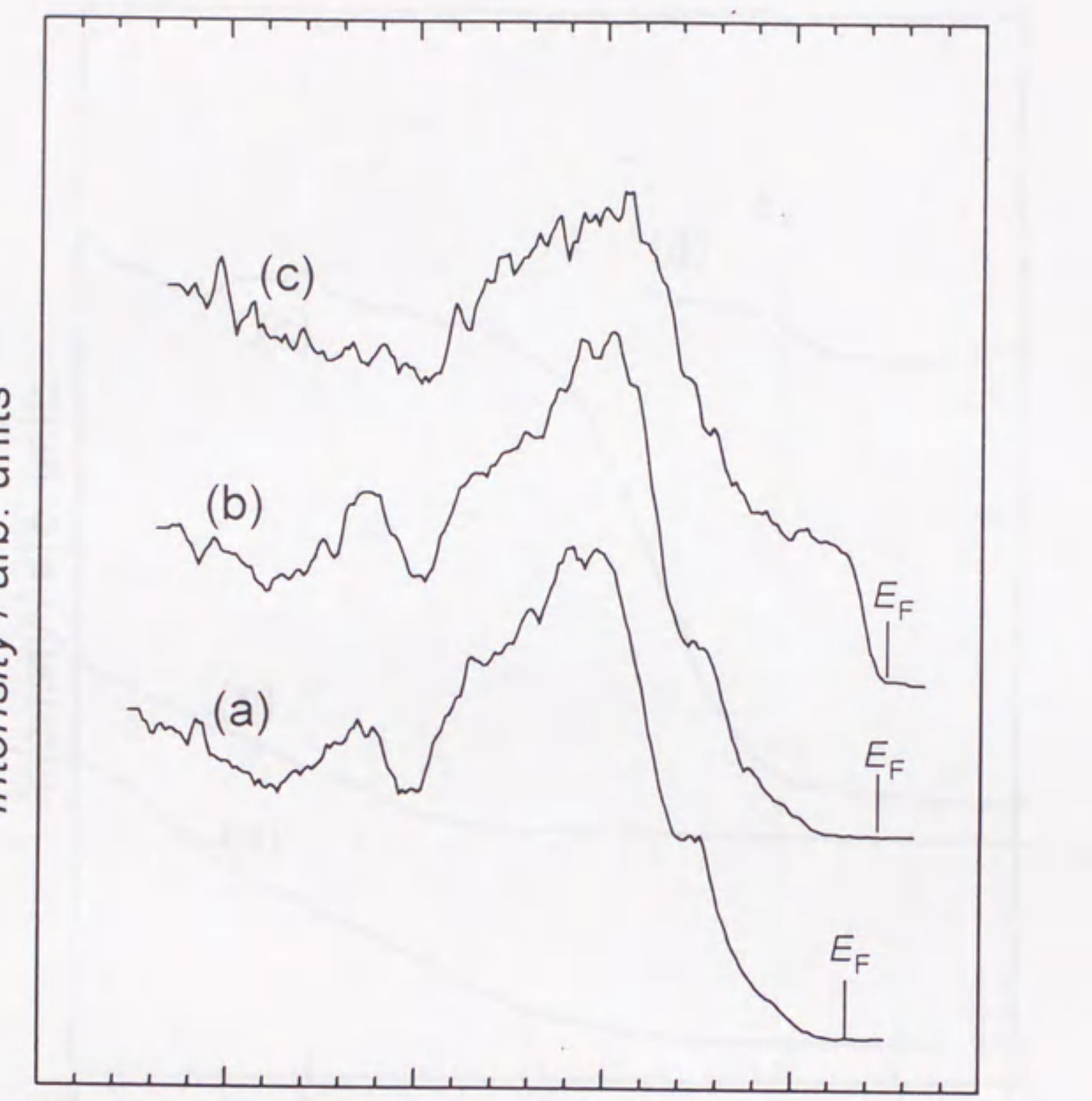

Figure 1

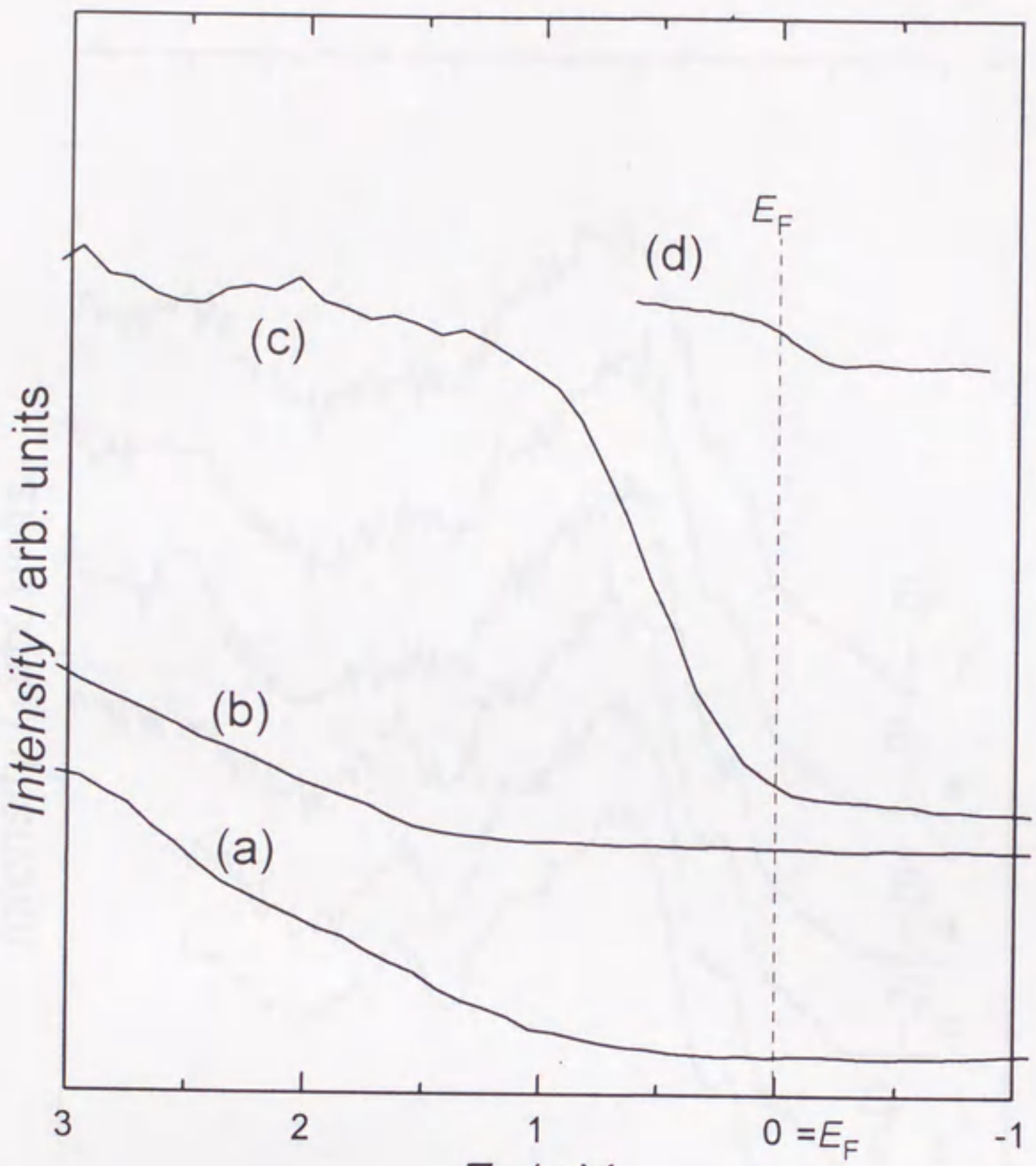

Figure 2

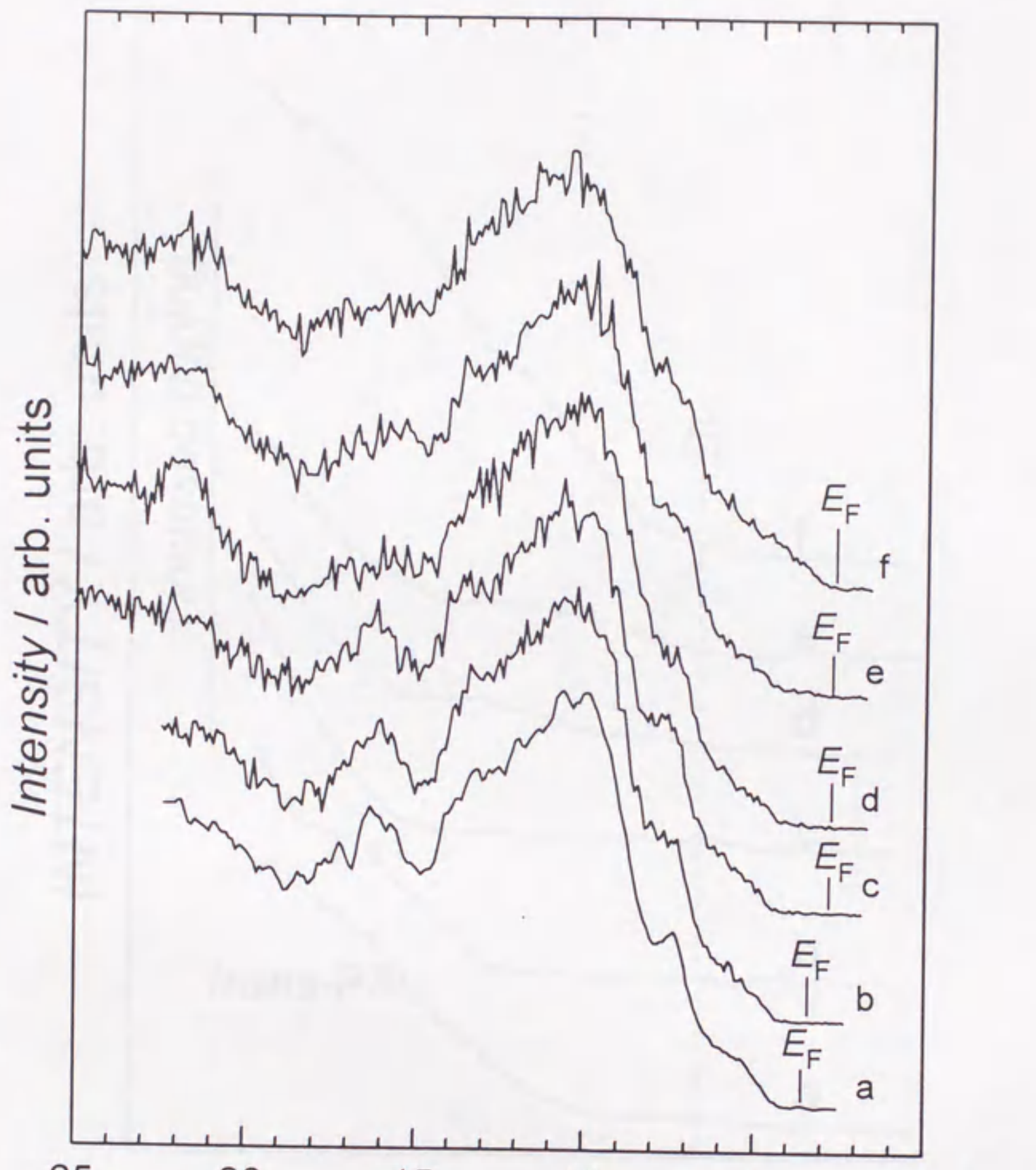
Intensity / arb. units
E_F
f
E_F
e
E_F
d
E_F
c
E_F
b
E_F
a
25
20
15
10
5
0=E_{vac}
E_b / eV

Figure 3

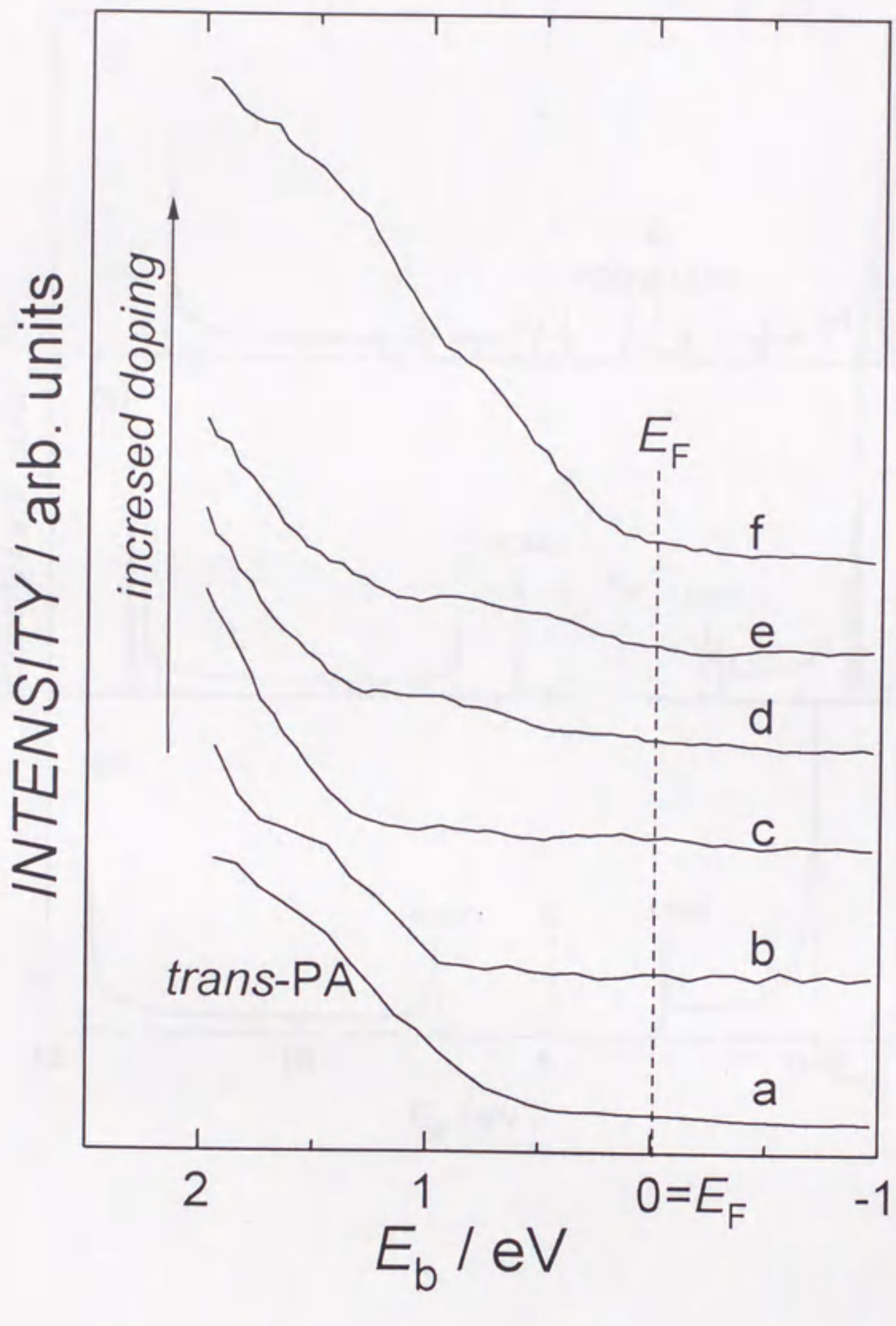
INTENSITY / arb. units
increased doping
E_F
f
e
d
c
b
a
trans-PA
2
1
0=E_F
-1
E_b / eV

Figure 4

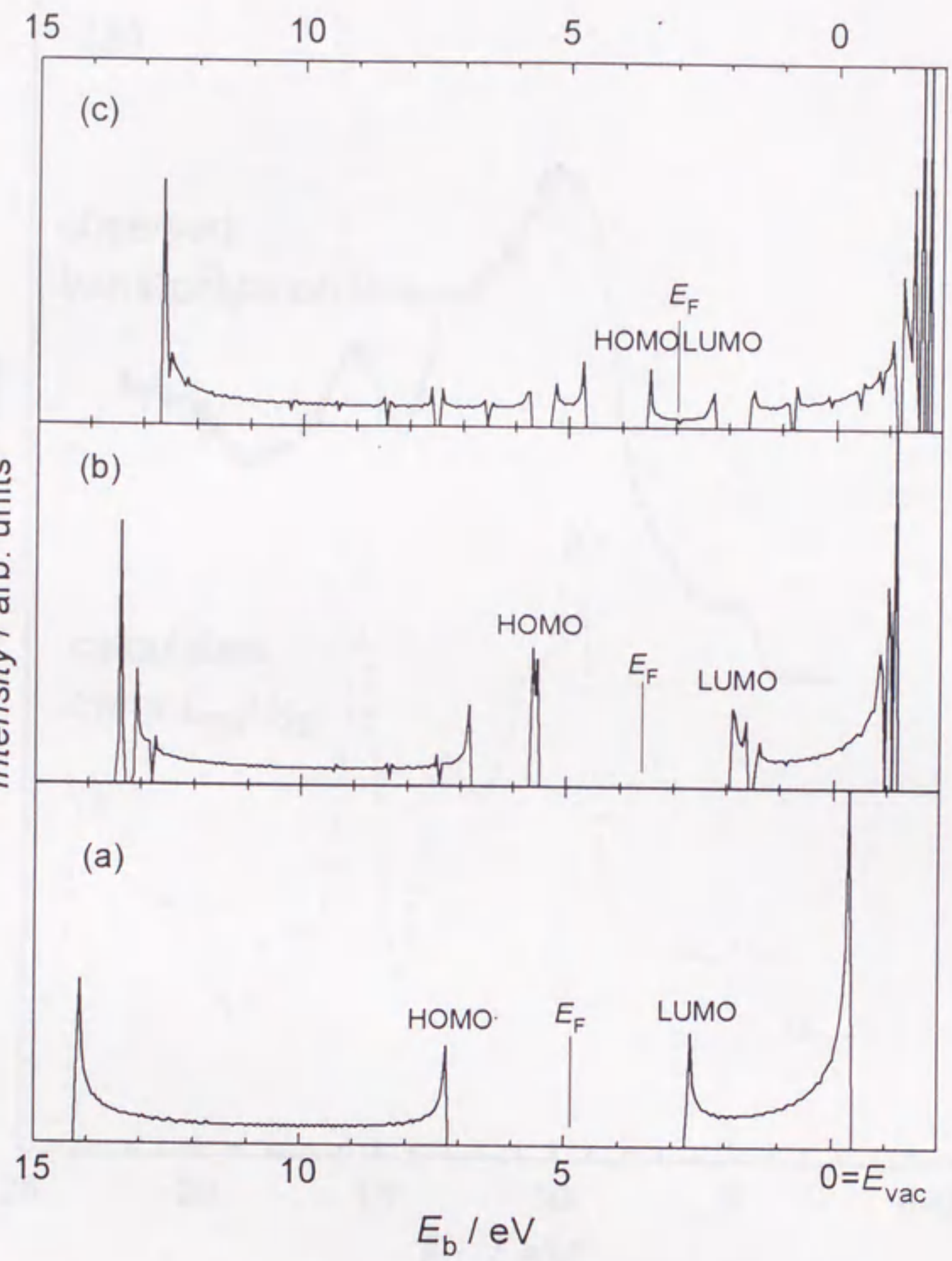
15
10
5
0
(c)
E_F
HOMO LUMO
(b)
HOMO
E_F
LUMO
(a)
HOMO
E_F
LUMO
15
10
5
0=E_{vac}
Intensity / arb. units
E_b / eV

Figure 5

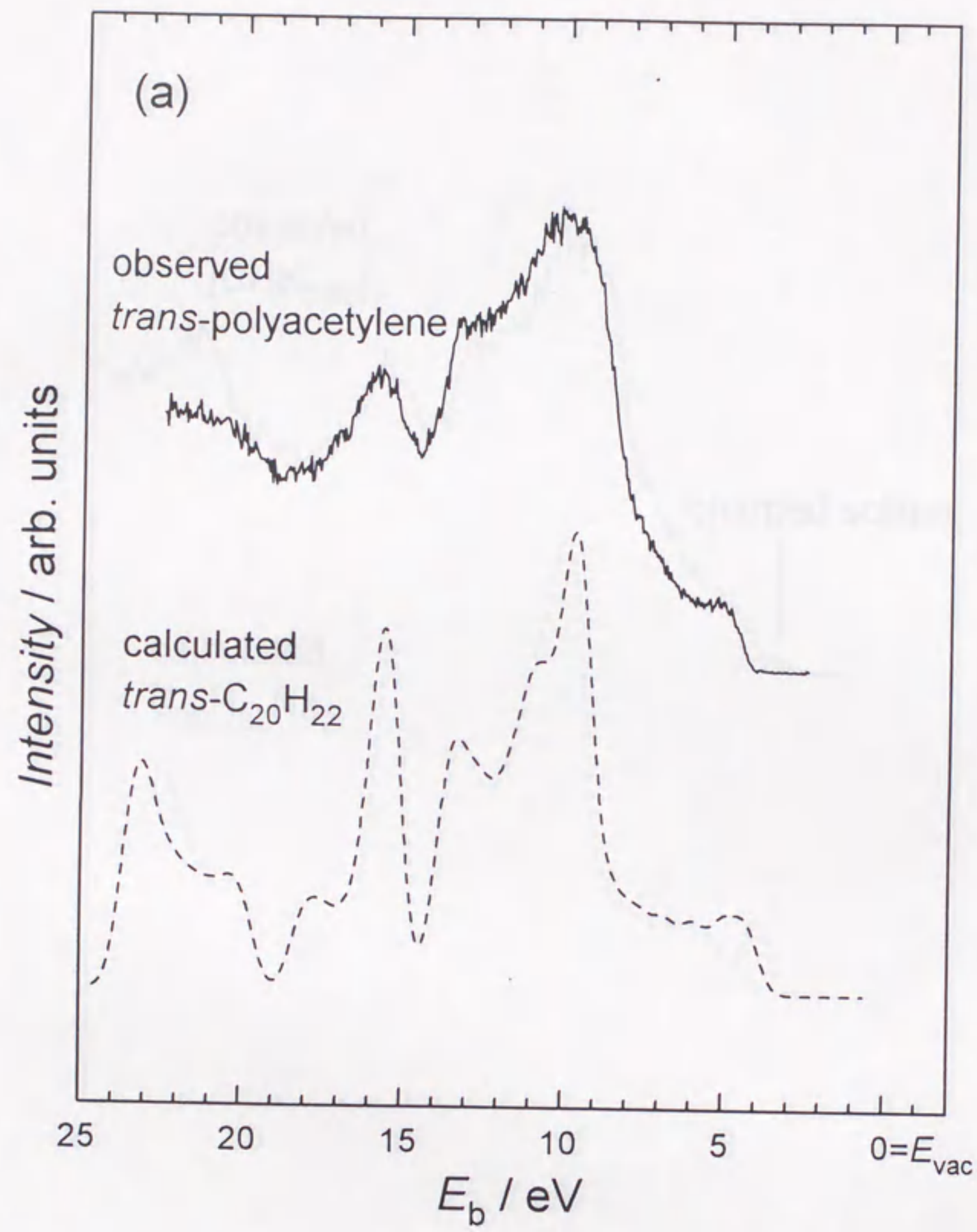
(a)
observed
trans-polyacetylene
calculated
trans-$C_{20}H_{22}$
Intensity / arb. units
25
20
15
10
5
0=E_{vac}
E_b / eV

Figure 6 (a)

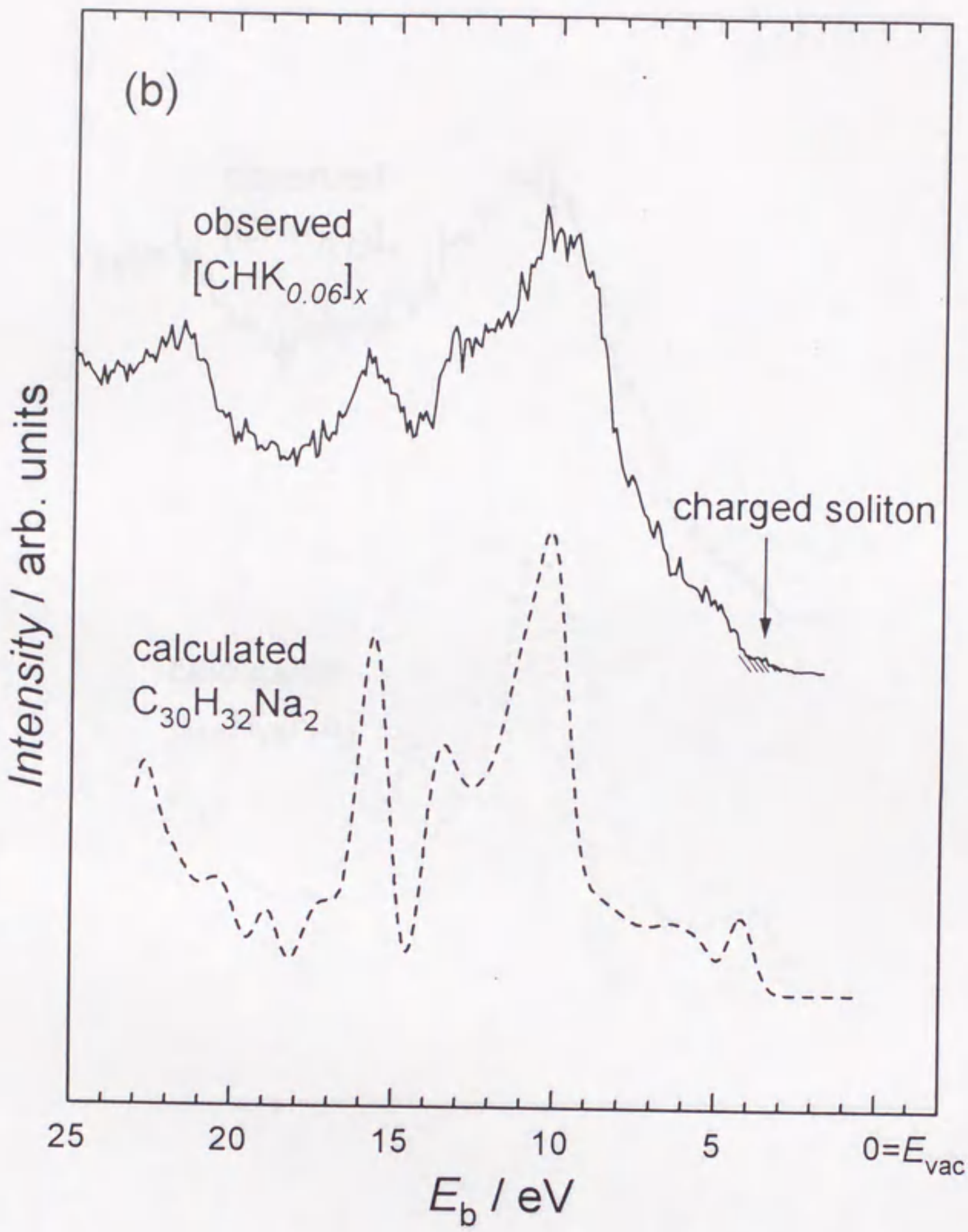
(b)
observed
[CHK0.06]x
charged soliton
calculated
C30H32Na2
Intensity / arb. units
25
20
15
10
5
0=Evac
Eb / eV

Figure 6 (b)

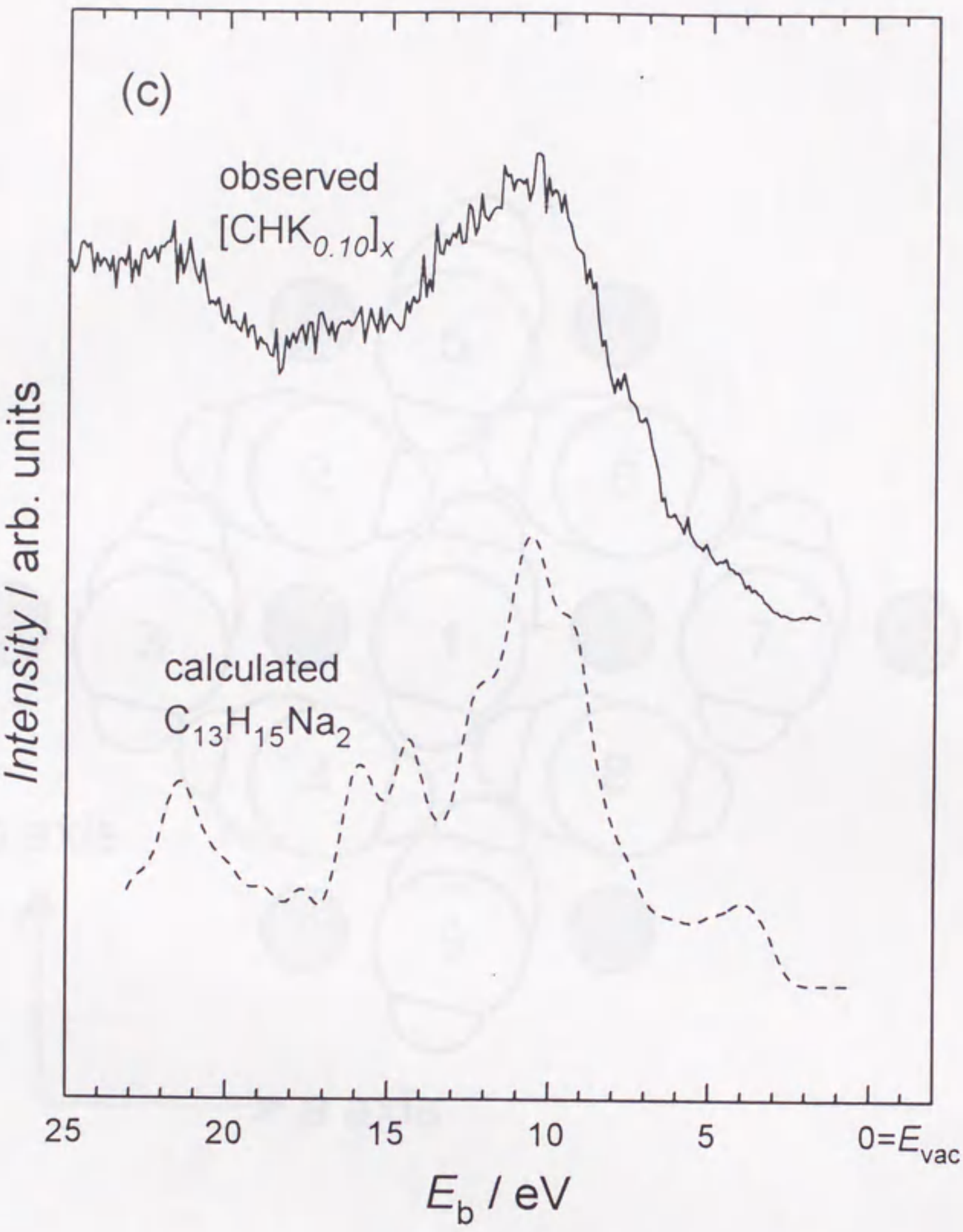
(c)
observed
[CHK0.10]x
calculated
C13H15Na2
Intensity / arb. units
25
20
15
10
5
0=Evac
Eb / eV

Figure 6 (c)

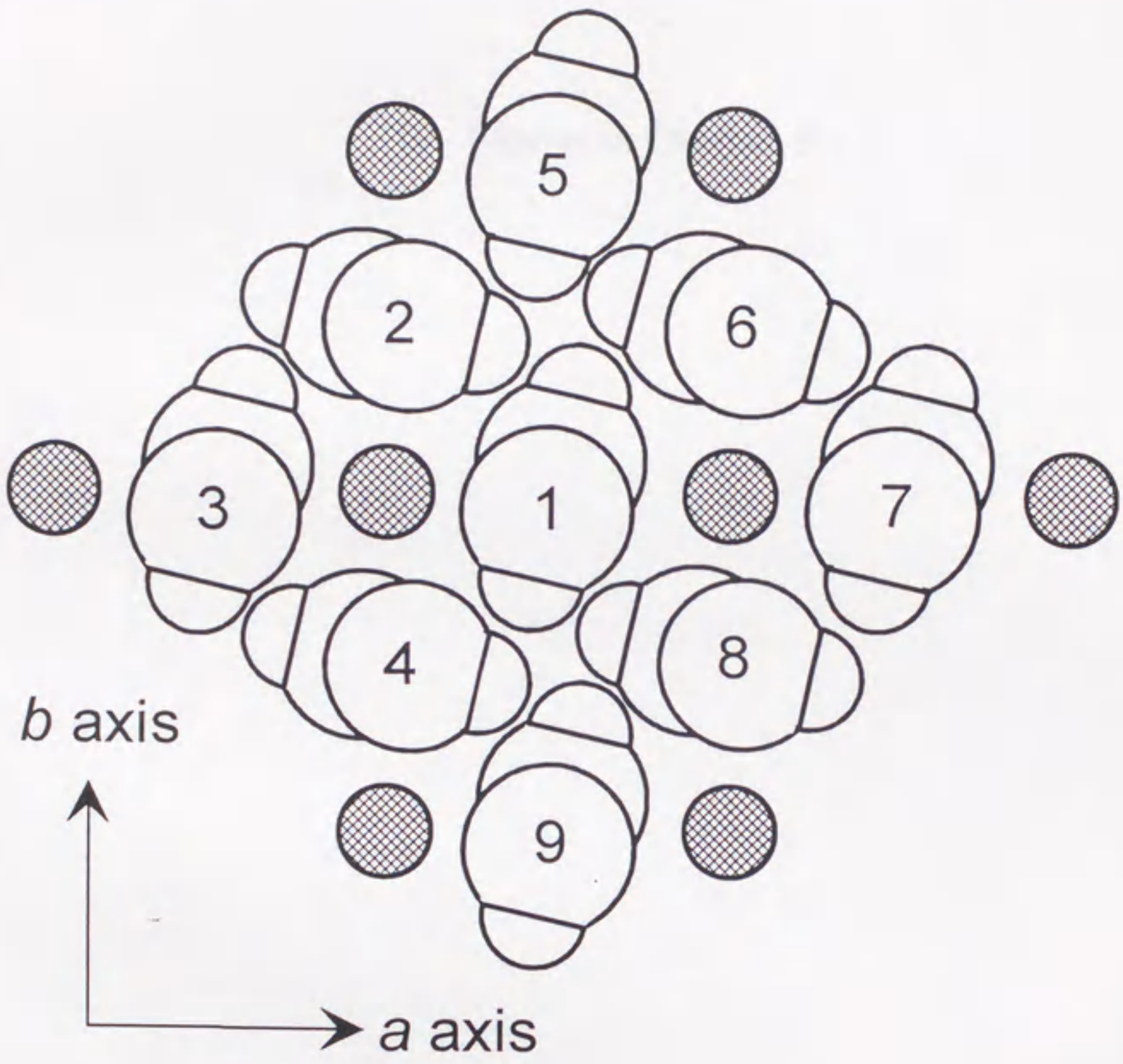

Figure 7

10. Figures in Chapter 5

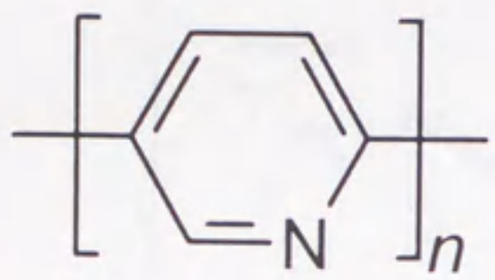

(a) PPy

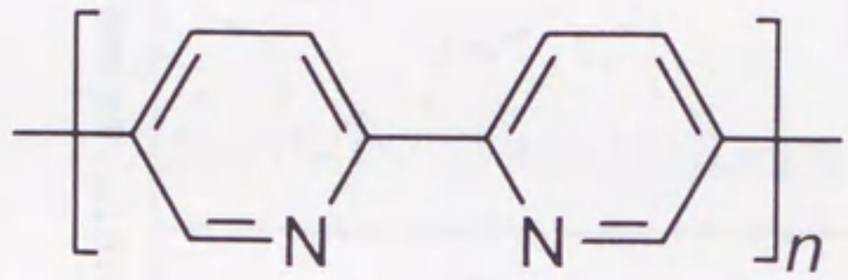

(b) PBPy

Figure 1

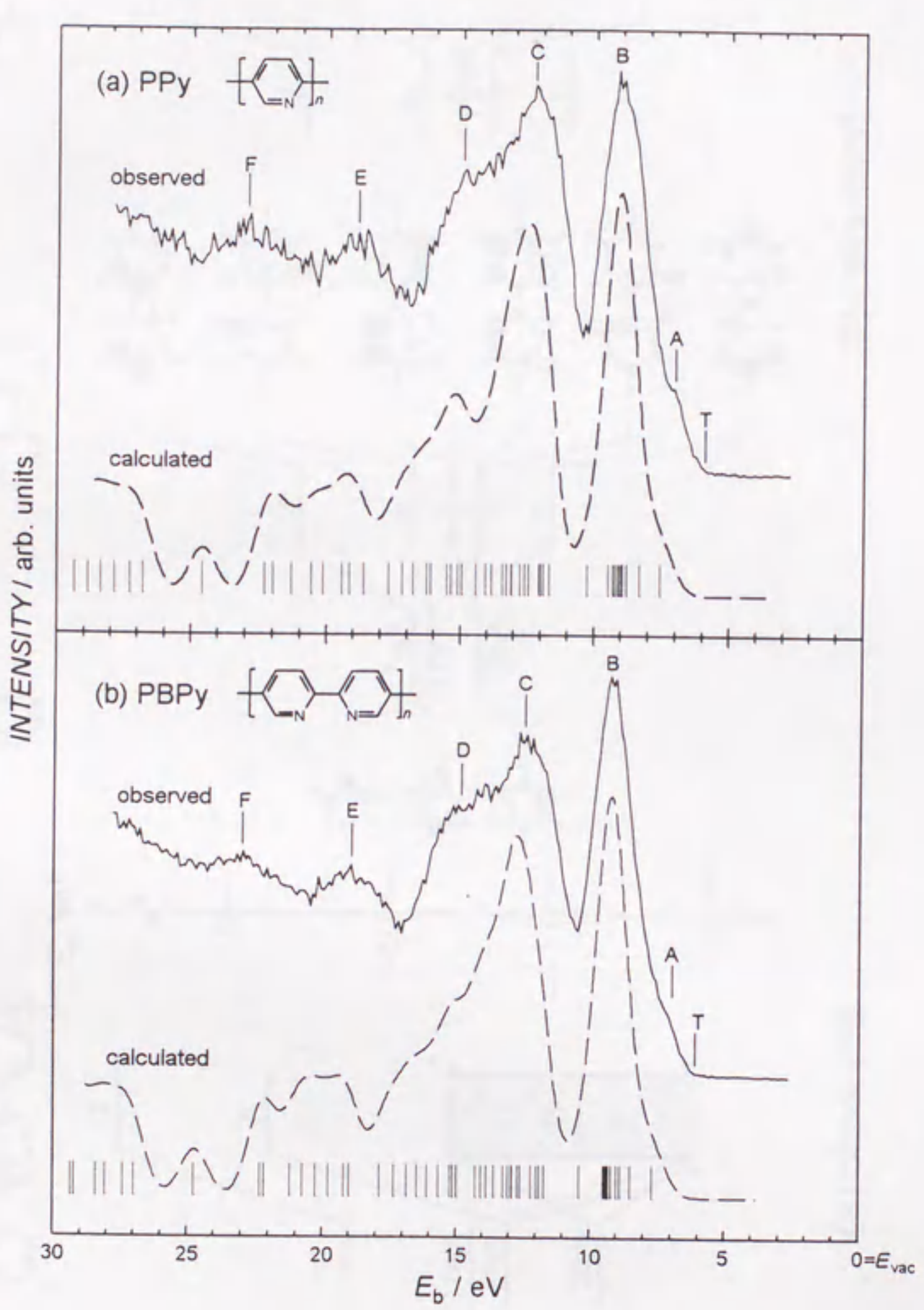
(a) PPy
observed
calculated
F
E
D
C
B
A
T
(b) PBPy
observed
calculated
F
E
D
C
B
A
T
INTENSITY / arb. units
30
25
20
15
10
5
0=E_{vac}
E_b / eV

Figure 2

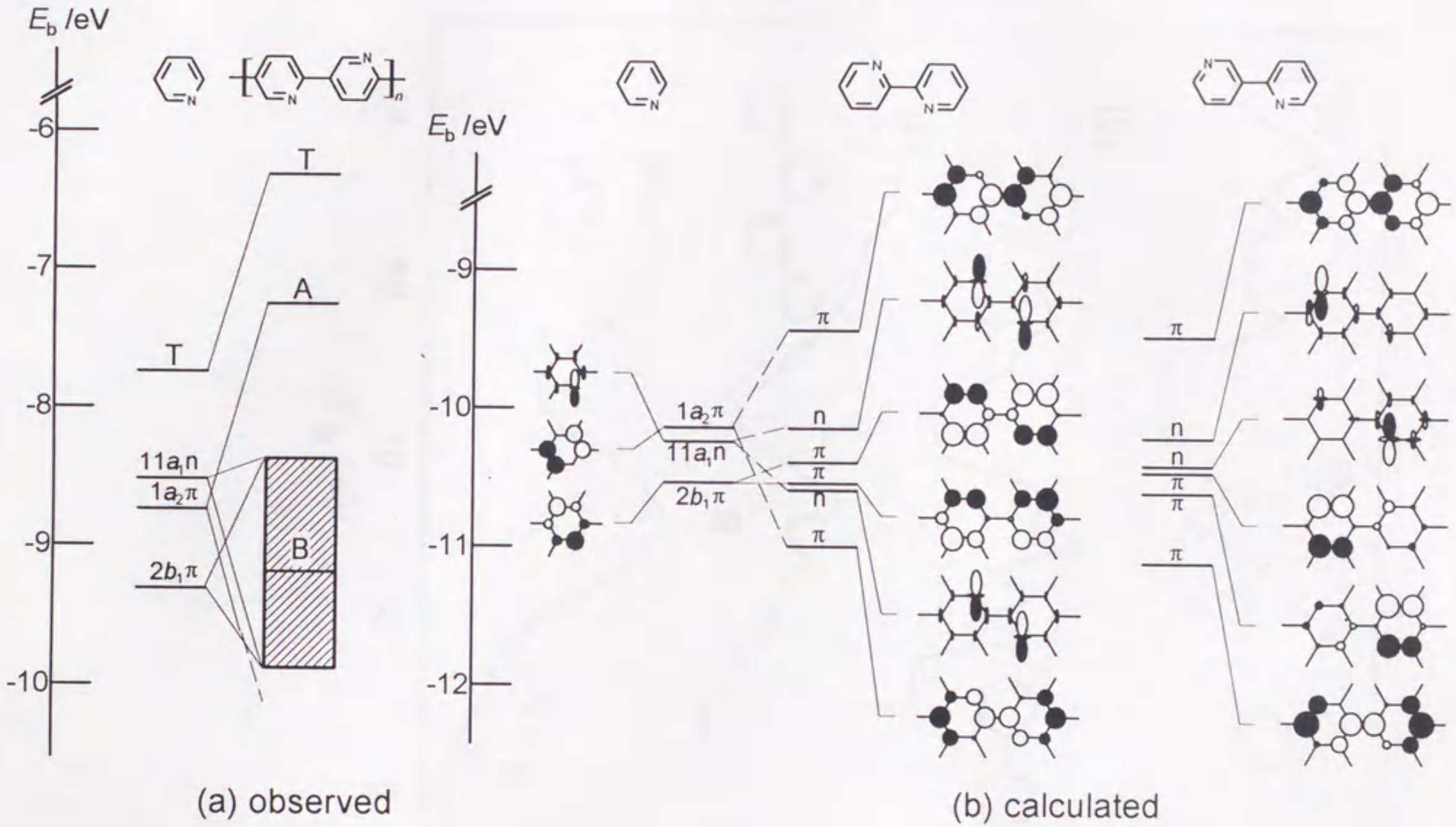

(a) observed

(b) calculated

Figure 3

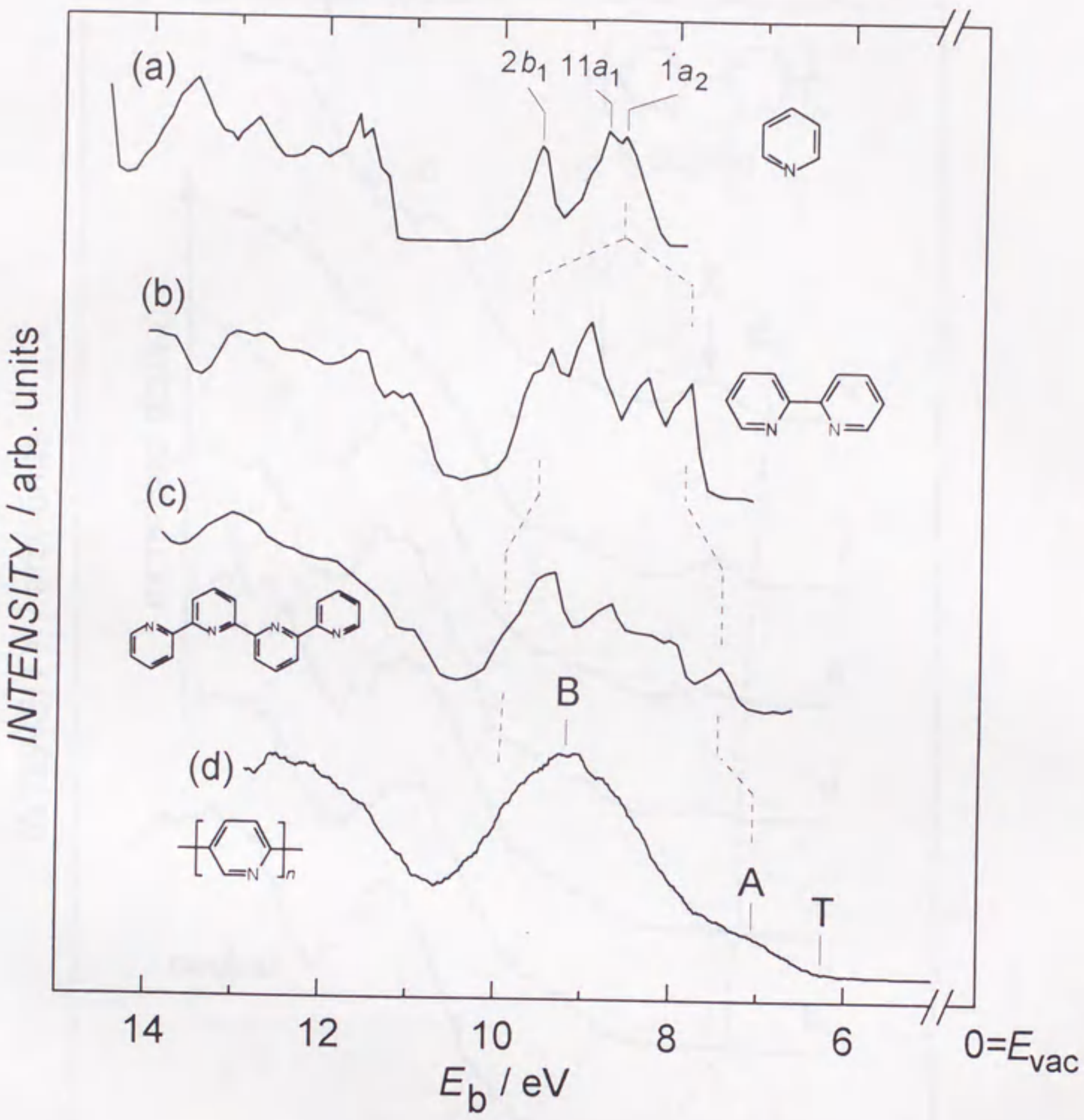
(a)
2b1 11a1 1a2
(b)
(c)
B
(d)
A
T
14
12
10
8
6
0=Evac
Eb / eV
INTENSITY / arb. units

Figure 4

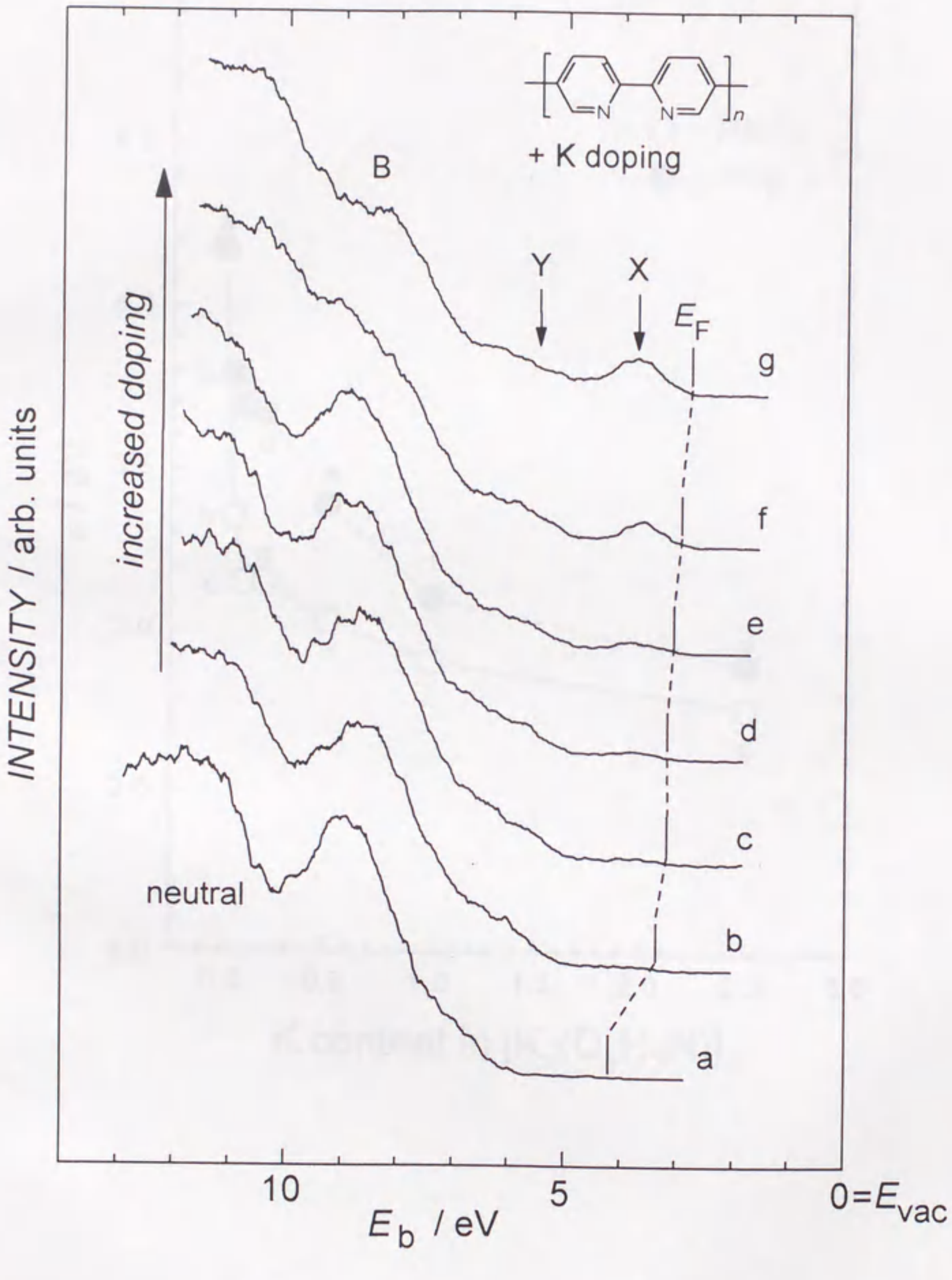
N
N
n
+ K doping
B
Y
X
E_F
g
f
e
d
c
b
a
neutral
increased doping
INTENSITY / arb. units
10
5
0=E_{vac}
E_b / eV

Figure 5

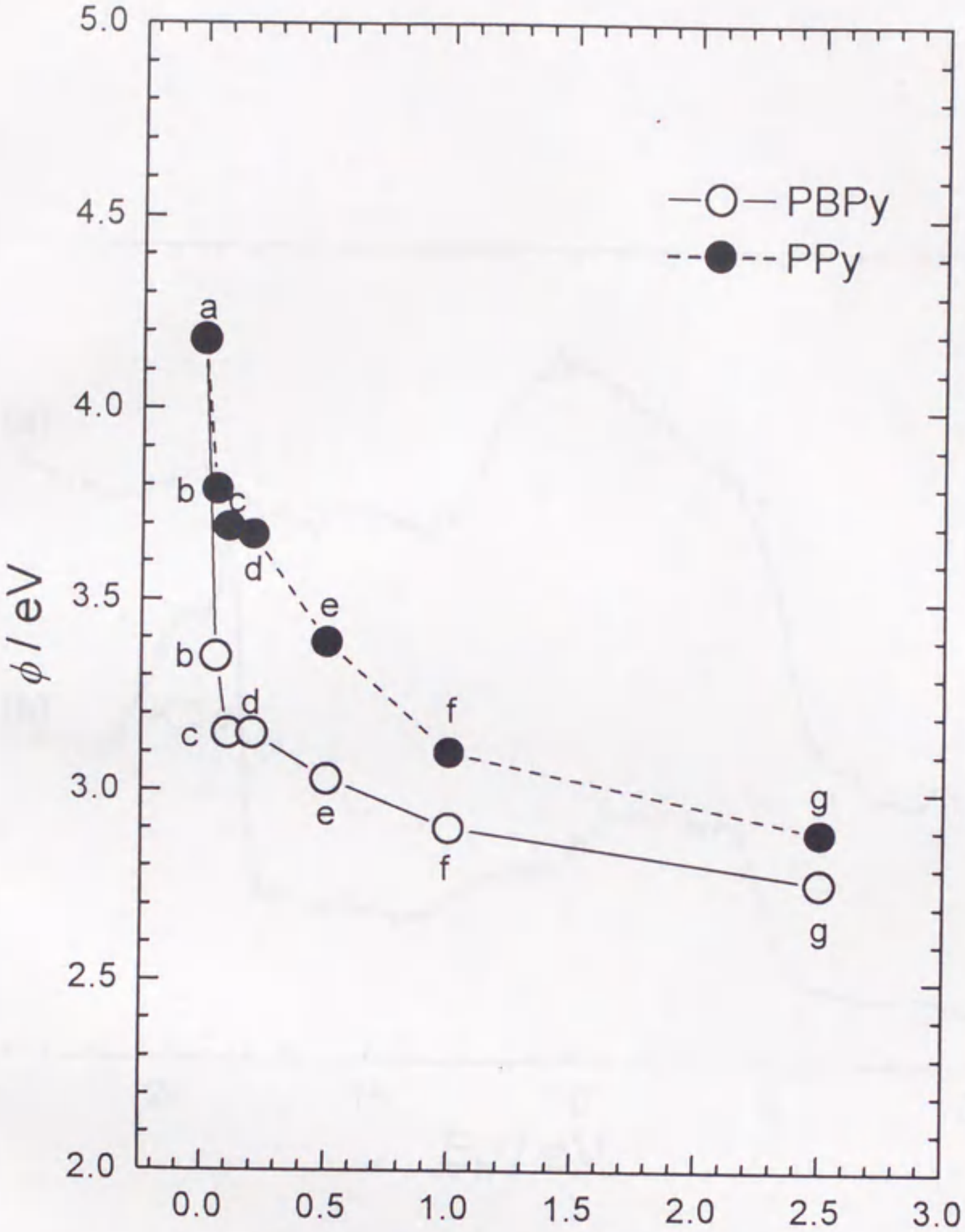
5.0
4.5
4.0
3.5
3.0
2.5
2.0
φ / eV
—O— PBPy
--●-- PPy
a
b
c
d
e
f
g
b
c
d
e
f
g
0.0
0.5
1.0
1.5
2.0
2.5
3.0
K content in [K$_x$(C$_5$H$_3$N)]$_n$

Figure 6

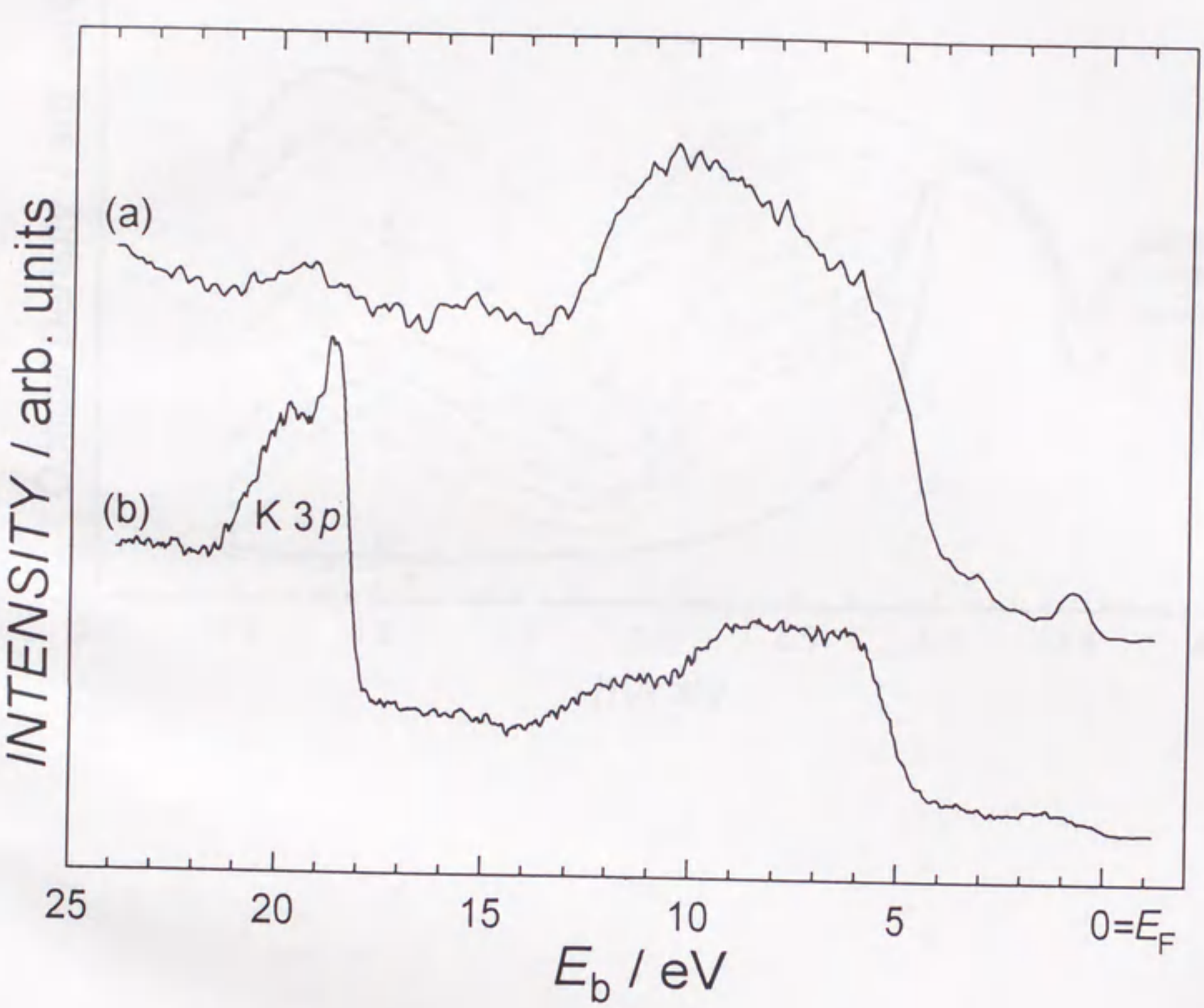

Figure 7

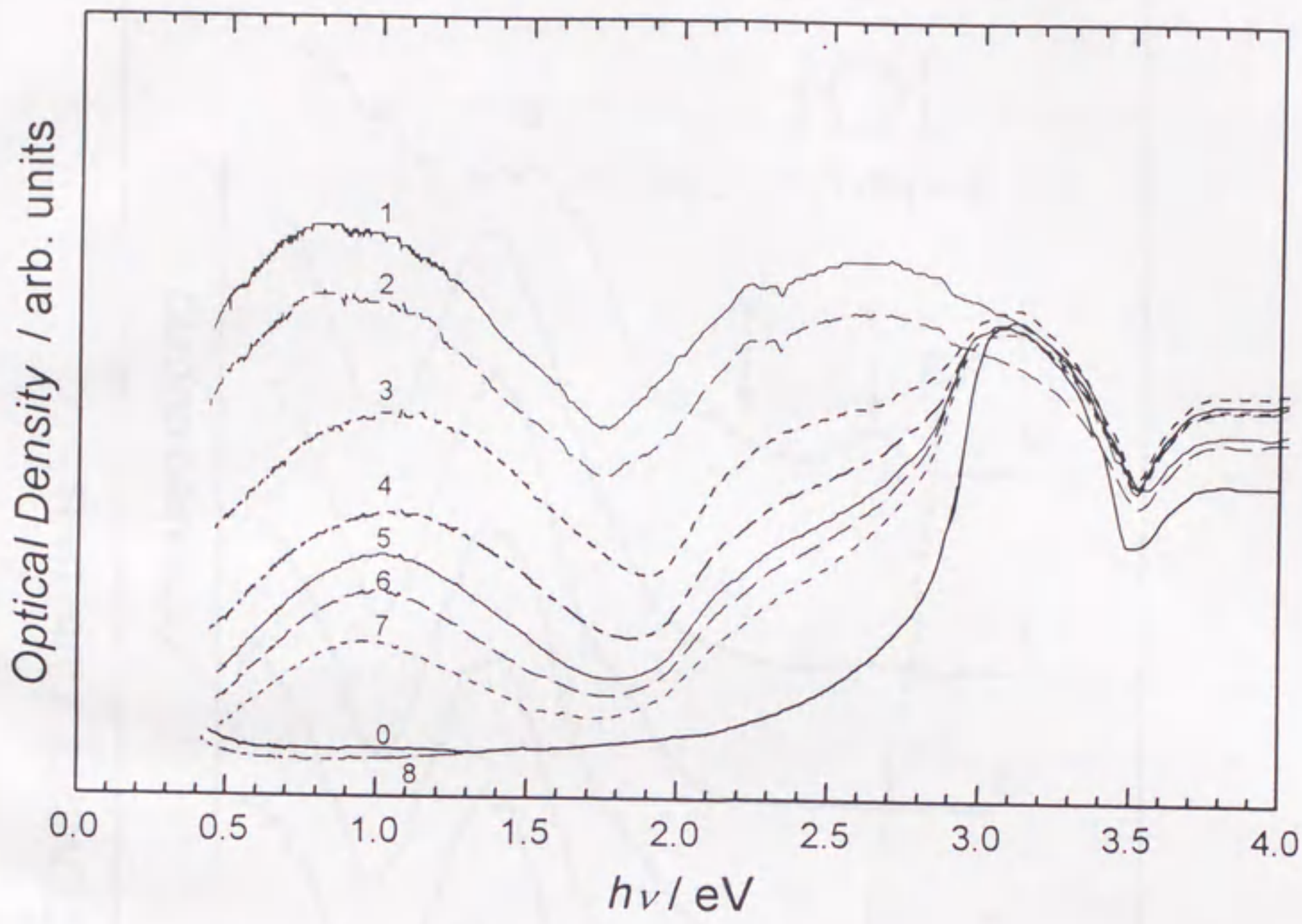
Optical Density / arb. units
1
2
3
4
5
6
7
0
8
0.0
0.5
1.0
1.5
2.0
2.5
3.0
3.5
4.0
hν / eV

Figure 8

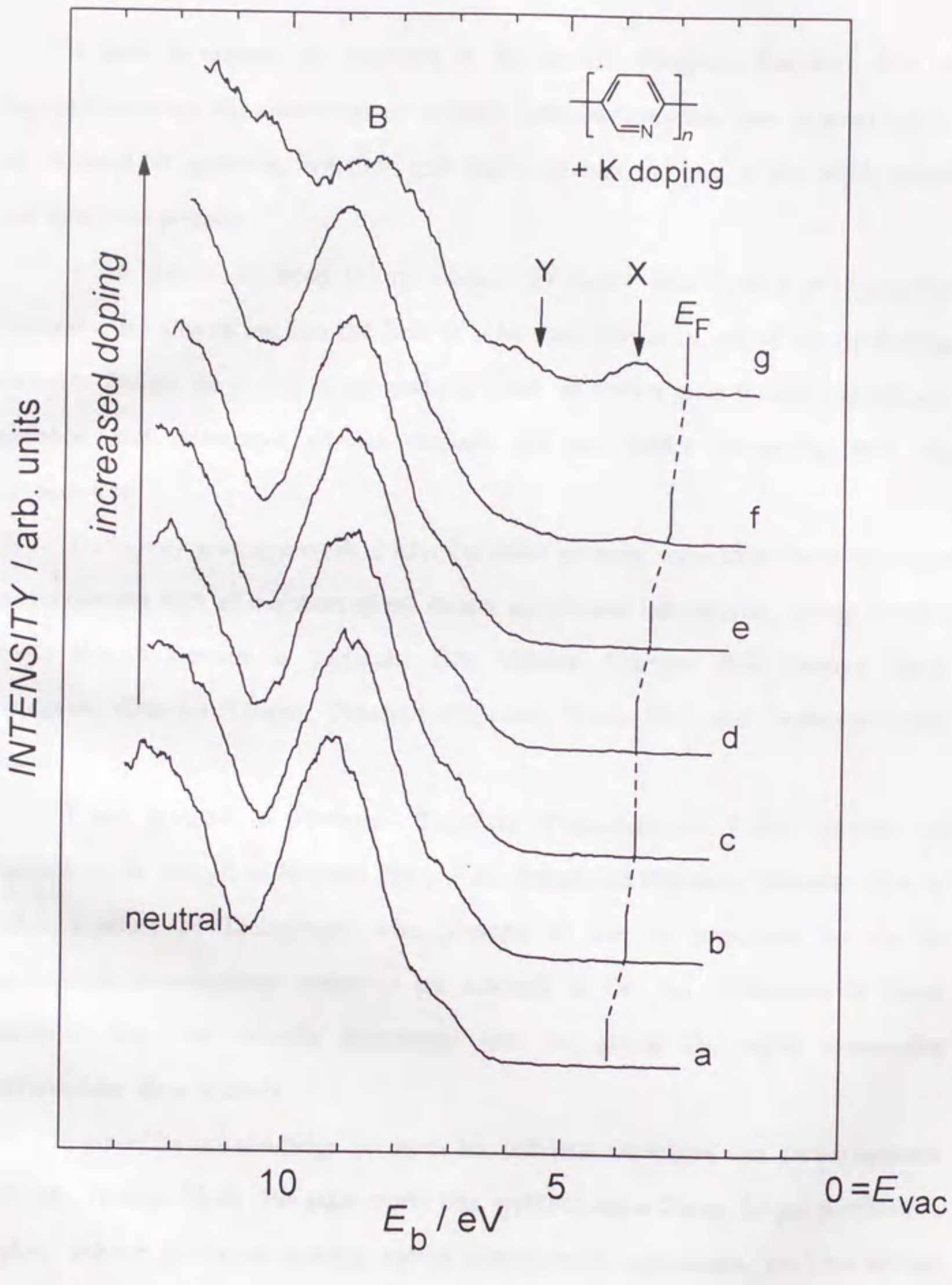
B
+ K doping
Y
X
E_F
g
f
e
d
c
b
a
neutral
increased doping
INTENSITY / arb. units
10
5
0 = E_{vac}
E_b / eV

Figure 9

Acknowledgements

I have to express my gratitude to my adviser, Professor Kazuhiko Seki of Nagoya University. His knowledge of the solid state chemistry has been of great help to me. Without his guidance, criticism, and encouragement, no part of this work would have ever been possible.

I am greatly indebted to my adviser, Professor Jiro Tanaka of Kanagawa University. He allured me into the field of solid state chemistry and of the conducting polymers. During the course of my graduate work, he always gives kindful suggestions, guidance, and instructive advices through out the works concerning with the polyacetylene.

During my graduate work, I have benefited in many ways from discussions and encouragement with all members of my former and present laboratories, among whom I would like to mention in particular Drs. Masaaki Shimizu, Koji Kamiya, Shinji Hasegawa, Chizuko Tanaka, Takafumi Miyazaki, Hisao Ishii, and Professor Yukio Ouchi.

I am grateful to Professor Takakazu Yamamoto of Tokyo Institute of Technology for the gift of PPy and PBPy. I am thankful to Professor Takehiko Mori of Tokyo Institute of Technology, who consents to use the apparatus for the dc conductivity measurements readily. I am indebted to Dr. Jun Tsukamoto of Toray Industries, Inc. for valuable discussions and for giving the highly conductive polyacetylene films willingly.

I gratefully acknowledge so much his technical assistance and encouragement with Mr. Toshiaki Noda. His glass works (the synthetic apparatuses, Ar gas purification system, solvent distillation systems, optical measurement apparatuses, etc.) are always thoughtful designed for purpose and ingeniously.

Lastly, heartfelt thanks go to the members of the Laboratory of Quantum Chemistry, who have given the author so much assistance and encouragement during this study.

I thanks the Japan Society for the Promotion of Science for the Fellowship for Japanese Junior Scientists. The part of this work is supported by a Grant-in-Aid for International Cooperative Research Program on Molecular Metals, NEDO, Japan.

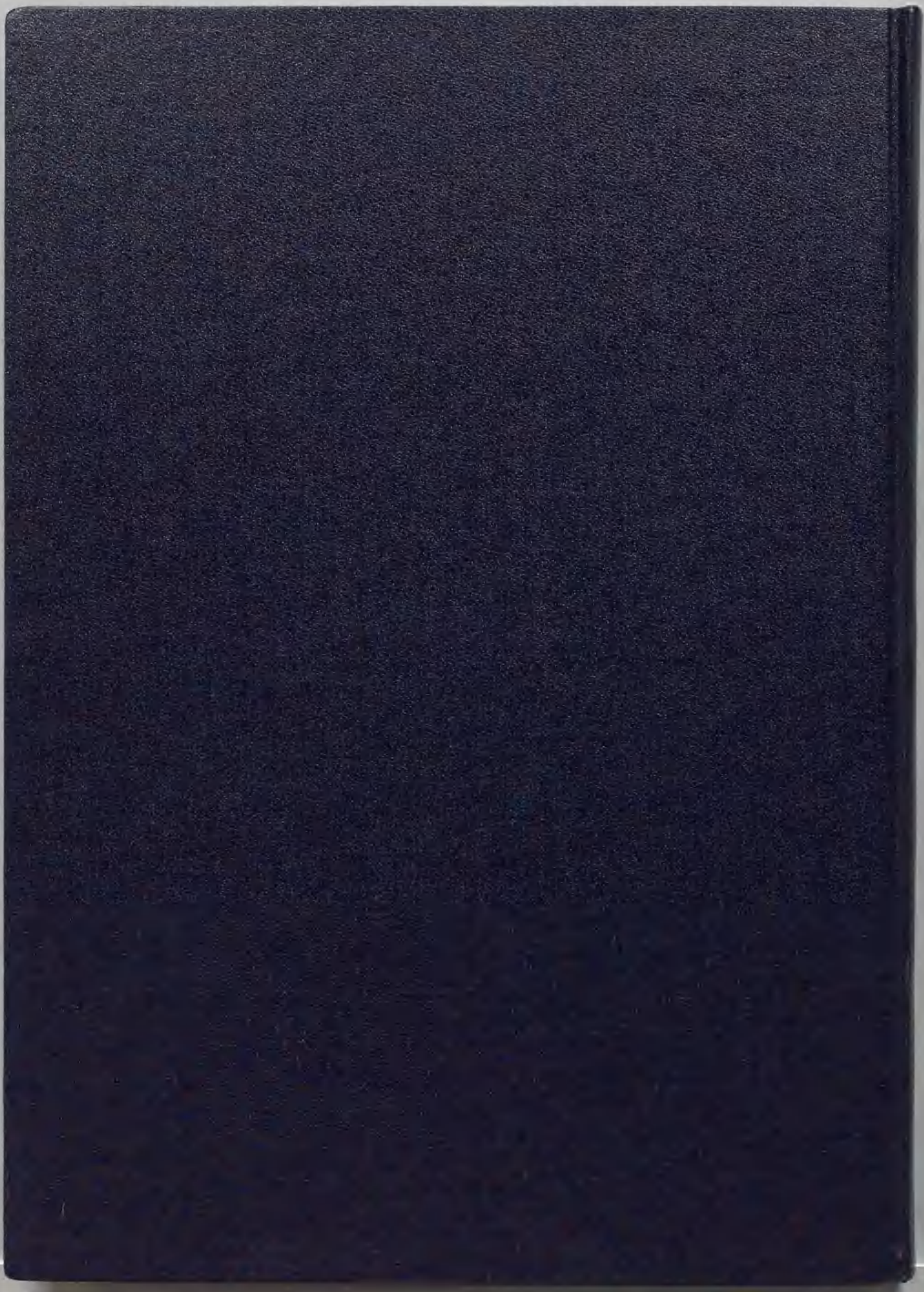

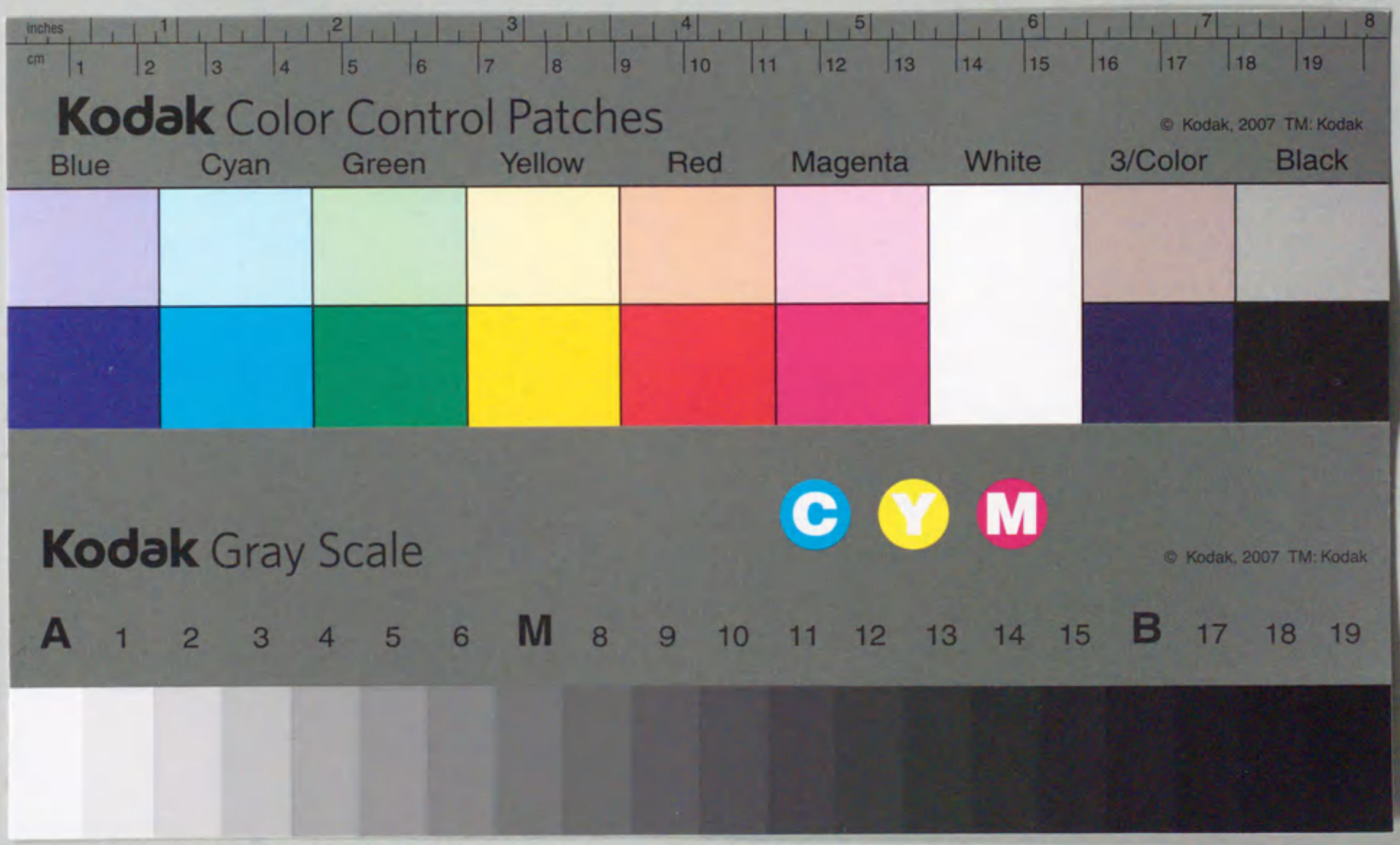
inches
cm
Kodak Color Control Patches
© Kodak, 2007 TM: Kodak
Blue
Cyan
Green
Yellow
Red
Magenta
White
3/Color
Black
Kodak Gray Scale
C
Y
M
© Kodak, 2007 TM: Kodak
A 1 2 3 4 5 6 M 8 9 10 11 12 13 14 15 B 17 18 19